



Durham E-Theses

Third generation fermions as probes of new physics

Bullock, Ben Kasmin

How to cite:

Bullock, Ben Kasmin (1994) *Third generation fermions as probes of new physics*, Durham theses, Durham University. Available at Durham E-Theses Online: <http://etheses.dur.ac.uk/5487/>

Use policy

The full-text may be used and/or reproduced, and given to third parties in any format or medium, without prior permission or charge, for personal research or study, educational, or not-for-profit purposes provided that:

- a full bibliographic reference is made to the original source
- a [link](#) is made to the metadata record in Durham E-Theses
- the full-text is not changed in any way

The full-text must not be sold in any format or medium without the formal permission of the copyright holders.

Please consult the [full Durham E-Theses policy](#) for further details.

Third generation fermions as probes of new physics

Ben Kasmin Bullock

Department of Physics, University of Durham

Submitted for the degree of Doctor of Philosophy

April 12, 1994

The copyright of this thesis rests with the author.
No quotation from it should be published without
his prior written consent and information derived
from it should be acknowledged.

The copyright of this thesis rests with the author. No quotation from it should be published without his prior written consent and information derived from it should be acknowledged.



7 JUN 1994

Contents

Abstract	3
List of Tables	4
List of Figures	6
Acknowledgments	7
Declaration	8
1 Introduction	9
2 Decay of polarised tau leptons	14
2.1 Introduction	14
2.2 Polarised tau decay distributions	17
2.3 The $\tau \rightarrow \rho \rightarrow 2\pi$ and $\tau \rightarrow a_1 \rightarrow 3\pi$ polarimeters.	22
2.3.1 The ρ decay mode	25
2.3.2 The a_1 decay mode	25
2.4 Detecting the charged Higgs	31
2.5 Detecting the neutral Higgs using decay correlations	33
2.6 Comparison of measurement errors for various decay modes	42
2.6.1 Measuring P_τ from τ^\pm decays	43
2.6.2 Measuring P_τ from $X \rightarrow \tau^- \tau^+$ events	47
2.6.3 Measuring P_τ at hadron colliders	48
2.7 Conclusions	50
3 Radiative corrections to top quark production and decay	52
3.1 Approach to the problem.	54
3.2 Kinematics	55
3.3 Spinors	57
3.4 Tree level amplitudes	60
3.5 Box diagrams	62

3.5.1	Amplitudes	62
3.5.2	Reduction of the D_{1n} and D_{2n} form factors	66
3.6	Vertex diagrams	68
3.6.1	Vertices with external on-shell fermions	69
3.6.2	e^+e^- vertex corrections	76
3.6.3	$t\bar{t}$ vertex corrections	77
3.6.4	tbW vertex corrections	77
3.7	Self energy diagrams	80
3.8	Renormalisation	85
3.9	The total cross section	87
3.10	Conclusions	88
Appendices		93
A.	Gamma matrices	93
B.	Rougé's formula	94
C.	The Standard Model Lagrangian	96
D.	One loop integrals	100
Bibliography		103

Abstract

This thesis concerns the properties of two particles, the top quark and the tau lepton, the heaviest of the quarks and leptons, respectively, in the standard model of elementary particle physics.

After a chapter introducing the standard model, the second concerns the tau lepton. Amongst all the quarks and leptons, the tau has the unique property that its polarisation can readily be measured at high energy colliders. We propose and develop new methods of using this unique property to search for new physics, such as Higgs bosons. and also for making an accurate measurement of the polarisation of taus produced via Z decay leading to a precision determination of the electroweak coupling.

The third chapter of this thesis concerns the top quark. We perform the complete one-loop radiative corrections to the helicity amplitudes within the standard model. Even though the radiative corrections to top quark production and decay have already been calculated separately, our work makes it possible to combine the sequence of events by keeping full information on the correlations among final state particles.

List of Tables

2.1	Fraction of the leading ‘particles’ in the decays of τ_L^- and τ_R^- for different values of minimum detectable particle energy fraction	33
2.2	The ideal errors associated with each of the major τ decay modes with and without the ρ and a_1 decay to pions as polarimeters.	44
2.3	Examples of the improvement in total accuracy in measuring τ polarisation when the ρ and a_1 decays to pions are used as polarimeters.	45
2.4	The errors associated with measuring the τ^- polarisation from a massive spin one boson X decaying as $X \rightarrow \tau^- \tau^+ \rightarrow A^- B^+ \nu$'s (or $X \rightarrow A^+ B^- \nu$'s).	48
2.5	The errors associated with measuring the τ^- polarisation at a hadron collider.	50
3.1	Radiative corrections to e^+e^- vertex	76
3.2	Radiative corrections to $t\bar{t}$ vertex	90
3.3	The radiative corrections to tbW vertex which do not involve virtual photon corrections	91
3.4	The radiative corrections to the tbW vertex that involve virtual photons. The fictitious mass of the photon is denoted λ	92

List of Figures

2.1	The fractional energy distributions of polarised ρ and a_1 vector mesons arising from τ_L^- or τ_R^+ decays and τ_R^- or τ_L^+ decays for zero width ρ or a_1 mesons.	21
2.2	As Fig. 2.1 but with non-zero ρ and a_1 widths.	23
2.3	The $\tau_{L,R} \rightarrow \nu\nu$ distributions assuming no information on the vector meson polarisation.	24
2.4	The Dalitz plots for $a_1 \rightarrow 3\pi$ using the Kühn and Santamaria and Isgur <i>et al.</i> models for the decay.	27
2.5	The scatter plots for transversely and longitudinally polarized $a_1 \rightarrow 3\pi$ decays in the laboratory frame.	29
2.6	Plots of the correlation in energy fractions in $X \rightarrow \tau^- \tau^+ \rightarrow A^- B^+ \nu$'s, where X is either a spin-one or spin-zero boson.	35
2.7	As Fig. 2.6	36
2.8	As Fig. 2.6	37
2.9	As Fig. 2.6	38
2.10	As Fig. 2.6	39
2.11	As Fig. 2.6	40
2.12	The polarized a_1 decay distributions as functions of the energy fraction of the distinguishable pion in $a_1 \rightarrow 3\pi$ decays).	46
3.1	Momenta of e^- , e^+ , t , \bar{t} , b , W^+ , \bar{b} and W^-	55
3.2	The Feynman diagram for $e^+e^- \rightarrow t\bar{t} \rightarrow bW^+ \bar{b}W^-$ at tree level	61
3.3	The three box diagrams.	62
3.4	The uncrossed (a) and crossed (b) box diagrams with their assignments of momenta.	63
3.5	The locations of the vertex radiative corrections to $e^+e^- \rightarrow t\bar{t} \rightarrow bW^+ \bar{b}W^-$ shown by shaded circles on the Feynman diagram	69
3.6	The six possible structures of one loop vertex occurring in the standard model	71

3.7	Conventions for the vertex one loop diagrams	72
3.8	Soft photon radiative corrections to $t \rightarrow bW^+$	78
3.9	Fermionic self energy Feynman diagram.	84
B.1	The angle ψ between the normal, n , to the plane that the three decaying bodies make in their parent's rest frame and the direction of motion of the parent particle in the lab frame.	94
D.1	The A, B, C, D classification scheme for one loop integrals.	101

Acknowledgments

I would like to thank Dr. Kaoru Hagiwara of K.E.K. for the patient advice and help he has given me on all the work I have done for this thesis. I would also like to thank Professor Alan Martin, my PhD supervisor at Durham University, particularly for his help in making the work in this thesis more comprehensible, and to acknowledge Dr. Nicholas d'Ambrumenil of Warwick University for his help in enabling me to come here to do this PhD.

Declaration

I declare that no material in this thesis has previously been submitted for a degree at this or any other University.

The work described in this thesis has previously appeared in the following publications:

- **Tau pair polarisation correlations as a signal for Higgs bosons**
B.K. Bullock, K. Hagiwara and A.D. Martin, Physics Letters B 273 (26th December 1991) 501.
- **Tau polarisation as a signal of charged Higgs bosons**
B.K. Bullock, K. Hagiwara and A.D. Martin, Physical Review Letters Vol. 67, No. 22 (25th November 1991) 3055.
- **Tau polarisation and its correlations as a probe of new Physics**
B.K. Bullock, K. Hagiwara and A.D. Martin, Nuclear Physics B 395 (1993) 499-533.

The copyright of this thesis rests with the author.

Chapter 1

Introduction

In this introduction I give a brief summary of current knowledge in elementary particle physics and how the material of this thesis relates to it.

Elementary particle physics is the branch of physics concerned with the interactions of the fundamental particles of which we believe all material objects are composed. The progress of fundamental physics can in part be regarded as the discovery of smaller and smaller levels of structure. At one time the atom was believed to be a fundamental particle of which all other materials were formed. Later the nucleus and electrons were believed to be fundamental. With the discovery of the photoelectric effect and Planck's explanation of black body radiation, the "electromagnetic field" came to be seen as composed of particles, photons. As more careful and ingenious experiments were performed, yet more particles were discovered, such as the neutrino observed in the beta decay of the nucleus, and the neutrons and protons from which the nucleus is composed. At even smaller scales, or equivalently, at higher energies, the W and Z bosons which mediate beta decay, and the quarks and gluons which comprise the proton and neutron, were observed. Also, particles which mysteriously duplicated the known particles, the muon, the tau lepton, the muon neutrino, and the tau neutrino, and the strange, charm and bottom quarks appeared.

In the standard model these particles are grouped into generations, with the first generation comprising the electron, electron neutrino, and up and down quarks, the second generation comprising the muon, the muon neutrino, and the charm and strange quarks, and the third generation, from which this thesis takes its title, comprising the tau lepton, the tau neutrino, and the top and bottom quarks.

generation	1	2	3
charge $+\frac{2}{3}$ quark	u	c	t
charge $-\frac{1}{3}$ quark	d	s	b
lepton	e	μ	τ
neutrino	ν_e	ν_μ	ν_τ

We now have a theory which encompasses all the interactions of these particles except the gravitational ones. However, the theory is not complete. For its consistency it requires two particles which are as yet unobserved, the top quark and the Higgs boson. Also, the model contains various input parameters, such as masses of the particles and strengths of couplings which cannot be predicted but can only be determined from experiment. It can be speculated, based on past experience, where simple structures revealed themselves as the scale of investigation became smaller, that these apparently arbitrary numbers may be predicted by some deeper theory.

The standard model of particle physics models electromagnetism, weak interactions and strong interactions. Electromagnetic interactions are responsible for most of the everyday phenomena that surround us. Therefore it is not surprising that we have a complete theory, called quantum electrodynamics, of the electromagnetic interaction. This is one of the most accurately tested of all physics models. The weak interaction was first observed less than one hundred years ago, in the beta decay of nuclear matter. The strong force was first observed as the force that holds neutrons and protons together in the nucleus. There exists both a theory of weak interactions, which combines them with electromagnetic interactions, known as the electroweak standard model, and a theory of strong interactions, known as Quantum Chromodynamics, or QCD, which binds together hadrons. Unfortunately the nature of the strong interaction makes comparison of QCD with experiment difficult, since no-one has solved the theory from first principles for even the simplest cases of bound states of quarks, the only state in which the strong interaction has been observed. The best hope at present seems to be the attempt to solve numerically the QCD problem using the lattice method, where the interior of a hadron is modeled as a lattice of points in four dimensional space. Comparison of the weak interaction with experiment is also difficult for the opposite reason. Because of their weakness, weak interactions can be calculated using perturbation theory, but are hard to test in experiment since at low energies the force is so weak in comparison to the electromagnetic and strong forces that its interactions are difficult to discern.

In a framework of relativistic quantum field theory, the notion of gauge fields has been imposed to model the electromagnetic and weak fields. Originally an observation regarding the theory of the classical electromagnetic force, that an absolute electromagnetic potential

could not be measured, and that the only meaningful notion was of a difference in potential, the notion of gauge symmetry was found to have deep consequences for the quantum theory of electromagnetism. The freedom to choose an arbitrary “gauge” or basic potential, was found to correspond to the invariance of the quantum electrodynamic Lagrangian under a shift of the vector potential A^μ by the derivative of an arbitrary function $\partial^\mu\chi$ without changing the physical consequences. This in turn is related to the local conservation of charge, that is, charge cannot disappear from one location and appear at another location without making a continuous journey from one location to the other.

This gauge property was found to be related to the renormalisability properties of the theory, which is the property that the theory contains dimensionless couplings and can be dealt with in a way that is consistent in perturbation theory.

We now believe that the weak and strong interactions can also be modeled by a gauge theory. In the case of the strong interactions the field is described by a symmetry group called SU(3), the group of 3×3 unitary matrices with determinant one. The gauge bosons which carry the QCD force are spin one bosons denoted gluons.

The weak interaction is unified with electromagnetism in an $SU(2) \times U(1)$ gauge group, the direct product of the group of 2×2 unitary matrices with determinant one, SU(2), and the group of complex numbers with modulus 1, U(1), which is broken by the “Higgs mechanism”. The standard model Higgs field consists of an SU(2) doublet of fields which gains a vacuum expectation value.

$$\frac{1}{\sqrt{2}} \begin{pmatrix} \chi^1 + i\chi^2 \\ H + i\chi^3 \end{pmatrix} \rightarrow \frac{1}{\sqrt{2}} \begin{pmatrix} \chi^1 + i\chi^2 \\ v + H + i\chi^3 \end{pmatrix}. \quad (1.1)$$

where v is the vacuum expectation value that the field H acquires. The component of the field that has this expectation value interacts with the electroweak bosons. This breaks the $SU(2) \times U(1)$ symmetry into a residual U(1) gauge symmetry. The residual U(1) symmetry is not the same as the one we started out with. This residual symmetry is the gauge group of the massless photon. The other three degrees of freedom in $SU(2) \times U(1)$ become the massive gauge bosons, the charged W and the neutral Z boson. From this mechanism, the gauge bosons acquire a mass, thus making the force weak at energies far below their mass, where the weak gauge bosons can only be produced in virtual states.

The SU(2) component of the weak boson field interacts only with the negative helicity states of the fermions. In order for consistency we must assume that initially the fermions are all massless, since only for massless fermions is helicity conserved. Therefore the fermion mass is also generated by the Higgs mechanism.

This model can be criticised for a number of reasons. It does not tell us anything about

why the masses of the fermions have the value they do, and in effect we are just reparametrising the masses of the fermions as couplings to the Higgs field. The model itself is inconsistent within quantum field theory, since the contribution of self-energy graphs to the vacuum expectation value of the Higgs field is not renormalisable - the corrections caused by tadpole graphs create quadratic divergences which cannot be consistently reabsorbed into measured values in perturbation theory.

The other major question that faces fundamental physics is that of the unification of all the forces. Since so many different phenomena have gradually been reduced to such a small set of fundamental laws, it is widely believed that further unification of the forces of nature must come about somehow. This is because of the similarity between the electromagnetic, weak and strong forces, which all interact via spin-one gauge bosons. No-one yet has any evidence for any such unification, but many speculative theories exist. Since the scale of any unification is so far beyond what can possibly be achieved at current experiments, each piece of experimental information that we have, in particular highly accurate measurements of coupling constants, must be exhaustively scrutinised for clues.

The only remaining part of fundamental physics that has not been mentioned here is gravity. This has been successfully described to the limits of experimental measurement by Einstein's theory of General Relativity. However it is theoretically inconsistent with the other theories of the forces of nature, since it predicts absolute motion with no quantum uncertainty, and it is speculated that it cannot be possible to have this kind of unquantised force which could in principle be used to deduce the absolute position and momentum of a particle, contradicting quantum theory. Therefore efforts have been made to formulate a quantum theory of gravity, and to unify the gravitational force with the other three forces of nature. With little possibility of experimental inputs due to the extremely weak nature of the gravitational field, and intractable mathematics even within unquantised General Relativity, the problems of quantised models are formidable and so far no success whatsoever has been achieved in testing any models of quantum gravity against experiments.

We concentrate here on what can be achieved experimentally to test the standard model. In particular, this thesis concentrates on two members of the third generation of fermions, the tau lepton and the top quark, and how their behaviour can be used to probe beyond the standard model for new physics.

In the first part of the thesis, we examine how the tau can be used to probe both the Higgs sector of the theory, and the unification of electroweak and strong forces through accurate measurements of the electroweak coupling. The tau is the heaviest of the leptons, and because its mass is sufficient for it to decay into hadrons, its decay can serve as a polarimeter. Also

its couplings to Higgs bosons will be much greater than the electron or muon, and thus it may be possible to use the tau for detecting Higgs bosons.

In the second part of the thesis we give complete analytic formulae for the electroweak radiative corrections to $t\bar{t}$ production at an e^+e^- linear collider and top quark and anti-top quark decay within the standard model. This will serve as a background for future studies on the effect of new physics on these radiative corrections.

Chapter 2

Decay of polarised tau leptons

2.1 Introduction

The electron, muon and tau are believed to have identical properties, apart from their mass. Indeed why nature chooses to have two “identical” copies of itself is one of the great unsolved problems. We speak of e, μ and τ universality; and experiment has confirmed the equality of their couplings to the gauge bosons to a considerable degree of accuracy. However for practical purposes the τ , as a consequence of its much greater mass; behaves differently from the e and μ . First the τ has hadronic decay modes (e.g. $\tau \rightarrow \pi\nu, \rho\nu, a_1\nu \dots$) which allow an efficient measurement of its polarization, and second its coupling to the Higgs boson is expected to dominate those of the e and μ . We shall see that these two distinctive features allow the τ to be a rather special experimental probe of new physics.

The first property is being exploited at LEP to make a precision measurement of $\sin^2\theta_W$ by studying the tau polarization P_τ , in the process $e^-e^+ \rightarrow \tau^-\tau^+$. For example if we retain only the $e^-e^+ \rightarrow Z \rightarrow \tau^-\tau^+$ contribution we have

$$P_\tau \equiv \frac{\sigma(\tau_R) - \sigma(\tau_L)}{\sigma(\tau_R) + \sigma(\tau_L)} \simeq -2(1 - 4\sin^2\theta_W)$$

where $\sigma(\tau_{R,L})$ are the cross sections for producing τ^- with right- and left-handed helicities respectively. A measurement of P_τ therefore determines $\sin^2\theta_W$ with an accuracy $\delta(\sin^2\theta_W) \simeq \frac{1}{8}\delta P_\tau$. The electron distribution from the purely leptonic decay mode, $\tau^- \rightarrow e^-\bar{\nu}_e\nu_\tau$, is not very sensitive to whether the parent is τ_R or τ_L because of the two missing neutrinos in this decay. However the distributions of the final state hadrons in the hadronic decay modes allow a much better determination of P_τ . For $\tau^\pm \rightarrow \pi^\pm\nu$, for example, the pion energy distributions are of the form [1]

$$\frac{1}{\Gamma_\tau} \frac{d\Gamma_\pi}{dz} = B_\pi [1 \mp P_\tau(2z - 1)]$$

where $B_\pi = B(\tau \rightarrow \pi\nu)$ is the decay branching fraction and $z = E_\pi/E_{beam}$ is the energy fraction carried by the pion in the laboratory frame of the e^-e^+ collider. Moreover, as we shall discuss in detail, the distributions of the outgoing pions in the decays [2, 3, 4]

$$\tau \rightarrow \rho\nu \rightarrow (2\pi)\nu$$

$$\tau \rightarrow a_1\nu \rightarrow (3\pi)\nu$$

allow comparably sensitive measurements of P_τ [5, 6, 7].

We shall see that it is the possibility of measuring its polarisation which best allows the τ to probe new physics beyond the standard model. Recall that the most unsatisfactory feature of the standard model, which is so successful in other respects, is our lack of knowledge of the actual mechanism that breaks the electroweak gauge symmetry and generates the particle masses. In the minimal model the breaking is accomplished by a complex Higgs doublet, three components of which become the longitudinal polarisation states of the massive vector gauge bosons, while the remaining component manifests itself as a neutral massive scalar Higgs particle, H^0 . On the other hand the minimal supersymmetric model contains two Higgs doublets; again three of the fields are taken by the vector bosons and the remaining five components become physical particles: a pair of charged bosons H^\pm , two scalars $H_{1,2}^0$ and one pseudoscalar A . More complicated models of mass generation have been proposed (including composite Higgs scalar particles), but a common feature of all models is that the couplings of the ‘‘Higgs’’ particles to fermions increase with the mass of the fermion. Thus the τ couples preferentially in comparison with either the μ or the e . There are two different ways in which measurements of the polarisation of the τ can help to probe the Higgs sector; first they offer a distinctive signal for charged Higgs bosons via $H^\pm \rightarrow \tau^\pm\nu$ [7, 8, 9] and second they provide a way to identify the decay $H^0 \rightarrow \tau^-\tau^+$ [10]. We discuss the two cases in turn.

Although the charged Higgs bosons, H^\pm , exist in most extensions of the minimal model, there are surprisingly few viable ways in which they may be detected [11, 12]. However, due to the massiveness of the top quark, it is quite possible that $m(H^\pm) < m_t$. In this circumstance H^+ (or H^-) can be produced via $t \rightarrow H^+b$ (or $\bar{t} \rightarrow H^-\bar{b}$) and, as we shall see, it may then be detected via the subsequent decays $H^\pm \rightarrow \tau^\pm\nu$. The event rate [11, 13] depends on the branching fractions of these decays, which in turn depend on the magnitude of the Yukawa couplings. The main background is $W^\pm \rightarrow \tau^\pm\nu$, where, in addition to $t \rightarrow W^+b$ (and $\bar{t} \rightarrow W^-b$), the W boson can also be produced by the Drell-Yan mechanism. To identify $H \rightarrow \tau\nu$ simply from an excess of $\tau\nu$ events over the known $W \rightarrow \tau\nu$ event rate would require high statistics and a good control of the experimental systematic errors. However

a measurement of the τ polarisation can give a much cleaner separation of the $H \rightarrow \tau\nu$ signal from the $W \rightarrow \tau\nu$ background. To be specific we discuss the τ^- channel. The crucial observation [7] is that the τ^- leptons arising from $H^- \rightarrow \tau^-\bar{\nu}$ decays are almost all purely right-handed in contrast with the left-handed τ 's which arise from W^- decays, $W^- \rightarrow \tau_L^-\bar{\nu}_R$. This is a consequence of the helicity flip nature of the Yukawa couplings of the Higgs fields, and, indeed, the distinctive $H^- \rightarrow \tau_R^-\bar{\nu}_R$ character of the decay is true in all models containing only left-handed neutrinos (and right-handed antineutrinos). Since the pion distributions resulting from the $\tau^- \rightarrow \pi^-\nu$, $(2\pi)^-\nu$, $(3\pi)^-\nu$ differ significantly depending on whether the τ is left- or right-handed, we should be able to identify $H^- \rightarrow \tau_R^-\bar{\nu}$ decays amongst the $W^- \rightarrow \tau_L^-\bar{\nu}$ events. It has been shown [9] that τ polarisation can be used to improve the charged Higgs boson signal by a factor of ~ 3 in hadron collider experiments.

The polarisation of the τ can also be exploited to identify a neutral Higgs boson via the decay $H^0 \rightarrow \tau^-\tau^+$. Any experimental observation which breaks e, μ, τ universality, by favouring $\tau^-\tau^+$ events, could be an indication of the presence of a neutral Higgs scalar. Here the background is Z (or γ) $\rightarrow \tau^-\tau^+$ events. Whenever such a departure from lepton universality is observed, there exists a simple helicity correlation test which, in principle, will clearly indicate the presence of τ pairs of Higgs origin among the background $Z \rightarrow \tau^-\tau^+$ events. The crucial observation [10] is that vector bosons, Z or γ , decay into either $\tau_L^-\tau_R^+$ or $\tau_R^-\tau_L^+$, whereas the scalar Higgs boson decays into either $\tau_L^-\tau_L^+$ or $\tau_R^-\tau_R^+$. Thus a polarization correlation test can be performed, using the distributions of the final decay products, which is sensitive to the admixture of the H^0 and (Z, γ) parentage of the τ pairs.

In addition, τ polarisation measurements are essential in identifying the quantum numbers of a new heavy W boson or a Z' boson [14, 15]. The use of the 2π and 3π decay modes of τ 's will significantly improve experimental sensitivity, especially at hadron colliders.

In this chapter, we present details of our studies [7, 10] of the use of $\tau \rightarrow \rho\nu_\tau$ and $\tau \rightarrow a_1\nu_\tau$ decay modes at collider energies. In Section 2.2 we present the distributions of the final state particles from polarized τ decays. We are particularly concerned with fast taus which arise from a ‘‘heavy’’ parent (a gauge boson or Higgs scalar), and so accurate final state angular distributions are not accessible experimentally. It is more useful, therefore, to present the decay distributions in the collinear approximation. We have carefully treated the effects of the large widths of the ρ and a_1 . Section 2.3 is devoted to a detailed study of the ρ and a_1 decay modes of polarised τ leptons. In particular we examine the model dependence of the description of the $\tau \rightarrow (3\pi)\nu$ decay. In section 2.4 we discuss how τ polarisation can be used for detecting a charged Higgs boson. In section 2.5 we present the τ pair polarization correlations for the various decay combinations. In section 2.6 we compare quantitatively

errors in measuring tau polarisation using the lepton, π , ρ and a_1 modes of τ decay, and the subsequent decay to pions of the a_1 and the ρ . In particular, we demonstrate that the τ polarisation measurement can be improved significantly, even if a single π^0 cannot be distinguished from multiple π^0 's (for instance $\rho^\pm \rightarrow \pi^\pm \pi^0$ from $a_1^\pm \rightarrow \pi^\pm \pi^0 \pi^0$). The effect of using the $\tau^- \tau^+$ polarisation correlation in the P_τ measurements at LEP is also studied quantitatively. Section 2.7 contains our conclusions.

2.2 Polarised tau decay distributions

In this section we present the distributions of the charged particles which arise from the various (primary) decay modes of polarised τ leptons. First we give the decay distributions in the τ rest frame, although the frame is not accessible experimentally on account of the missing neutrinos. Since we are primarily concerned with the decay of fast moving taus (with energy $E_\tau \gg m_\tau$) it is sufficient to obtain the distributions in the limit in which the tau and its decay products are moving collinearly:

$$\frac{d\Gamma}{dz}(\tau^- \rightarrow A^- \nu \text{'s})$$

where z is the fraction of the tau's energy which is carried by the observable decay particle A , that is $z = E_A/E_\tau$. To be precise we present distributions for $A = e, \pi, \rho, a_1$ arising respectively from the $\tau^- \rightarrow e^- \bar{\nu}_e \nu_\tau$, $\pi^- \nu_\tau$, $\rho^- \nu_\tau$, $a_1^- \nu_\tau$ decay modes. For τ^+ decays, due to CP invariance, we need simply replace P_τ by $-P_\tau$.

The simplest mode is the decay $\tau^- \rightarrow \pi^- \nu_\tau$. In the τ rest frame we have

$$\frac{1}{\Gamma_\tau} \frac{d\Gamma_\pi}{d \cos \hat{\theta}} = B_\pi \frac{1}{2} \left[1 + P_\tau \cos \hat{\theta} \right] \quad (2.1)$$

where B_π is the branching fraction of $\tau \rightarrow \pi \nu_\tau$, P_τ is the polarisation of the τ and $\hat{\theta}$ is the angle between the direction of motion of the outgoing pion and the tau spin quantisation axis, which is chosen so as to coincide with the τ momentum direction when we boost to the laboratory frame. In terms of the variable $z = E_\pi/E_\tau$ we have

$$\cos \hat{\theta} = \frac{2z - 1 - a^2}{\beta(1 - a^2)} \quad (2.2)$$

where $a = m_\pi/m_\tau$ and β is the velocity of the τ . Hence we obtain

$$\frac{1}{\Gamma_\tau} \frac{d\Gamma_\pi}{dz} = B_\pi \frac{1}{\beta(1 - a^2)} \left[1 + P_\tau \frac{2z - 1 - a^2}{\beta(1 - a^2)} \right] \quad (2.3)$$

which can also be applied to other spin zero decay modes such as $\tau^- \rightarrow \pi'^- \nu$ with $a = m_{\pi'}/m_\tau$. The collinear limit is found by taking the $\beta = 1$ limit. The polarisation $P_\tau = +1$ and -1 for a τ^- lepton with right- and left-handed helicity respectively. For the pion decay mode it is reasonable to make the further approximation that $a = 0$, and so we obtain the familiar result

$$\frac{1}{\Gamma_\tau} \frac{d\Gamma}{dz} (\tau^\pm \rightarrow \pi^\pm \nu_\tau) = B_\pi [1 \mp P_\tau (2z - 1)]. \quad (2.4)$$

For the purely leptonic decay process $\tau^- \rightarrow e^- \bar{\nu}_e \nu_\tau$ the polarisation of the outgoing electron (or muon) is essentially unmeasurable at high energies and so we sum over the two polarisation states. In the τ rest frame the energy-angle distribution of the outgoing lepton is

$$\frac{d\Gamma}{dE d\cos\hat{\theta}} (\tau^- \rightarrow \ell^- \bar{\nu}_\ell \nu_\tau) \sim pE \left[3E_{\max} - 2E - \frac{m_\ell^2}{E} + P_\tau \cos\hat{\theta} \frac{p}{E} \left(E_{\max} - 2E + \frac{m_\ell^2}{m_\tau} \right) \right] \quad (2.5)$$

where $E = (p^2 + m_\ell^2)^{\frac{1}{2}}$ is the energy of the decay lepton and E_{\max} is its maximum value

$$E_{\max} = \frac{m_\tau^2 + m_\ell^2}{2m_\tau}. \quad (2.6)$$

As before, $\hat{\theta}$ is the angle between the lepton momentum and the tau spin quantisation axis. The energy fraction E_ℓ/E_τ in the frame where the τ velocity is β is expressed as

$$z \equiv \frac{E_\ell}{E_\tau} = \frac{E + \beta p \cos\hat{\theta}}{m_\tau}. \quad (2.7)$$

This enables us to obtain the z distribution from (2.5). In the limits $\beta = 1$ and $m_\ell = 0$ we find

$$\frac{1}{\Gamma_\tau} \frac{d\Gamma}{dz} (\tau^- \rightarrow \ell^- \bar{\nu}_\ell \nu_\tau) = B_\ell \frac{1}{3} (1 - z) \left[(5 + 5z - 4z^2) + P_\tau (1 + z - 8z^2) \right], \quad (2.8)$$

where B_ℓ is the branching fraction of $\tau \rightarrow \ell \bar{\nu}_\ell \nu_\tau$, which yields a relatively weak dependence of the electron distribution on P_τ .

We now turn to the vector meson decay modes, $\tau^- \rightarrow v \nu_\tau$ where $v = \rho$ or a_1 . Since the subsequent $\rho \rightarrow 2\pi$ and $a_1 \rightarrow 3\pi$ decay distributions differ according to whether the vector mesons are transversely (T) or longitudinally (L) polarised we study the $\tau \rightarrow v(T)$ and $\tau \rightarrow v(L)$ decay distributions separately. In the τ rest frame, the amplitudes, $\mathcal{M}_{\lambda_\tau \lambda_v}(\hat{\theta})$, describing the $\tau_L^- \rightarrow v \nu_\tau$ decay are of the form

$$\mathcal{M}_{--} = \sqrt{2} \cos \frac{1}{2} \hat{\theta}, \quad \mathcal{M}_{-0} = \frac{m_\tau}{m_v} \sin \frac{1}{2} \hat{\theta}, \quad (2.9)$$

and for $\tau_R^- \rightarrow \nu\nu_\tau$ are

$$\mathcal{M}_{++} = -\sqrt{2} \sin \frac{1}{2}\hat{\theta}, \quad \mathcal{M}_{+0} = \frac{m_\tau}{m_\nu} \cos \frac{1}{2}\hat{\theta} \quad (2.10)$$

where λ_ν is the vector meson helicity and where the τ subscripts R,L refer respectively to helicity $\lambda_\tau = +\frac{1}{2}$ and $-\frac{1}{2}$ in the laboratory frame. We note that τ_L^- cannot decay into a $\lambda_\nu = +1$ state (and τ_R^- cannot decay into $\lambda_\nu = -1$) due to angular momentum conservation. It follows directly that the angular distributions of transversely (T) and longitudinally (L) polarised vector mesons are

$$\frac{1}{\Gamma_\tau} \frac{d\Gamma_\nu^T}{d\cos\hat{\theta}} = B_\nu \frac{m_\nu^2}{m_\tau^2 + 2m_\nu^2} (1 - P_\tau \cos\hat{\theta}) \quad (2.11)$$

$$\frac{1}{\Gamma_\tau} \frac{d\Gamma_\nu^L}{d\cos\hat{\theta}} = B_\nu \frac{\frac{1}{2}m_\tau^2}{m_\tau^2 + 2m_\nu^2} (1 + P_\tau \cos\hat{\theta}) \quad (2.12)$$

where $\nu = \rho$ or a_1 and B_ν is the branching fraction of the $\tau \rightarrow \nu\nu_\tau$ decay mode.

As expected, the form of the P_τ dependence shown in (2.12) for the $\lambda_\nu = 0$ longitudinal state is the same as that of (2.1) for the $\tau^- \rightarrow \pi^- \nu_\tau$ decay, whereas P_τ enters with the opposite sign for the $|\lambda_\nu| = 1$ vector meson decay modes. Thus, from (2.11) and (2.12), we see that the $\tau \rightarrow \nu\nu_\tau$ decay events should be equally good at determining the τ polarisation as the $\tau \rightarrow \pi\nu_\tau$ events, provided that we can distinguish longitudinally from transversely polarised vector mesons. If no attempt is made to measure the polarisation of the vector mesons then we must average (2.11) and (2.12) and the sensitivity to P_τ is suppressed by a factor $(m_\tau^2 - 2m_\nu^2)/(m_\tau^2 + 2m_\nu^2)$ which is about 0.46 for $\nu = \rho$, and almost vanishes for $\nu = a_1$.

Since we do not sum over the polarisation states of the vector meson the boost to the collinear frame is not as straightforward as it was for the single pion or purely leptonic decay mode. We must first perform a Wigner rotation [16] of the vector meson spin quantisation axis,

$$\mathcal{M}'_{\lambda_\tau \lambda'_\nu} = \sum_{\lambda_\nu} d_{\lambda'_\nu \lambda_\nu}^{\lambda_\tau}(\omega) \mathcal{M}_{\lambda_\tau \lambda_\nu}, \quad (2.13)$$

which relates the $\tau \rightarrow \nu\nu_\tau$ helicity amplitudes \mathcal{M}' in the collinear frame to the amplitudes \mathcal{M} of (2.9) and (2.10). The angle of rotation is given by

$$\cos \omega = \frac{1 - a^2 + (1 + a^2)\beta \cos\hat{\theta}}{\sqrt{(\cos^2\hat{\theta} + \gamma^{-2} \sin^2\hat{\theta})(1 - a^2)^2 + 2(1 - a^4)\beta \cos\hat{\theta} + \beta^2(1 + a^2)^2}} \quad (2.14)$$

which in the collinear limit ($\beta = 1$) becomes

$$\cos \omega = \frac{1 - a^2 + (1 + a^2) \cos\hat{\theta}}{1 + a^2 + (1 - a^2) \cos\hat{\theta}} \quad (2.15)$$

where $a = m_v/m_\tau$ and $\gamma = (1 - \beta^2)^{-1/2} = E_\tau/m_\tau$ is the boost factor. Using the rotated amplitudes \mathcal{M}' we find the collinear decay distributions

$$H_v^T(z, m_v^2) = \frac{a^2}{(1-a^2)(1+2a^2)} \left[\frac{\sin^2 \omega}{a^2} + 1 + \cos^2 \omega + P_\tau \cos \hat{\theta} \left(\frac{\sin^2 \omega}{a^2} - \frac{\sin 2\omega}{a} \tan \hat{\theta} - 1 - \cos^2 \omega \right) \right] \quad (2.16)$$

$$H_v^L(z, m_v^2) = \frac{a^2}{(1-a^2)(1+2a^2)} \left[\frac{\cos^2 \omega}{a^2} + \sin^2 \omega + P_\tau \cos \hat{\theta} \left(\frac{\cos^2 \omega}{a^2} + \frac{\sin 2\omega}{a} \tan \hat{\theta} - \sin^2 \omega \right) \right] \quad (2.17)$$

where $z = E_v/E_\tau$ and where $\cos \hat{\theta}$ is given by (2.2) with $a = m_v/m_\tau$. These distributions are shown in Fig. 2.1 normalised such that in the zero-width limit of the ρ and a_1 mesons, the z distributions of v_T and v_L are given by

$$\frac{1}{\Gamma_\tau} \frac{d\Gamma}{dz}(\tau \rightarrow \nu_\tau v_\alpha) = B_v H_v^\alpha(z, m_v^2) \quad (2.18)$$

where B_v is the branching fraction $B(\tau \rightarrow \nu v_\tau)$ and where $\alpha = T$ (transverse) or L (longitudinal). It can be clearly seen that the leading vector bosons arising from τ_L^- (τ_R^-) decays are predominantly transversely (longitudinally) polarised.

To obtain realistic distributions we must include the widths of the vector meson states. To do this we average the above distributions over the vector resonance shapes $F_v(m^2)$ for the unpolarised $\tau \rightarrow \nu v_\tau$ decays, where

$$F_v(m^2) = \left(1 - \frac{m^2}{m_\tau^2}\right)^2 \left(1 + \frac{2m^2}{m_\tau^2}\right) |D_v(m^2)|^2 f_v(m^2) \quad (2.19)$$

Here m is the invariant mass of the off-shell v (2π for $v = \rho$, 3π for $v = a_1$), and

$$D_v(m^2) = \frac{1}{m^2 - m_v^2 + im\Gamma_v(m^2)} \quad (2.20)$$

is the vector boson propagator with the running width

$$\Gamma_v(m^2) = \Gamma_v \frac{m f_v(m^2)}{m_v f_v(m_v^2)}. \quad (2.21)$$

In this way we obtain the collinear decay distributions for the 2π (' ρ ') and 3π (' a_1 ') states

$$\frac{1}{\Gamma_\tau} \frac{d\Gamma(\tau \rightarrow \nu_\tau + 'v_\alpha')}{dz} = B_v \frac{1}{N_v} \int_{(nm_\pi)^2}^{2m_\tau^2} F_v(m^2) H_v^\alpha(z, m^2) dm^2 \quad (2.22)$$

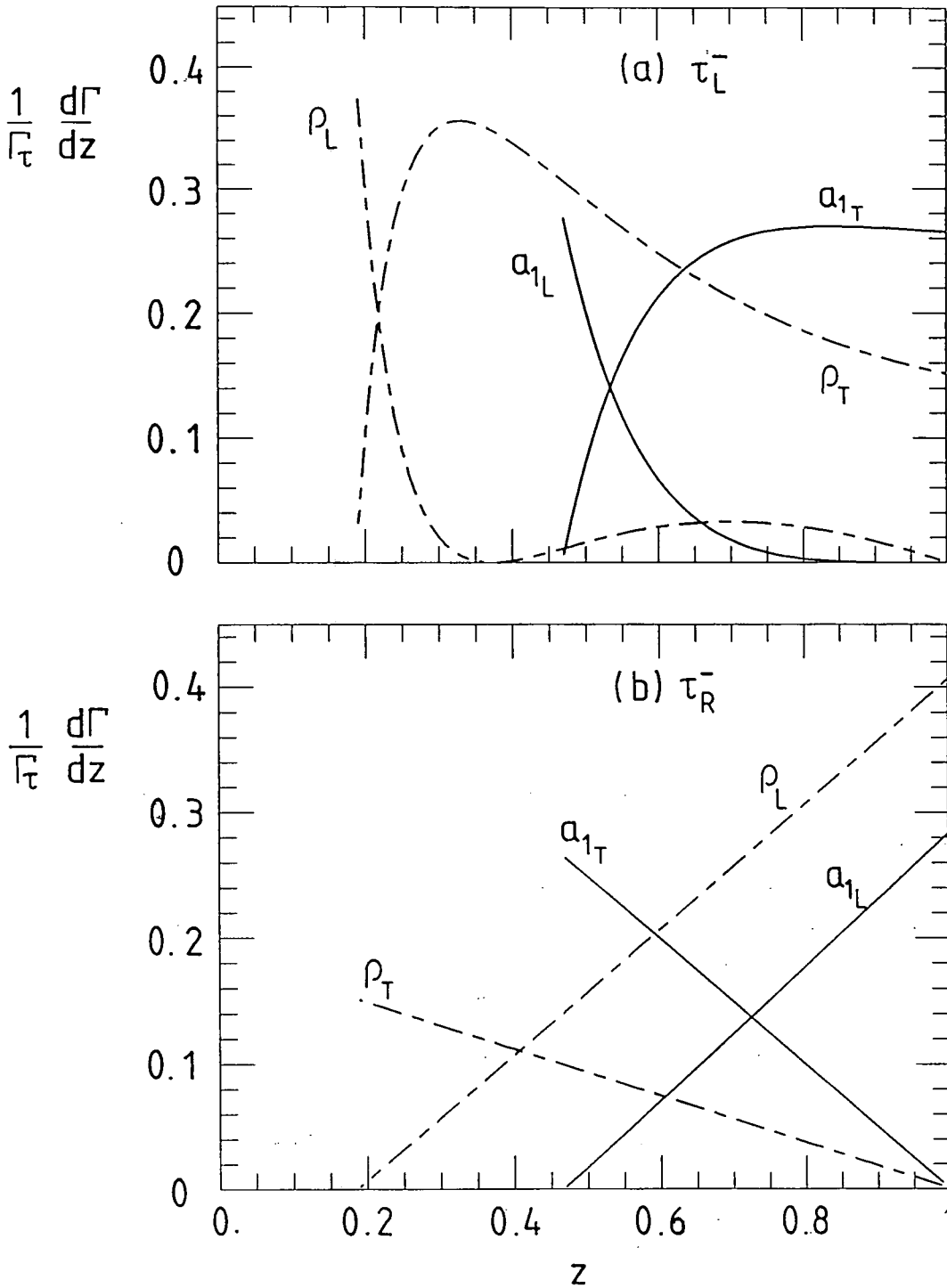


Figure 2.1: The fractional energy distributions of polarised ρ and a_1 vector mesons arising from (a) τ_L^- or τ_R^+ decays, (b) τ_R^- or τ_L^+ decays. The energy fraction $z \equiv E_\nu/E_\tau$, where E_ν is the vector meson laboratory energy in the collinear limit ($E_\tau \gg m_\tau$). The masses of the ρ , a_1 mesons are taken to be 0.77 GeV, 1.22 GeV respectively and the widths are set to zero. In each plot the sum of the v_T and v_L distributions are normalised to the $\tau \rightarrow \nu\nu$ branching fractions. The L and T subscripts refer to longitudinally and transversely polarized vector mesons respectively.

where $\alpha = T$ or L , and the normalisation factor

$$N_v = \int_{(m_\pi)^2}^{m_\tau^2} F_v(m^2) dm^2. \quad (2.23)$$

The ρ meson line shape factor in (2.21) is

$$f_\rho(m^2) = \left(1 - \frac{4m_\pi^2}{m^2}\right)^{3/2}, \quad (2.24)$$

which takes account of the P-wave threshold behaviour of the $\rho \rightarrow \pi\pi$ decay. For the a_1 meson we use the parameterisation of Kühn and Santamaria [17]

$$f_{a_1}(m^2) = \begin{cases} \frac{4.1}{m^2}(m^2 - 9m_\pi^2)^3[1 - 3.3(m^2 - 9m_\pi^2) + 5.8(m^2 - 9m_\pi^2)^2] & \text{if } m^2 < (m_\rho + m_\pi)^2, \\ 1.623 + \frac{10.38}{m^2} - \frac{9.32}{m^4} + \frac{0.65}{m^6} & \text{if } m^2 > (m_\rho + m_\pi)^2, \end{cases} \quad (2.25)$$

where the masses are in GeV units.

The collinear distributions, (2.22), which include the effects of the vector meson widths, are shown in Fig. 2.2. It is interesting to contrast these distributions with the zero-width approximation of Fig. 2.1. For completeness, we also include the $\tau \rightarrow \pi\nu$, $l\nu\bar{\nu}$ decay distributions in Fig. 2.2. Fig. 2.3 shows the decay distributions for τ to unpolarised ρ and a_1 mesons. The insensitivity of $\tau \rightarrow a_1\nu$ to the polarisation of the τ is apparent; it is crucial to measure the polarisation of the a_1 to obtain information on P_τ from this decay mode.

We see that the energy distributions from the τ_L^- events are significantly different from those of the τ_R^- events. In particular, the most energetic particles from τ_L^- decays are transversely polarized ρ and a_1 mesons, whereas the energetic particles arising from τ_R^- decays are π^- and longitudinally polarized ρ and a_1 mesons. Therefore the polarisation measurement can be considerably enhanced if we can use the subsequent $\rho \rightarrow 2\pi$ and $a_1 \rightarrow 3\pi$ decay distributions to distinguish between transversely and longitudinally polarized ρ and a_1 mesons.

2.3 The $\tau \rightarrow \rho \rightarrow 2\pi$ and $\tau \rightarrow a_1 \rightarrow 3\pi$ polarimeters.

In this section we discuss how the pion spectra arising from the two-stage decays

$$\tau \rightarrow \rho\nu \rightarrow (2\pi)\nu$$

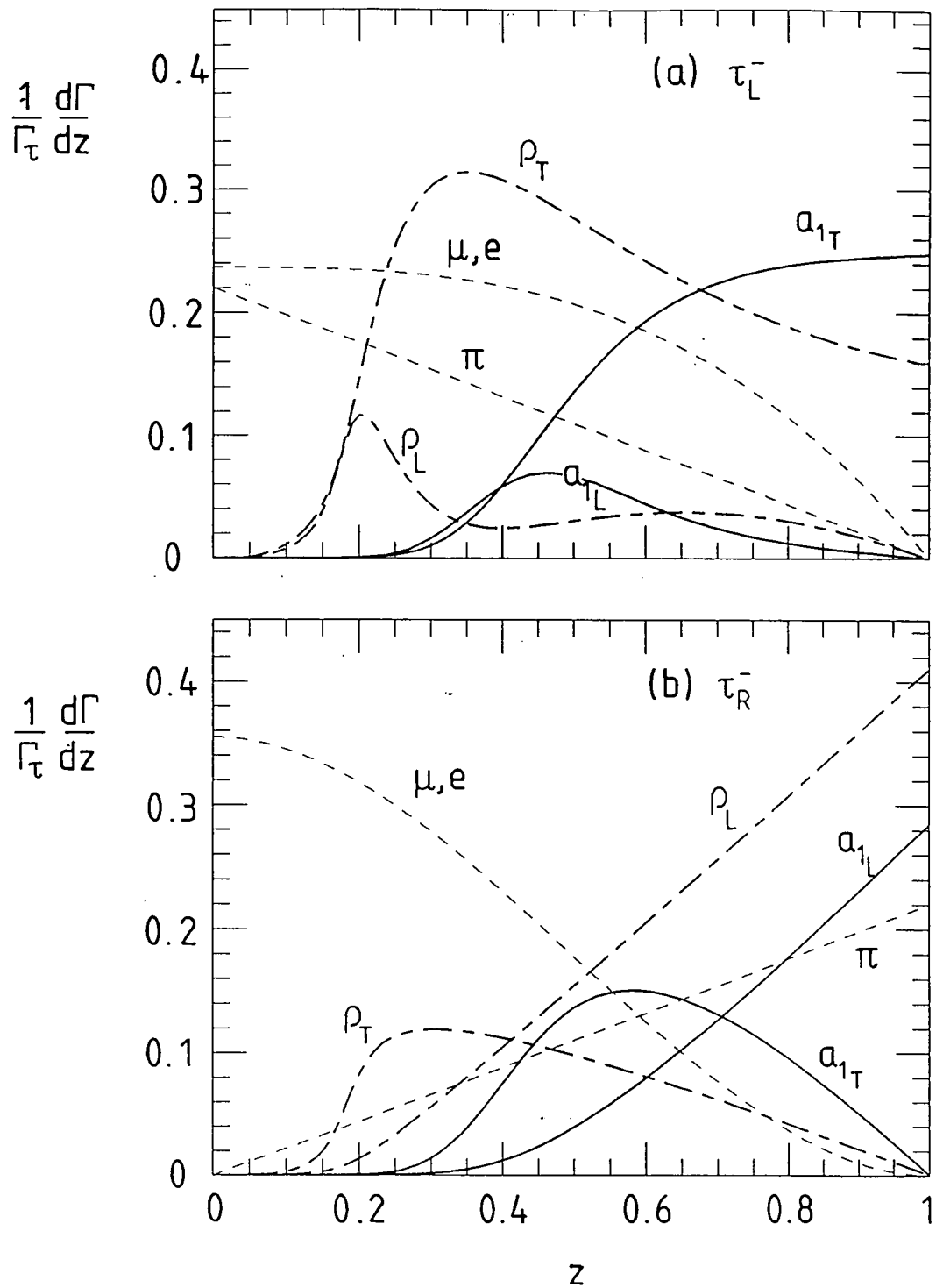


Figure 2.2: As Fig. 2.1, but with the ρ and a_1 widths taken to be 0.15 GeV and 0.42 GeV respectively. We also show the fractional energy distributions for τ decays to muons (or electrons) and pions normalised to the respective branching fractions. We have assumed that the electron and muon are massless, and so the electron distribution is identical to that of the muon.

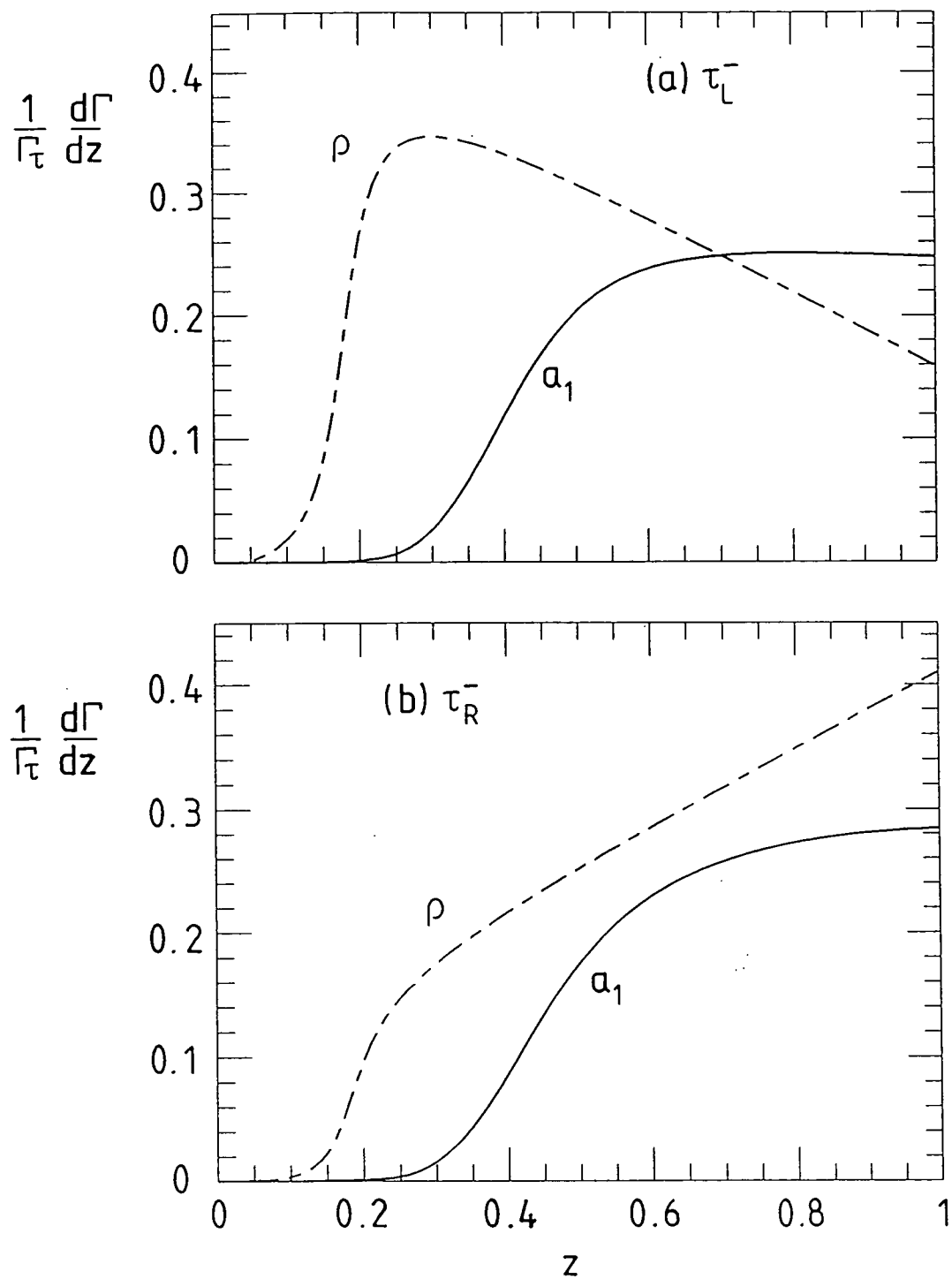


Figure 2.3: The $\tau_{L,R} \rightarrow \nu\nu$ distributions assuming no information on the vector meson polarisation. That is the sum $v_T + v_L$ of the distributions of Fig. 2.2 for $v = \rho$ and a_1 .

$$\tau \rightarrow a_1 \nu \rightarrow (3\pi)\nu$$

can be used to determine the polarisation of the vector mesons, which in turn act as polarisation analyzers of the parent τ .

2.3.1 The ρ decay mode

The mode of decay $\tau \rightarrow \rho \nu_\tau$ accounts for approximately 22% of all τ decays. The ρ decays via $\rho^\pm \rightarrow \pi^\pm \pi^0$. Treatment of $\rho \rightarrow 2\pi$ is straightforward. By the conserved vector current (CVC) hypothesis, the ρ mode of decay can be completely described by the four-vector current

$$J^\nu(\rho \rightarrow \pi^\pm \pi^0) = f_\rho(m_\rho^2)(p_{\pi^\pm} - p_{\pi^0})^\nu. \quad (2.26)$$

The most general current [18] should include an additional term proportional to $(p_{\pi^\pm} + p_{\pi^0})^\nu$ when the ρ meson is off-shell, but it gives a negligible effect. Previous studies [5] of the ρ mode concluded that there would be a dramatic improvement in the measurement of P_τ if measurements were made, not just of the ρ energy, but also that of the produced pions.

The matrix elements

$$\mathcal{M} = \epsilon_\nu^{T,L}(\rho) J^\nu(\rho \rightarrow \pi^\pm \pi^0), \quad (2.27)$$

where ϵ_ν^T and ϵ_ν^L are the polarisation vectors of ρ_T and ρ_L respectively, then lead to the decay angular distributions

$$\frac{d\Gamma(\rho_T \rightarrow 2\pi)}{d \cos \hat{\theta}} \sim \frac{1}{2} \sin^2 \hat{\theta}, \quad (2.28)$$

$$\frac{d\Gamma(\rho_L \rightarrow 2\pi)}{d \cos \hat{\theta}} \sim \cos^2 \hat{\theta}, \quad (2.29)$$

in the ρ rest frame about the ρ polarisation axis. In the laboratory frame, we obtain [5]

$$\frac{d\Gamma(\rho_T \rightarrow 2\pi)}{dx} \sim 2x(1-x) - \frac{2m_\pi^2}{m_\rho^2}, \quad (2.30)$$

$$\frac{d\Gamma(\rho_L \rightarrow 2\pi)}{dx} \sim (2x-1)^2, \quad (2.31)$$

where x is the energy fraction E_π/E_ρ , in the collinear limit.

2.3.2 The a_1 decay mode

Approximately 14% of all τ decays are believed to go through an intermediate a_1 resonant state, which itself subsequently decays dominantly via an intermediate ρ which then decays to 2π ;

$$a_1 \rightarrow \pi \rho \rightarrow 3\pi.$$

The decay of the charged a_1 meson must always produce one distinguishable and two identical pions, since either $a_1^\pm \rightarrow \pi^\pm \rho^0 \rightarrow \pi^\mp 2\pi^\pm$ or $a_1^\pm \rightarrow \pi^0 \rho^\pm \rightarrow \pi^\pm 2\pi^0$. The branching fractions for these two final states are equal. We denote the two identical pions as π_1, π_2 and the distinguishable pion as π_3 .

If the widths of the a_1 (and ρ) mesons could be neglected in the decay chain

$$\tau \rightarrow a_1 \nu \rightarrow \rho \pi \nu \rightarrow 3\pi \nu,$$

then the parameterisation of the decay would be relatively straightforward. Problems arise, however, from the ambiguities of taking the vector mesons off their mass-shells. The most exhaustive discussion of this decay process is given by Isgur *et al.* [18]. From the results given in the appendices to their paper we find that the current describing the $a_1 \rightarrow 3\pi$ decay has the approximate form

$$J^\nu \sim D_{a_1}(s) D_\rho(s_{13}) f_{\rho\pi\pi}(s_{13}) \left[f_{a\rho\pi}(s, s_{13}) (p_3^\nu - p_1^\nu) - g_{a\rho\pi}(s, s_{13}) \frac{s_{21} - s_{23}}{2} (p_3^\nu + p_1^\nu) \right] + 1 \leftrightarrow 2, \quad (2.32)$$

where $s_{13} = (p_1 + p_3)^2$, $s_{23} = (p_2 + p_3)^2$, $s = (p_1 + p_2 + p_3)^2 \equiv Q^2$ and the vertex form factors $f_{\rho\pi\pi}$, $f_{a\rho\pi}$, $g_{a\rho\pi}$ are listed in Appendix B of [18]. D_ν is the vector meson propagator

$$D_\nu(s) = \frac{1}{s - m_\nu^2 + i\sqrt{s}\Gamma_\nu(s)}. \quad (2.33)$$

A simpler parameterisation of $a_1 \rightarrow 3\pi$ decay current can be found in Kühn and Santamaria [17]. Making use of the chiral limit (conserved axial vector current) approximation, they find

$$J^\nu \sim D_{a_1}(s) [D_\rho(s_{13})(\tilde{p}_3 - \tilde{p}_1)^\nu + D_\rho(s_{23})(\tilde{p}_3 - \tilde{p}_2)^\nu], \quad (2.34)$$

where $\tilde{p}_i = p_i - Q_i(p_i \cdot Q)/Q^2$. Kühn and Santamaria parameterise the energy dependence of the widths $\Gamma_\nu(s)$ occurring in the Breit-Wigner forms, D_ν , as described in Section 2.2 (see (2.21) onwards), while Isgur *et al.* use more involved expressions, see [18].

We compare the predictions of these two models in Fig. 2.4. These scatter plots show the $s_{13} - s_{23}$ invariant mass squared distributions of pion pairs which result from on-shell a_1 decays; “13” and “23” are the two possible ρ meson channels. The two orthogonal ρ bands are clearly visible in each of these plots. The agreement between Fig. 2.4(a) and 2.4(b) is good. There are slight differences, which originate from the additional $g_{a\rho\pi}$ terms in the Isgur *et al.* model, (2.32), which give small contributions near the edges of the plot of Fig. 2.4(b).

We are now ready to discuss the experimental determination of the polarisation of the a_1 (and hence of the τ). The polarisation of the a_1 is measured by observing the $a_1 \rightarrow 3\pi$ decay

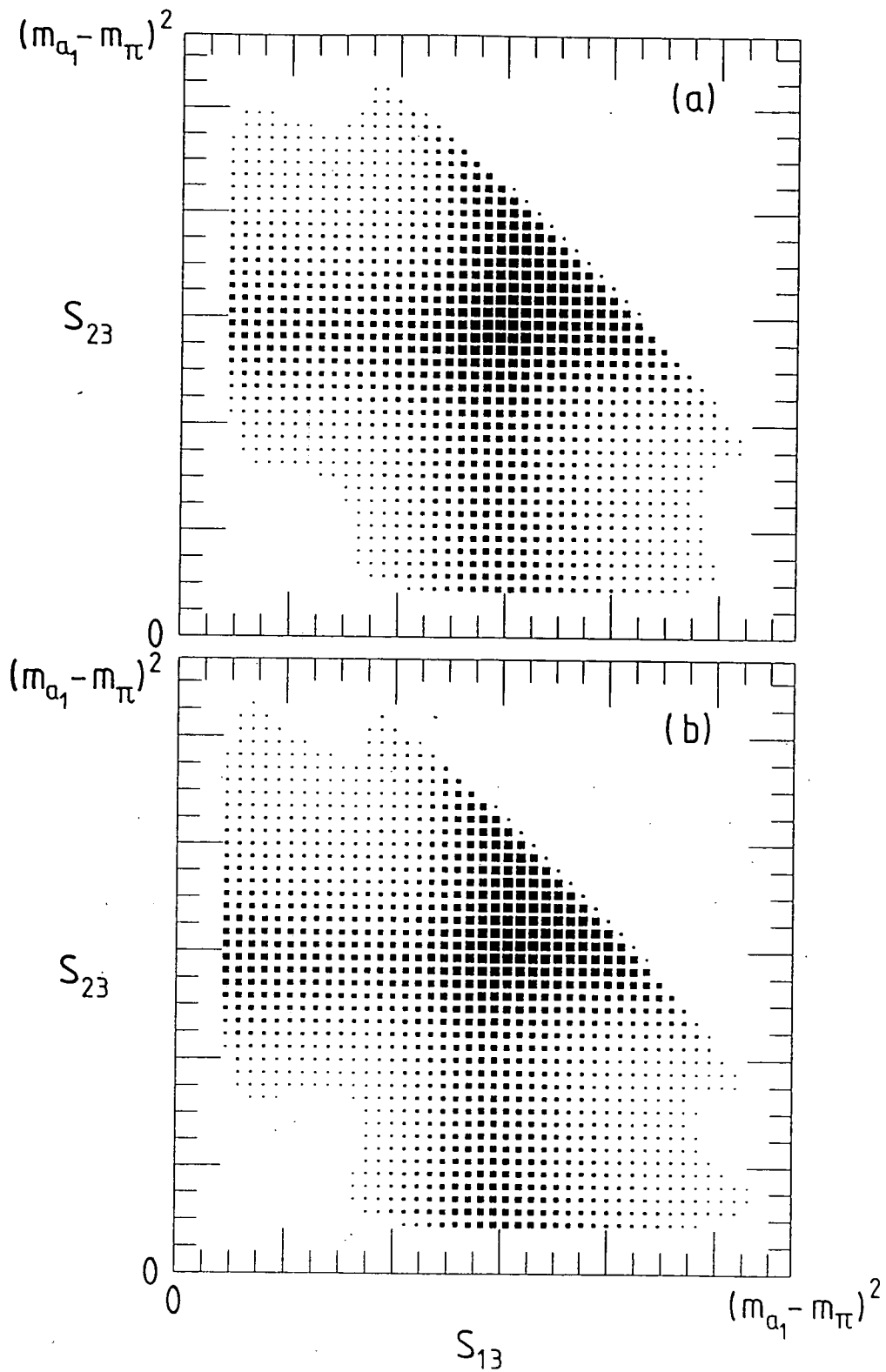


Figure 2.4: The Dalitz plots for $a_1 \rightarrow 3\pi$ using the (a) Kuhn and Santamaria [17] and (b) Isgur *et al.* [18] models for the decay. The variables are $s_{13} = (p_1 + p_3)^2$ and $s_{23} = (p_2 + p_3)^2$ where p_i is the four-momentum of pion i . These are the two channels that contain the ρ meson.

angular distribution. A natural polarisation observable is the angle ψ between the direction of the normal to the plane defined by the 3-momenta of the three pions in the 3π rest frame and the laboratory direction of the 3π system [19]. Rougé [6] has given an expression for $\cos\psi$ in terms of the laboratory 3-momenta \mathbf{p}_i of the three pions;

$$\cos\psi = \frac{8s\mathbf{p}_1 \cdot (\mathbf{p}_2 \times \mathbf{p}_3)/|\mathbf{p}_1 + \mathbf{p}_2 + \mathbf{p}_3|}{\sqrt{-\lambda(\lambda(s, s_{12}, m_\pi^2), \lambda(s, s_{13}, m_\pi^2), \lambda(s, s_{23}, m_\pi^2))}} \quad (2.35)$$

where s and s_{ij} are the invariant mass squared of the 3π and 2π systems, and $\lambda(a, b, c) = a^2 + b^2 + c^2 - 2ab - 2bc - 2ac$. A polarised spin one boson decaying to three pions has $\cos\psi$ angular distributions in the laboratory frame of the form [19]

$$\frac{1}{\Gamma_{a_1 T}} \frac{d\Gamma_{a_1 T}}{d\cos\psi} = \frac{3}{8}(\cos^2\psi + 1), \quad (2.36)$$

$$\frac{1}{\Gamma_{a_1 L}} \frac{d\Gamma_{a_1 L}}{d\cos\psi} = \frac{3}{4}\sin^2\psi. \quad (2.37)$$

The $\cos\psi$ distribution is therefore an excellent a_1 polarimeter if we are able to measure the three-momenta of each of the three outgoing pions accurately. However, measurement of such an angular distribution is difficult when the a_1 meson energy (zE_τ) greatly exceeds its mass. In such configurations, all three pion momenta are essentially collinear and only the collinear energy fractions $x_i = E_i/(E_1 + E_2 + E_3)$ may be measured accurately. We should therefore look for an a_1 polarimeter in the collinear limit.

First we consider the decays of polarised on-shell a_1 mesons. Our method is to perform numerical simulations of polarised a_1 decay to 3 pions. The $a_1^{T,L} \rightarrow 3\pi$ amplitudes

$$\mathcal{M} = \epsilon_\nu^{T,L}(a_1) J^\nu(a_1 \rightarrow 3\pi) \quad (2.38)$$

are squared and integrated over phase space with the usual symmetry and flux factors using Monte Carlo techniques. Unlike the $\cos\psi$ distributions, these collinear decay distributions depend on specific dynamical assumptions about the $a_1 \rightarrow 3\pi$ decay. We examined the above two models, (2.32) and (2.34), for the $a_1 \rightarrow 3\pi$ current J^ν . The results for the scatter plot

$$\frac{1}{\Gamma_{a_1 T,L}} \frac{d\Gamma(a_1 T,L \rightarrow \pi_1 \pi_2 \pi_3)}{dxdy} \quad (2.39)$$

for the collinear energy fractions x_i of the pions are shown in Fig. 2.5. The x variable is x_3 and $y = \min(x_1, x_2)$, the minimum of the two fractions of a_1 energy carried by the two identical pions. The results shown in Fig. 2.5 are for the Kühn and Santamaria parameterisation (2.34). However the model of Isgur *et al.*, [18], gives essentially identical distributions.

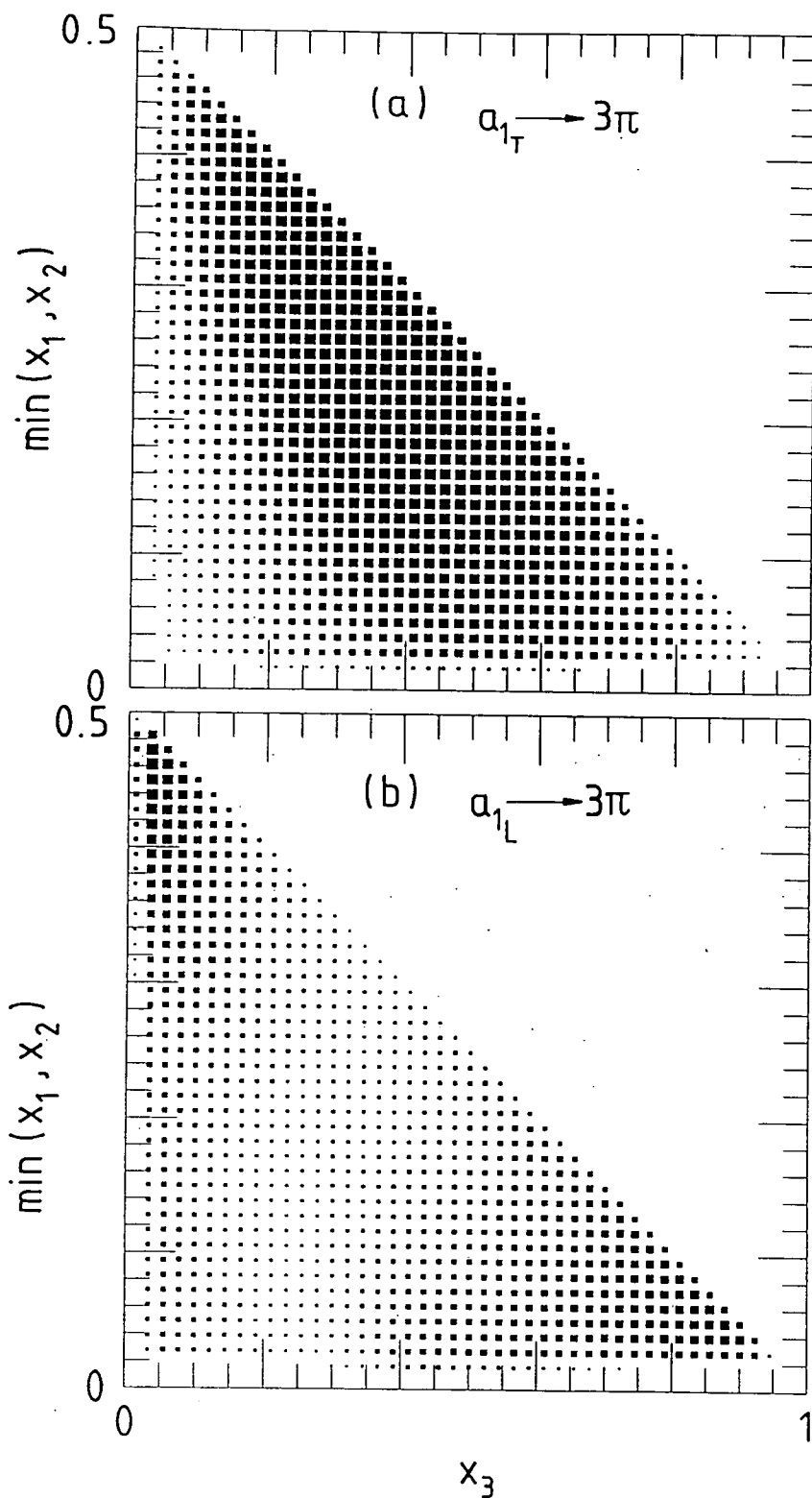


Figure 2.5: The scatter plots for (a) transversely and (b) longitudinally polarized $a_1 \rightarrow 3\pi$ decays, where x_i are the energy fractions carried by three pions (with pions 1 and 2 having identical charges) in the laboratory frame. The x -variable is x_3 , the energy fraction of the distinguishable pion π_3 (see section 2.3) and the y variable is $\min(x_1, x_2)$ the minimum of the two energy fractions of the two identical pions. It is assumed that $m_{3\pi} = m_{a_1} = 1.22$ GeV.

The difference between the scatter plots for the a_{1L} and a_{1T} decays is striking. For a_{1T} decays, Fig. 2.5(a), all three pions have a tendency to share equally the energy. On the contrary for a_{1L} decays, Fig. 2.5(b), the favoured configurations are those in which one or two of the three pions are soft; the upper densely populated corner of the plot corresponds to π_3 being soft and π_1, π_2 sharing all the energy, whereas the right-hand populated corner corresponds to both π_1, π_2 being soft and π_3 energetic.

Our numerical results are consistent with the $\cos\psi$ result proposed by Rougé. For a transverse a_1 , the distribution (2.36) has a maximum when the decay plane is perpendicular to the a_1 polarisation axis and so the pion momenta will tend to be transverse to this axis. Thus, after a boost into the laboratory frame, an equal distribution of energy of the three pions will be most favoured. On the other hand for a longitudinal a_1 , the distribution (2.37) has a maximum when the polarisation axis is coincident with the decay plane. This suggests that a longitudinal a_1 will prefer to decay to pions whose direction in the a_1 rest frame has a large component along the polarisation axis. On boosting along this axis, larger differences between the pion energies are therefore to be expected. However, the energy distributions of Fig. 2.5(a) and (b) cannot be determined simply by (2.36) and (2.37) respectively, since the $\cos\psi$ distribution says nothing about the distribution of the three pions of $a_1 \rightarrow 3\pi$ in the decay plane.

It is remarkable, and fortunate, that the energetic $n\pi$ systems from τ_L and τ_R decays are predicted to be so very different. For the τ_L decays the leading particle is either ρ_T or a_{1T} (see Fig. 2.5(a)), both of which prefer their energy to be equally shared between the outgoing pions; whereas the leading particle resulting from τ_R decays is either π , ρ_L or a_{1L} , where the subsequent ρ_L decay gives rise to one energetic pion and the a_{1L} decay contains either a single energetic pion or two energetic identical pions. We notice in passing that these characteristic differences in the multiparticle distributions of polarized τ decays will affect the efficiency of detectors to isolate the τ decay signal from the low multiplicity hadronic background in hadronic collisions.

We cannot, of course, distinguish ρ_T from ρ_L (or a_{1T} from a_{1L}) on an event-by-event basis. Rather, in a quantitative study we can measure the probability P_L of a 2π (or 3π) event arising from the decay of a longitudinally polarized meson as a function of the kinematic variables of the decay. For example, the ‘‘polarimeter’’, P_L , of a $\pi^-\pi^0$ system of momentum fraction z ($= E_{2\pi}/E_\tau$) may be readily determined by comparing the observed x ($= E_{\pi^-}/E_\tau$) distribution with the form

$$[1 - P_L(z)] \frac{d\Gamma(\rho_T)}{dx} + P_L(z) \frac{d\Gamma(\rho_L)}{dx}. \quad (2.40)$$

Similarly the polarization of a 3π system may be extracted by comparing the observed scatter plot distribution with

$$[1 - P_L(z)] \frac{d\Gamma(a_{1T})}{dx dy} + P_L(z) \frac{d\Gamma(a_{1L})}{dx dy}. \quad (2.41)$$

In fact, it is a good approximation to simply take $d\Gamma/dx$ in (2.40) to be (2.30), (2.31) evaluated at $m_{2\pi} = m_\rho$, and $d\Gamma/dx dy$ in (2.41) to be those of Fig. 2.5 (which were obtained using $m_{3\pi} = m_{a_1} = 1.22$ GeV), for all values of z , except those at low z ($z < m_\rho^2/m_\tau^2$) where the $n\pi$ system is forced off the vector-meson mass shell.

2.4 Detecting the charged Higgs

As noted in the introduction, the charged Higgs boson may be produced at hadron colliders at a significant rate if its mass is lower than the mass of the top quark. Its decay branching ratio to $\tau^\pm \bar{\nu}_\tau^{(-)}$ is then expected to be appreciable, providing an opportunity for its detection [8, 11, 13, 9]. In this case, the major background comes from the decays of W^\pm produced in the decay $t \rightarrow bW$, or directly with associated jet activities.

In e^+e^- collisions, H^\pm would be produced in pairs, which may possibly be identified from their $\tau^\pm \bar{\nu}_\tau^{(-)}$ decays. The major background is again from $W^\pm \rightarrow \tau^\pm \bar{\nu}_\tau^{(-)}$, which is produced copiously in $e^+e^- \rightarrow W^+W^-$, or via cascade decays from $e^+e^- \rightarrow t\bar{t}$.

The successful detection of $W^\pm \rightarrow \tau^\pm \bar{\nu}_\tau^{(-)}$ decays [20] at $p\bar{p}$ colliders [22] encourages us to seriously pursue this search strategy. All the τ 's that have been observed at $p\bar{p}$ colliders are left-handed due to the left-handedness of the charged current, whereas the τ 's from H^- decays should be right-handed as long as the decay is associated with the standard right-handed antineutrino [7]. This is a consequence of the helicity-flip (-conserving) nature of the standard model Higgs (vector boson) couplings and holds quite generally.

We should therefore expect that τ signals resulting from H^\pm decays will be different to those arising from the standard W decay, as will those from the decay of a new heavy charged weak boson W_R that couples to a right handed current [14]. There is a striking contrast between the τ_L^- signal (from W^- or W_L^-) and the τ_R^- signal (from H^- or W_R^-) when the topology of the final state 2π and 3π systems is considered [7]. Previous studies [14, 15] did not find these striking differences because they studied only the simplest decay mode into a single π .

At hadron colliders, a clean τ signal is obtained only when the τ decay products carry away a large fraction z of the parent τ 's energy, that is for z in the interval $z_{\min} < z < 1$ where typically $z_{\min} > 0.5$. The signature is therefore a large missing transverse momentum

with an energetic, very narrow jet of small (1 to 3) charged multiplicity. Figs. 2.2(a) and (b) show that the leading particles of the collinear τ decay distributions are

$$\begin{aligned}\tau_L &\rightarrow a_{1T}, \rho_T && \text{from } W^-, W_L'^-, \\ \tau_R &\rightarrow a_{1L}, \rho_L, \pi && \text{from } H^-, W_R^-.\end{aligned}\quad (2.42)$$

Furthermore, the $\rho \rightarrow 2\pi$ decay distributions (2.30) and (2.31) and the $a_1 \rightarrow 3\pi$ decay distributions of Fig. 2.5 show that the leading particles from τ_L^- decay are

$$\tau_L^- \rightarrow \begin{cases} \text{symmetric } (\pi^- \pi^0), \\ \text{symmetric } (\pi^- \pi^0 \pi^0), \\ \text{symmetric } (\pi^+ \pi^- \pi^-). \end{cases}\quad (2.43)$$

where the decay pions share equally the energy of the tau. In contrast the leading particles from τ_R^- are

$$\tau_R^- \rightarrow \begin{cases} \pi^-, \\ \pi^- \text{ hard, and } \pi^0 \text{ or } \pi^0 \pi^0 \text{ soft,} \\ \pi^0 \text{ or } \pi^0 \pi^0 \text{ hard, and } \pi^- \text{ soft,} \\ \pi^+ \text{ hard and } \pi^- \pi^- \text{ soft,} \\ \pi^- \pi^- \text{ hard and } \pi^+ \text{ soft,} \end{cases}\quad (2.44)$$

where there is a strong tendency for either a single π or two identical π 's ($\pi^0 \pi^0$ or $\pi^- \pi^-$) to dominate the jet energy. These qualitative differences between the W (or W_L') signals from τ_L^- and the H^\pm (or W_R^\pm) signals from τ_R^- should be taken into account in the search for new physics.

In order to show the quantitative differences in the leading particle spectra of τ_L^- and τ_R^- decays, we list in Table 2.1 the fraction,

$$\frac{f_A(\tau_\alpha, z_{\min})}{\sum_A f_A(\tau_\alpha, z_{\min})},\quad (2.45)$$

of τ decays with leading particle with $z > z_{\min}$ which go through each particular decay mode $\tau_\alpha \rightarrow A$. Here we assume that the $A = \ell, \pi, \rho, a_1$ modes account for all the τ decays.

The fraction $f_A(\tau_\alpha, z_{\min})$ in (2.45) is given by

$$f_A(\tau_\alpha, z_{\min}) = \int_{z_{\min}}^1 dz \frac{1}{\Gamma_\tau} \frac{d\Gamma(\tau_\alpha \rightarrow A)}{dz},\quad (2.46)$$

where $\alpha = L$ or R . Clearly for very large z , the dominance of the leading particles as given in (2.42) is overwhelming. Choosing $z_{\min} = 0.9$, the sum of the leading modes of (2.42) account for about 88% of τ_L^- and 96% of τ_R^- decays.

The last column in Table 2.1 gives the total fraction,

$$f(\tau_\alpha, z_{\min}) = \sum_A f_A(\tau_\alpha, z_{\min}),\quad (2.47)$$

z_{\min}	parent	ℓ	π	a_{1L}	a_{1T}	ρ_L	ρ_T	$f(\tau_\alpha, z_{\min})$
0.9	τ_L^-	0.13	0.02	0.01	0.49	0.02	0.33	0.05
	τ_R^-	0.01	0.23	0.29	0.03	0.43	0.01	0.09
0.8	τ_L^-	0.21	0.04	0.01	0.42	0.03	0.29	0.12
	τ_R^-	0.03	0.22	0.26	0.06	0.41	0.02	0.18
0.7	τ_L^-	0.26	0.05	0.02	0.36	0.03	0.28	0.20
	τ_R^-	0.06	0.21	0.23	0.08	0.38	0.04	0.26

Table 2.1: Fraction of the leading ‘particles’ in the decays of τ_L^- and τ_R^- for different values of minimum detectable particle energy fraction z_{\min} as defined by (2.45). The final column is the total fraction of τ decay events in which the observed particles (ℓ, π, ρ, a_1) have energy fraction $z > z_{\min}$ as defined by (2.47).

of τ_α decays to particles ($A = \ell, \pi, \rho, a_1$) with energy fraction $z > z_{\min}$. Thus the fraction $f_A(\tau_\alpha, z_{\min})$ of any particular $\tau_\alpha \rightarrow A$ decays with $z > z_{\min}$ is found simply by multiplying the appropriate $\tau_\alpha \rightarrow A$ entry in Table 2.1 by the number in the end column.

We note in passing that these quantitative predictions can be used to measure the mean polarisation P_τ of τ in the decay of a new neutral vector boson Z' . This will give us essential information on the $Z'\ell\ell$ couplings [14, 15]. By fitting the observed $\pi, 2\pi$ and 3π distributions in the large z region to formulae like (2.40) and (2.41), the tau polarisation can be efficiently determined. Attempts to measure P_τ in standard model Z or W decays at the Tevatron could provide valuable experience for the use of the τ polarimeter as a means of identifying new physics in future experiments. For these analyses it is important to note that, in principle, we can measure the energy fraction z even in hadron collider experiments [15].

2.5 Detecting the neutral Higgs using decay correlations

In this section, we examine the use of the tau spin correlations in the decays

$$H \rightarrow \tau^- \tau^+ \text{ and } Z, Z', \gamma^* \rightarrow \tau^- \tau^+ \quad (2.48)$$

as a signal to distinguish the neutral Higgs boson from a new neutral vector boson Z' or other vector bosons (including the standard Z and virtual γ). In particular we study the polarisation correlation in various tau decay modes

$$X \rightarrow \tau_\alpha^- \tau_\beta^+ \rightarrow A^- B^+ + \nu\text{'s}$$

where X denotes either $V(Z, Z', \gamma^*)$ or H and where α, β are either L or R . We use A and B to each denote one of e, μ, π, ρ, a_1 arising from $\tau \rightarrow \ell \bar{\nu}_\ell \nu_\tau, \pi \nu_\tau, 2\pi \nu_\tau, 3\pi \nu_\tau$, where

the 2π and 3π states are well approximated by the ρ and a_1 mesons respectively [17, 18]. It is appropriate to work in the collinear limit since $m_\tau/m_X \ll 1$, and so the appropriate kinematic variables are the energy fractions

$$z = 2E_A/m_X, \quad \bar{z} = 2E_B/m_X, \quad (2.49)$$

in the X rest frame. We note in passing that the X rest frame can usually be reconstructed in e^+e^- production processes ($e^+e^- \rightarrow ZH, e^+e^- \rightarrow Z'$), and also in hadron collisions if m_X is known *a priori*, as should be the case for $Z' \rightarrow \tau^-\tau^+$ [15].

The τ pair joint decay distribution is of the form

$$\frac{d\Gamma(X \rightarrow A^-B^+ + \nu\text{'s})}{dzd\bar{z}} = \sum_{\alpha,\beta} C_{\alpha\beta}^X \frac{d\Gamma(\tau_\alpha^- \rightarrow A^-)}{dz} \frac{d\Gamma(\tau_\beta^+ \rightarrow B^+)}{d\bar{z}} \quad (2.50)$$

where the only non-zero correlation coefficients $C_{\alpha\beta}$ for the parity conserving $H \rightarrow \tau^+\tau^-$ decay are

$$C_{LL}^H = C_{RR}^H = \frac{1}{2}, \quad (2.51)$$

and for vector boson $V \rightarrow \tau^+\tau^-$ decay are

$$C_{LR}^V = \frac{1}{2}(1 - P_\tau), \quad C_{RL}^V = \frac{1}{2}(1 + P_\tau). \quad (2.52)$$

Here non-zero tau polarisation, P_τ , arises for $V = Z$ since the Z decay is not parity-conserving. On the Z boson pole ($V = Z$) we have $P_\tau = -2va/(a^2 + v^2)$ where $v = -\frac{1}{2} + 2\sin^2\theta_W$ and $a = -\frac{1}{2}$ are the vector and axial-vector couplings of the Z to the τ pair.

We now study the $H \rightarrow \tau^-\tau^+$ and $Z \rightarrow \tau^-\tau^+$ decay correlations for all the τ decay modes listed above. Figures 2.6-2.11 compare the correlations, $d^2\Gamma/dz d\bar{z}$, arising from the Higgs with those for the Z boson for all possible combinations of the 6 major τ decay modes, i.e. for the $(6 \times 6)/2$ different $\tau^-\tau^+ \rightarrow A^-B^+\nu$'s decays. Apart from the P_τ dependence ($P_\tau = -0.135$ for $V = Z$ with $\sin^2\theta_W = 0.233$), the correlation patterns are similar for any vector boson V . We present the correlation figures for all combinations, since they are needed to obtain an overall understanding of the expected correlation patterns.

The distributions of the $\pi^-\pi^+$ system, Fig. 2.6(a), are readily anticipated from the individual pion distributions of Fig. 2.2. The energy distribution of the pion arising from τ_L^- (or τ_R^+) has the form $f \sim 1 - z$, while from τ_R^- (or τ_L^+) it is $f \sim z$. Hence in $Z \rightarrow \tau_L^-\tau_R^+$ or $\tau_R^-\tau_L^+$ decays an energetic (a soft) π^\pm is most likely to be associated with an energetic (a soft) π^\mp , whereas precisely the opposite is favoured for $H \rightarrow \tau_L^-\tau_L^+$ or $\tau_R^-\tau_R^+$ decays. Therefore, if a possible excess of $\tau^+\tau^-$ events over e^+e^- or $\mu^+\mu^-$ events arises from Higgs decay, the

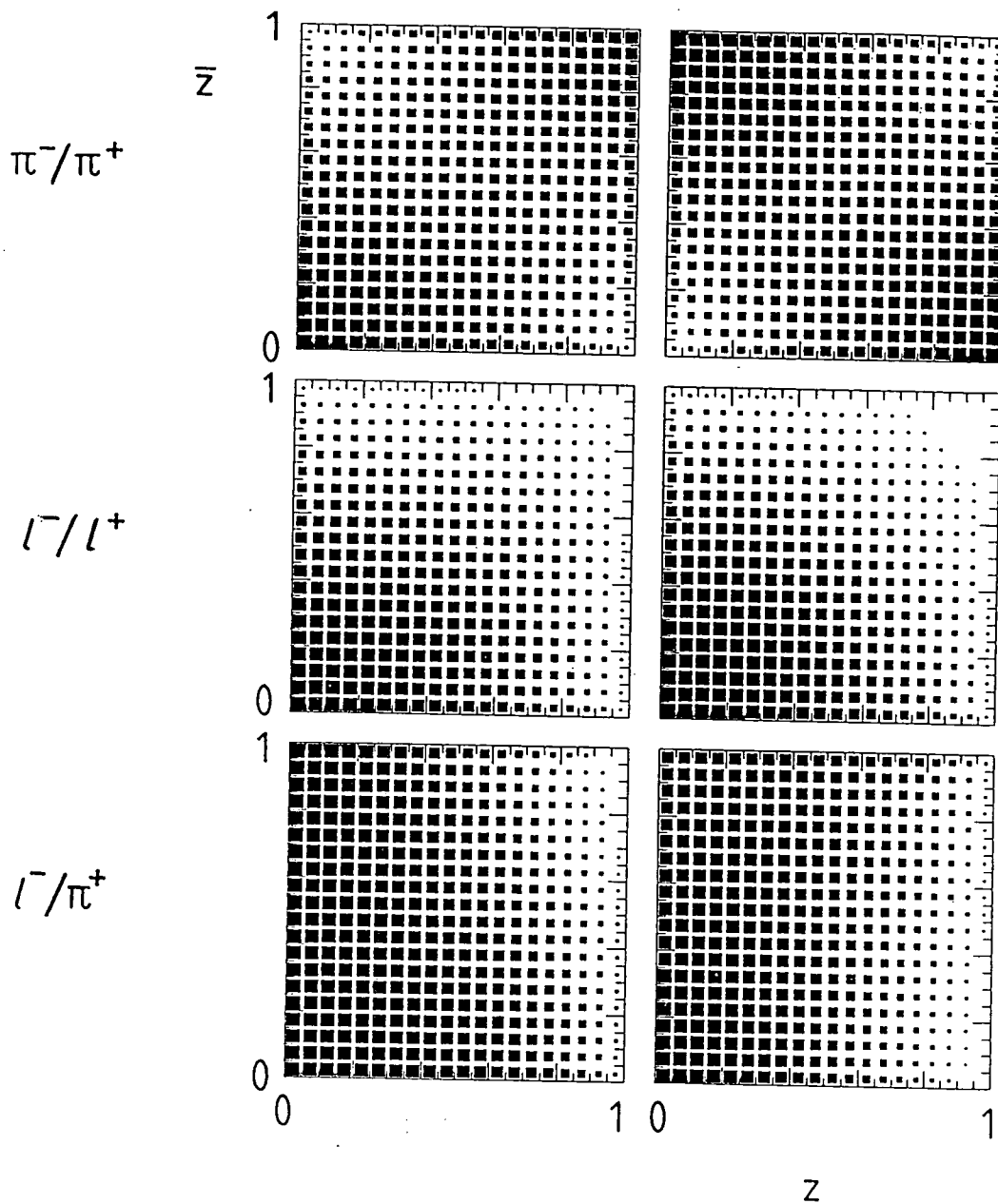


Figure 2.6: Plots of the correlation $d^2\Gamma/dz d\bar{z}$ in energy fractions in $X \rightarrow \tau^- \tau^+ \rightarrow A^- B^+ \nu$'s, where X is either a spin-one or spin-zero boson and $z = E_A/E_\tau$ and $\bar{z} = E_B/E_\tau$. If $A \neq B$ then the graphs with $A \leftrightarrow B$ can be obtained by reflection in the line $z = \bar{z}$. The first column shows the correlation when X is a Z boson and the second shows the correlation when X is a Higgs boson. In descending order the three pairs of plots are for the (τ^-, τ^+) pair decaying into (π^-, π^+) , (ℓ^-, ℓ^+) and finally (ℓ^-, π^+) with $\ell = e$ or μ .

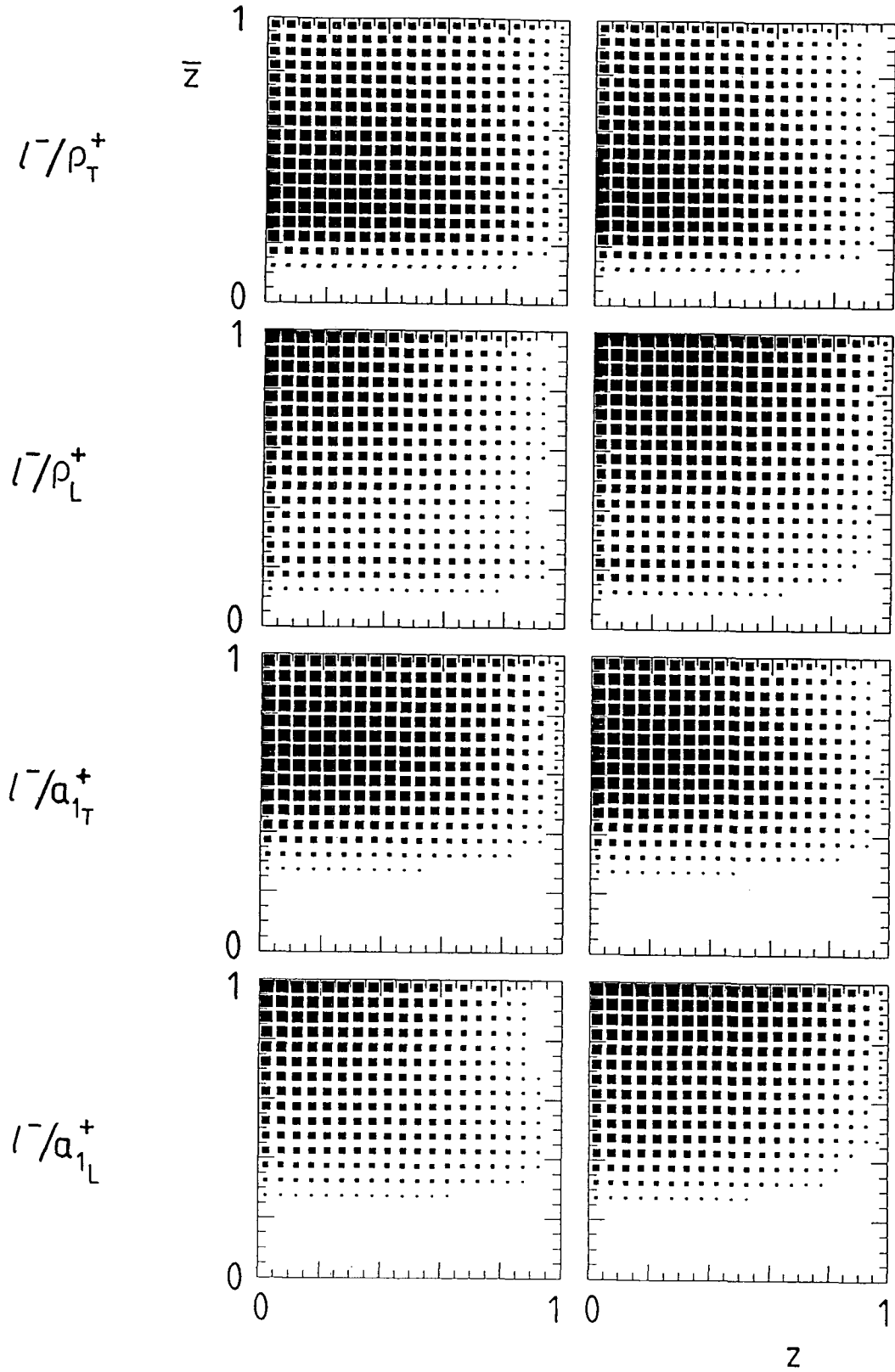


Figure 2.7: As Fig. 2.6 except where now, in descending order, the (τ^-, τ^+) pair decays into (l^-, ρ_T^+) , (l^-, ρ_L^+) , (l^-, a_{1T}^+) , (l^-, a_{1L}^+) respectively.

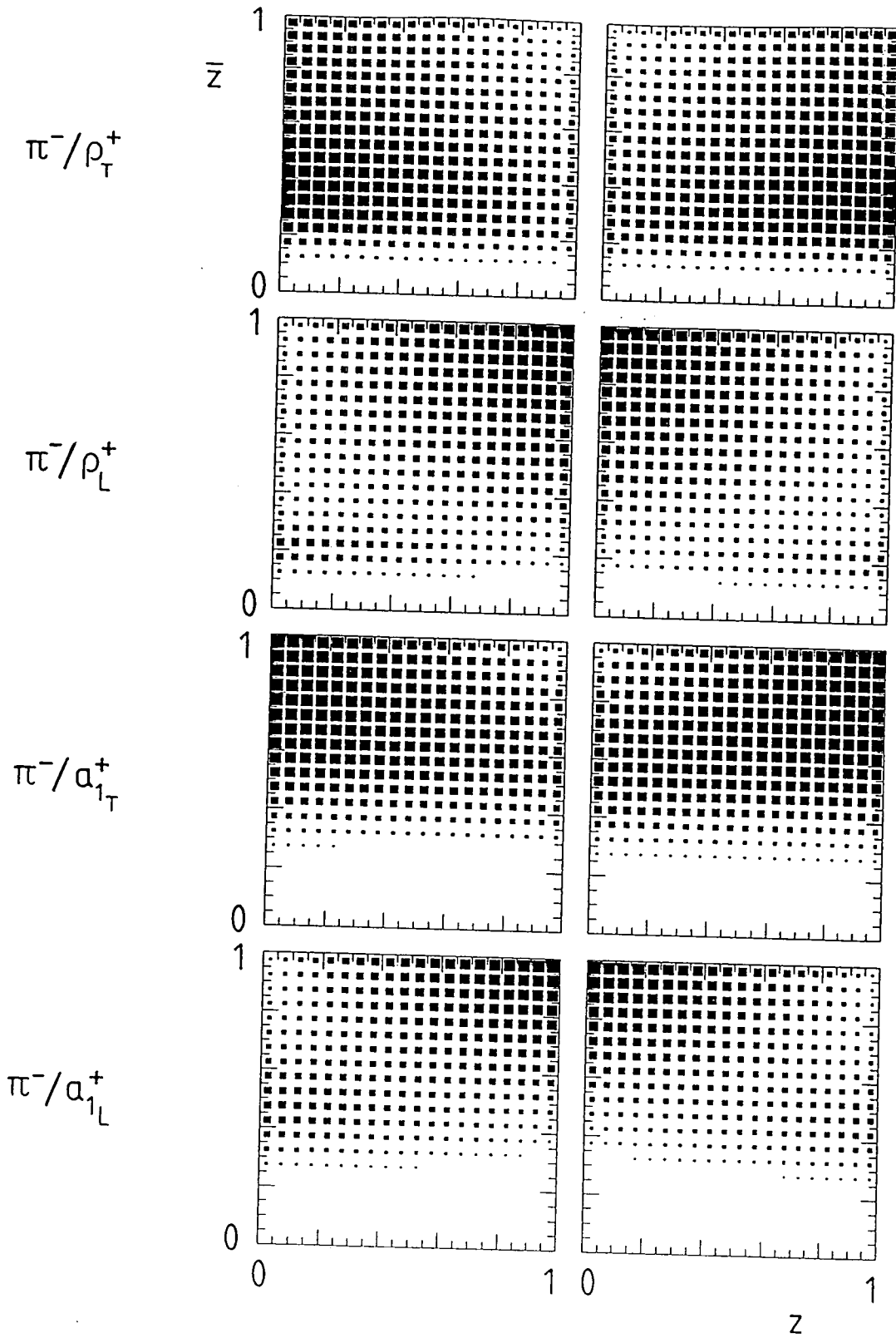


Figure 2.8: As Fig. 2.6 except where now, in descending order, the (τ^-, τ^+) pair decays into (π^-, ρ_T^+) , (π^-, ρ_L^+) , (π^-, a_{1T}^+) , (π^-, a_{1L}^+) respectively.

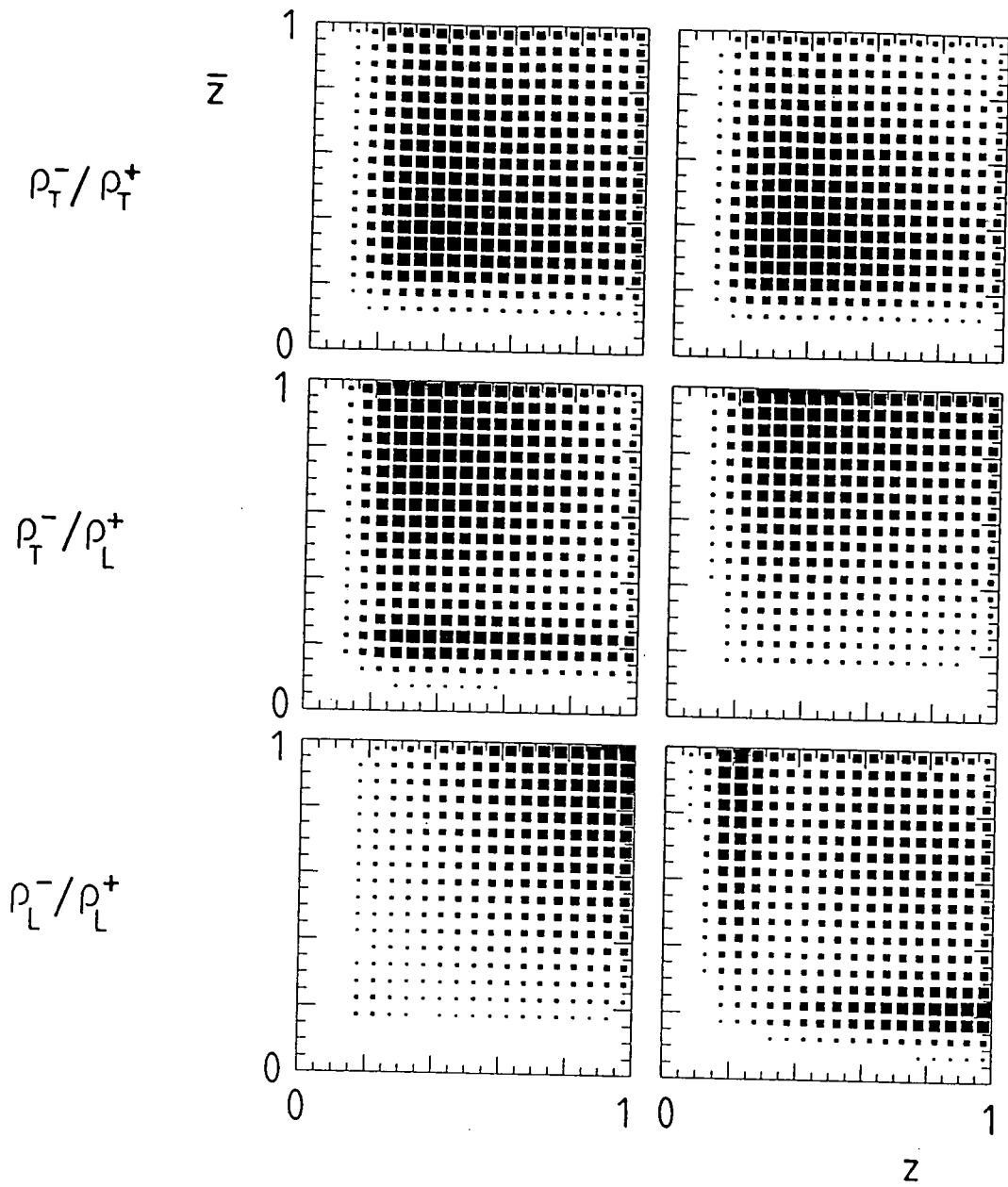


Figure 2.9: As Fig. 2.6 except where now, in descending order, the (τ^-, τ^+) pair decays into (ρ_T^-, ρ_T^+) , (ρ_T^-, ρ_L^+) , (ρ_L^-, ρ_L^+) respectively.

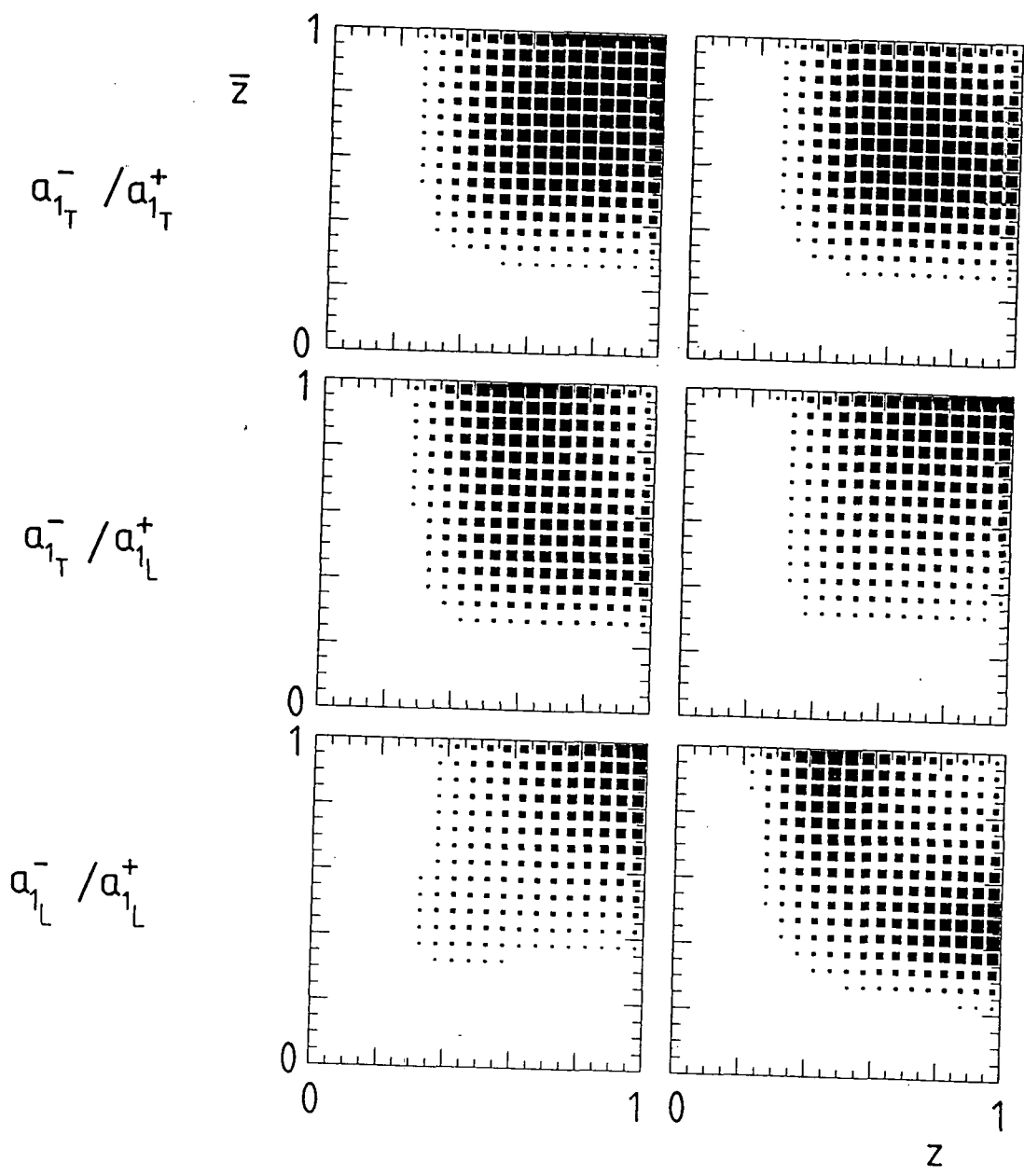


Figure 2.10: As Fig. 2.6 except where now, in descending order, the (τ^-, τ^+) pair decays into (a_{1T}^-, a_{1T}^+) , (a_{1T}^-, a_{1L}^+) , (a_{1L}^-, a_{1L}^+) respectively.

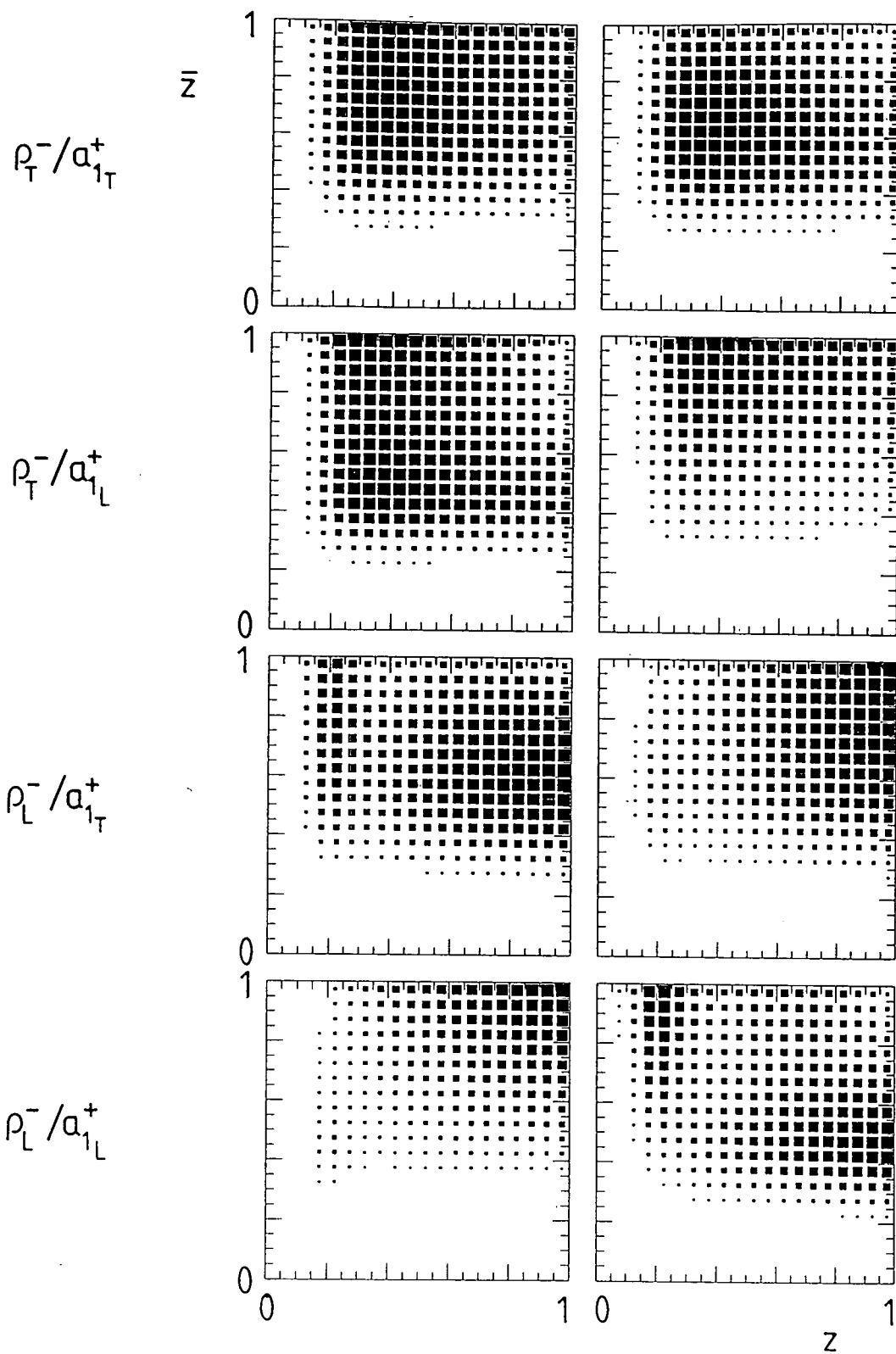


Figure 2.11: As Fig. 2.6 except where now, in descending order, the (τ^-, τ^+) pair decays into (ρ_T^-, a_{1T}^+) , (ρ_T^-, a_{1L}^+) , (ρ_L^-, a_{1T}^+) , (ρ_L^-, a_{1L}^+) respectively.

excess can be recognised in the $\pi^+\pi^-$ mode as an energetic π^\pm with a soft π^\mp . The effect of a small parity violation in Z decay ($P_\tau = -0.135$) leads to a slightly higher density when both π 's are soft. If $|P_\tau|$ is large, as expected for some proposed Z' 's, [21], then the asymmetry between soft and hard pions grows, but the positive energy-energy correlation between π^- and π^+ still holds, in contrast to the negative correlation in the $H \rightarrow \tau^-\tau^+ \rightarrow \pi^-\pi^+$ channel.

However although this is a clean signature for $H \rightarrow \tau^+\tau^-$ decays it accounts for only $(B_\pi)^2 \sim 1\%$ of the total τ -pair events. We therefore systematically studied all possible pairs of the decay modes shown in Fig. 2.2, which cover some 85% of τ decays. Since $|P_\tau|$ in (2.52) is small ($P_\tau = -0.135$ for $V = Z$) the double decay distributions of H and Z origin will be similar if either of the individual τ decay distributions are insensitive to the helicity of the τ . This is the case if $A = e$ (see Fig. 2.2), and indeed also for $A = \rho, a_1$ if we do not distinguish between the polarisation states of the vector meson. In fact we saw from Fig. 2.3 that the $\tau_L^- \rightarrow a_1$ and $\tau_R^- \rightarrow a_1$ distributions turn out to be essentially identical. A measurement of the vector meson polarization (from the distribution of its decay pions) is therefore crucial if we are to determine the spin of the τ -pair.

For example the $\pi^-\rho_L^+$ mode (see Fig. 2.8) arising from $Z \rightarrow \tau^-\tau^+$ decays favours events where both π^- and ρ_L^+ are energetic ($z \sim \bar{z} \sim 1$) whereas $H \rightarrow \tau^-\tau^+$ leads preferentially to asymmetric events with an energetic ρ_L^+ and a soft π^- . An energetic ρ_L tends to distribute its energy asymmetrically [5] and so the Higgs signal would be an asymmetric sharing of the energy between the π^- and the ρ_L^+ , and again between the π^+ and π^0 arising from the decay of the ρ . Similarly the $\rho_L\rho_L$ joint decay distribution (see Fig. 2.9) is strikingly different for the Z and H events, since for the former both ρ 's are energetic, whereas for the latter, one is energetic and the other soft (that is z or $\bar{z} \sim 0.5$). The a_{1L} acts very like the ρ_L and so the πa_{1L} (see Fig. 2.8) and $a_{1L}a_{1L}$ (see Fig. 2.10) modes can also distinguish H - from Z - τ pair decays.

Fig. 2.6 also shows the correlations between the μ (or e) and π modes. As expected, the distribution of the lepton modes is very similar for both the Higgs and the vector modes because of the similarity of $d\Gamma(\tau_\alpha \rightarrow \ell + \nu's)/dz$ for τ_L and τ_R that we found in Fig. 2.2. This similarity will hide nearly all the sensitivity of the distribution arising from the other τ decay, as can be seen in Fig. 2.7 and Fig. 2.6(c).

In Fig. 2.8 we show the combinations of the π channel with both longitudinal and transverse ρ and a_1 mesons. The effect of the opposite correlation on a pion mode (ignoring corrections of order $|P_\tau|$) is to reflect around the line $z = 0.5$ and thus the modes that show the greatest sensitivity to the spin of the parent are those where the difference between $d\Gamma/d\bar{z}$ for low and high \bar{z} is greatest for opposite parent τ helicities. Thus from Fig. 2.2 we see that

the longitudinal spin one meson modes should have good sensitivity, and this is demonstrated in Fig. 2.8 which displays the $\pi\rho$ and πa_1 correlations.

The strong sensitivity of longitudinal modes is repeated in Figs. 2.9, 2.10 and 2.11 which show respectively the distributions resulting from the various $\rho\rho$, $a_1 a_1$ and ρa_1 modes. It is clear that the greatest sensitivity to distinguishing between a Higgs and a vector parent arises from the $v_L v_L$ modes, where $v = \rho$ or a_1 , which is a consequence of the greater difference between the $\tau_L \rightarrow v_L$ and $\tau_R \rightarrow v_L$ distributions of Fig. 2.2, than between the $\tau_L \rightarrow v_T$ and $\tau_R \rightarrow v_T$ distributions.

2.6 Comparison of measurement errors for various decay modes

In this section, we present a comparison of the errors in measuring the τ polarisation using the various methods that we have studied. We first derive the formula used to calculate these errors.

Suppose that for a particular τ decay mode we have measurements of the distribution

$$\frac{1}{\Gamma} \frac{d\Gamma}{dz} = f(z) + P_\tau g(z), \quad (2.53)$$

in n_b bins of a region \mathcal{R} of z , where P_τ is the τ polarisation. We normalise the distribution so that over the observed z range

$$\frac{1}{\Gamma} \int_{z \in \mathcal{R}} \frac{d\Gamma}{dz} dz = 1. \quad (2.54)$$

We then define

$$N_i = N \int_{z \in \text{bin } i} f(z) dz, \quad M_i = N \int_{z \in \text{bin } i} g(z) dz \quad (2.55)$$

where N is the total number of τ events which make up the distribution (2.53) in region \mathcal{R} . We use a χ^2 fit to find the likeliest value of the parameter P_{input} , given the τ polarisation P_τ . χ^2 is given by

$$\chi^2(P_\tau) = \sum_{i=1}^{n_b} \left(\frac{N_i + P_{\text{input}} M_i - (N_i + P_\tau M_i)}{\sqrt{N_i + P_\tau M_i}} \right)^2 = \sum_{i=1}^{n_b} \frac{M_i^2}{N_i + P_\tau M_i} (P_{\text{input}} - P_\tau)^2. \quad (2.56)$$

Then trivially $P_\tau = P_{\text{input}}$ minimises χ^2 . The 1σ error of the P_τ measurement is determined by the condition

$$\chi^2(|P_\tau - P_{\text{input}}|) = 1. \quad (2.57)$$

If we write $P_\tau = P_{\text{input}} \pm \delta_P$ then this condition becomes $\chi^2(\delta_P) = 1$. We then solve (2.56) to find

$$\delta_P = \left(\sum_{i=1}^{n_b} \frac{M_i^2}{N_i + P_\tau M_i} \right)^{-1/2}. \quad (2.58)$$

We wish to present ‘ideal’ experimental errors independent of choice of bins, and thus we take $n_b \rightarrow \infty$ in (2.58) giving

$$\delta_P = \left(N \int_{\mathcal{R}} \frac{g(z)^2}{f(z) + P_\tau g(z)} dz \right)^{-1/2}. \quad (2.59)$$

This derivation can be extended to cases where more than one variable is involved by replacing the integral over dz by integration over all the variables.

We define $\hat{\delta}_P$ to be the value of δ_P in (2.59) when $N = 1$. We show tables of the value of $\hat{\delta}_P$ and $\hat{\delta}_P/\sqrt{B}$ for several modes, where B is the branching fraction of the mode. The statistical error of a ‘perfect’ experiment is then obtained by dividing $\hat{\delta}_P/\sqrt{B}$ by $\sqrt{N_{\text{event}}}$, where N_{event} is the number of τ events. For the simple case of the single pion, the integral can be performed analytically. For the other cases, the answers are obtained by numerical integration. When the ρ and a_1 pion decays are used as polarimeters, the sample data for the integration were taken from Monte Carlo simulations of $\tau \rightarrow \rho \rightarrow 2\pi$ and $\tau \rightarrow a_1 \rightarrow 3\pi$ decays. We used the subroutine package HELAS [23] to evaluate the helicity amplitudes for these decays. We have checked that the model dependence in the $a_1 \rightarrow 3\pi$ ’s decay amplitude, as discussed in Section 2.3.2, gives numerically negligible differences for the predictions of our Monte Carlo simulation.

2.6.1 Measuring P_τ from τ^\pm decays

Table 2.2 compares the errors for the various τ decay modes (unweighted and weighted by the appropriate branching fractions). These are calculated from (2.59), where we assume for simplicity that $P_\tau = 0$. If only the primary decay is observed we note from the upper portion of the Table that the π channel gives the best determination of P_τ , even after correcting for the branching factor. The $\tau \rightarrow \rho$ mode has the next best sensitivity, even though the ρ polarisation is not measured. The sum of the leptonic modes is comparable despite its large branching fraction. As anticipated from Fig. 2.3, the $\tau \rightarrow a_1$ decay mode has virtually no resolving power.

The middle section of Table 2.2 shows the improvement of the errors if the pion decays of the vector mesons are included. We present the results of the two dimensional analysis, in terms of the total energy fraction $z = \sum E_\pi/E_\tau$, and the fraction $x = E_{\pi^\pm}/(\sum E_\pi)$ of the

decay mode	$\hat{\delta}_P$	branching fraction, B	$\hat{\delta}_P/\sqrt{B}$
One dimensional results (z)			
π	1.73	0.11	5.22
$\mu + e$	4.49	0.355 (sum)	7.55
ρ	3.75	0.227	7.86
a_1	14.1	0.146	36.9
Two dimensional results (z, x_{π^\pm})			
$\rho (\pi^- \pi^0)$	2.15	0.227	4.51
$a_1 (\pi^- 2\pi^0)$	3.87	0.075	14.1
$\pi^- + \pi^0$'s	2.49	0.302	4.64
Three dimensional result ($z, \min(x_1, x_2), x_3$)			
$a_1 (\pi^+ 2\pi^-)$	3.76	0.071	14.1

Table 2.2: The ideal errors associated with each of the major τ decay modes with and without the ρ and a_1 decay to pions as polarimeters. The branching fractions are taken from [24]. The error $\hat{\delta}_P$ is per one event of each mode, whereas the error $\hat{\delta}_P/\sqrt{B}$ is per one tau.

total pion energy carried by the charged pion in the one-prong decays of the τ . We first give the results of the $\rho \rightarrow \pi^\pm \pi^0$ and $a_1 \rightarrow \pi^\pm 2\pi^0$ modes separately. We see that the polarimeter power of the ρ mode improves drastically, and that it now overwhelms that of the π mode, after allowing for the branching fraction. Even though we only use half of the a_1 decay modes and we do not measure the individual energies of the two outgoing π^0 mesons, the sensitivity of the a_1 mode improves by nearly a factor of three over the one dimensional analysis. If we were able to clearly distinguish a one π^0 event from a two π^0 event, then the two dimensional analysis should lead to a total resolving power of $\hat{\delta}_P/\sqrt{B} \sim (4.51^{-2} + 14.1^{-2})^{-1/2} = 4.30$. However, such a distinction may not be possible in realistic detectors. Thus the third entry assumes that one cannot distinguish between $\pi^\pm \pi^0$ and $\pi^\pm 2\pi^0$ events. Surprisingly, this does not strongly suppress the polarimeter power of the ρ mode, and we find a resolving power $\hat{\delta}_P/\sqrt{B} \sim 4.64$ which is almost as good as that of the pure ρ mode.

This fortunate situation can be easily understood if we examine the scatter plots shown in Fig. 2.5 for the a_1 decay. We first note that $x_{\pi^\pm} \equiv x_3 \equiv x$ in the $a_1^\pm \rightarrow \pi^\pm \pi^0 \pi^0$ decay mode. It is clearly seen from the plots that a_{1L} decays favour $x \sim 1$ or $x \sim 0$ (asymmetric in the charged and neutral energies), whereas a_{1T} decays favour $x \sim 0.5$ (symmetric). These trends are identical to those of ρ_L and ρ_T decays. Because of this similarity between the charged-to-neutral energy splitting of the ρ and a_1 modes, our inability to experimentally distinguish between the two modes does not significantly deplete the sensitivity to P_τ . Although our sample does not cover all $\tau^\pm \rightarrow (\pi^\pm + n\pi^0)\nu_\tau$ events, the $\rho^\pm \rightarrow \pi^\pm \pi^0$ and $a_1^\pm \rightarrow \pi^\pm \pi^0 \pi^0$ modes account for about 90% of the decays with a charged pion accompanied by neutral

pions. We therefore believe that our approach will be useful for very high τ energies when it will be difficult to distinguish between π^0 's.

The last entry in Table 2.2 is for the decay $a_1^\pm \rightarrow \pi^\pm \pi^\pm \pi^\mp$, where the integration is over z , $x = x_3$ and $y = \min(x_1, x_2)$, where $x_i = E_{\pi_i}/E_{a_1}$ and where π_3 is the distinguishable pion. Amusingly, this three-dimensional analysis does not significantly improve the polarimeter power of the two-dimensional analysis, where we used only the sum of the two π^0 energies in the $a_1^\pm \rightarrow \pi^\pm 2\pi^0$ mode. In other words, even if we do not measure the energies of the two identical pions separately, we essentially obtain the optimal measurement of P_τ in this mode. It is relevant to inspect Fig. 2.12 in which the continuous curves show the polarized a_1 decay distributions as a function of the energy fraction $x = x_3$ of the distinguishable pion. These curves are the projections of the scatter plots of Fig. 2.5 onto the $x = x_3$ axis. For comparison, the dashed lines show the corresponding single π energy fraction distributions arising from the decays of the polarised ρ mesons; see (2.30) and (2.31).

Using the values of $\hat{\delta}_P/\sqrt{B}$ listed in Table 2.2, we give in Table 2.3 some examples of how our methods can increase the accuracy of the measurement of τ polarisation. Because of their large branching fractions, the use of the leptonic modes is found to significantly improve the sensitivity of the single π analysis alone. As can be seen from the lepton distributions in Fig. 2.2, it is essential to be able to detect the leptonic modes over a wide range of the energy fraction z . Even if we were incapable of distinguishing a π^0 from two or more π^0 's, the use of the charged to neutral energy fraction data alone can reduce the error from 4.29 to 3.15. This reflects the approximate similarity evident in Fig. 2.12 between the single π distributions which arise from polarised ρ and a_1 decays. After combining all the modes considered so far, the P_τ polarimeter could be improved by approximately a factor of 1.7 as compared to just using single pion decays (that is the π error of 5.22 shown in Table 2.2 is reduced to 3.15).

modes	$\hat{\delta}_\Sigma$
π, μ, e	4.29
$\pi, \mu, e, \pi^\mp 2\pi^\pm$	4.1
$\pi, \mu, e, \pi^\pm \pi^0$'s	3.15
$\pi, \mu, e, \pi^\pm \pi^0$'s, $\pi^\mp 2\pi^\pm$	3.08

Table 2.3: Examples of the improvement in total accuracy in measuring τ polarisation when the ρ and a_1 decays to pions are used as polarimeters. These results are simply the errors of the rightmost column of Table 2.2 combined using $\hat{\delta}_\Sigma = \left(\sum(1/\hat{\delta}^2)\right)^{-1/2}$.

Finally we emphasize that the values given in Tables 2.2 and 2.3 (and also for Table 4

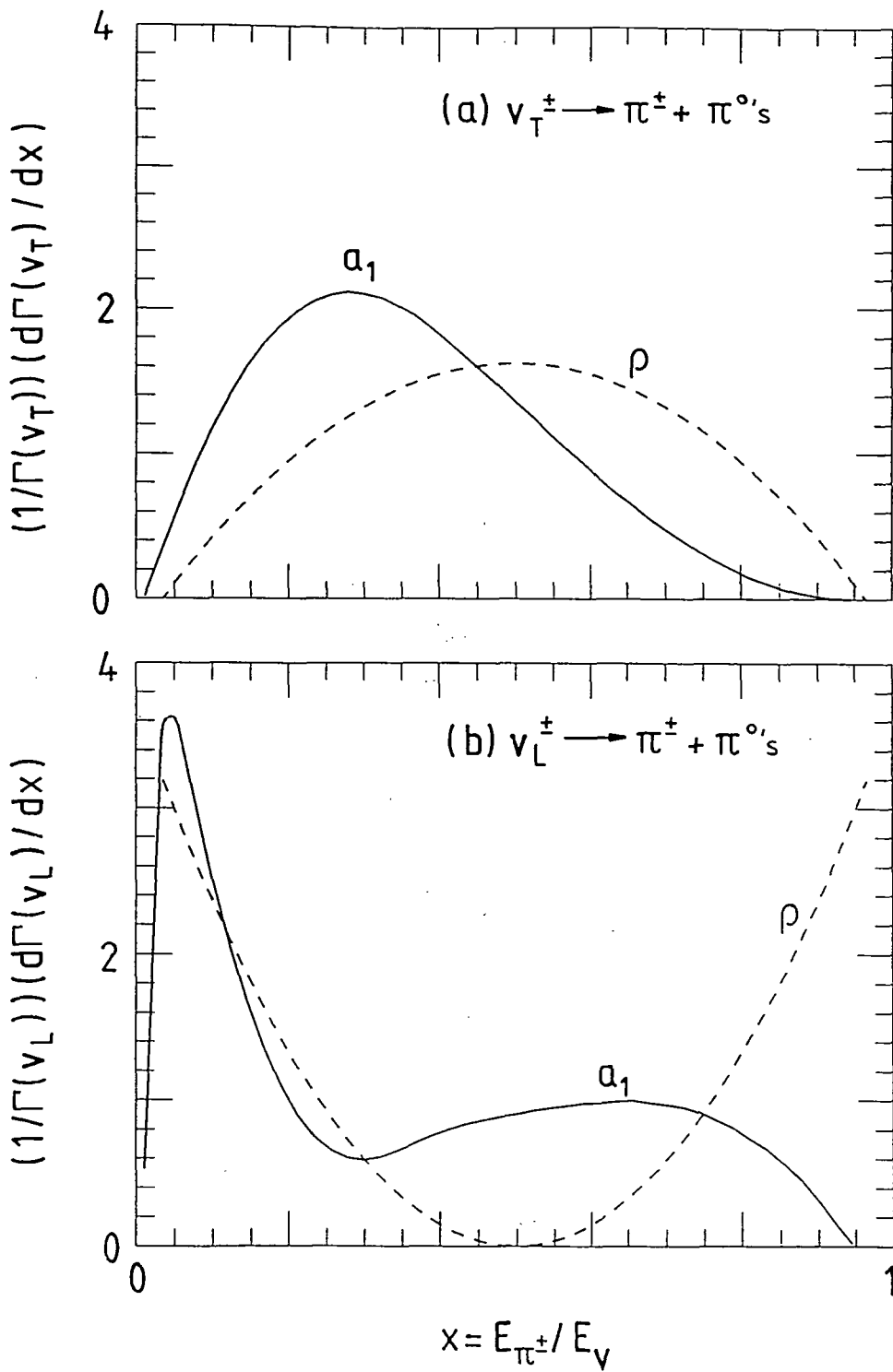


Figure 2.12: The polarized a_1 decay distributions as functions of the energy fraction $x_3 = E_3 / (E_1 + E_2 + E_3)$ of π_3 (the distinguishable pion in $a_1 \rightarrow 3\pi$ decays). These curves are the projections of the scatter plots of Fig. 2.5 onto the $x = x_3$ axis. For comparison, we also show with dashed lines the corresponding single π energy fraction distributions arising from polarized ρ decays; see eqs. (2.30) and (2.31).

below) are for the idealised situation in which the relevant decay pions can be detected over all phase space. In practice, particularly at hadronic colliders, this cannot be achieved and it will be necessary to impose cuts (e.g. $z > z_{\min}$) to enable the τ events to be tagged. It should be noted here that even at hadron colliders, the energy fraction z can be measured for W' or Z' [25] provided that the missing p_T can be well measured. Moreover the accuracy of the P_τ measurements given in the tables assumes that we can estimate reliably the total number of τ 's produced. At e^+e^- colliders where the τ pair events are detected with a high efficiency independent of their polarization, this requirement can be fulfilled with high statistics even for τ 's originating from H^0 or H^\pm . As noted in section 2.4, the requirement may also be fulfilled at hadron colliders for τ 's from W' or Z' , where the absolute τ event rate can be estimated from the associated e and μ events by assuming lepton universality. Uncertainty in the experimental normalisation (both statistical, from the number of observed events, and systematic, from detector efficiencies) will lead to an additional uncertainty in the measurement of P_τ .

2.6.2 Measuring P_τ from $X \rightarrow \tau^-\tau^+$ events

For the decays of the type

$$X \rightarrow \tau^-\tau^+ \rightarrow A^-B^+ + \nu\text{'s}$$

where the spin of the parent boson X is known, it is important to use the correlations between the decay modes of the τ^- and τ^+ to improve the accuracy in the measurement of P_τ over that which can be achieved using only one of the decays $\tau^- \rightarrow A^-$ or $\tau^+ \rightarrow B^+$. In this subsection we quantify the improvement in accuracy taking into account the polarimeter power of the subsequent $\rho \rightarrow 2\pi$ and $a_1 \rightarrow 3\pi$ decays. This is a considerable extension of previous studies [26] which have examined the use of correlations of the energies of the primary decay products, E_A and E_B . For the purposes of illustration we take the parent boson to have spin one.

We begin by using (2.53) to rewrite the joint decay distribution (2.50) for $X \rightarrow \tau^-\tau^+ \rightarrow A^-B^+ + \nu\text{'s}$ in the form

$$\frac{d\Gamma}{dz d\bar{z}} = f_A(z)f_B(\bar{z}) + g_A(z)g_B(\bar{z}) + P_\tau (f_A(z)g_B(\bar{z}) + g_A(z)f_B(\bar{z})), \quad (2.60)$$

where as before $z = 2E_A/m_X$ and $\bar{z} = 2E_B/m_X$. We then define

$$f(z, \bar{z}) = f_A(z)f_B(\bar{z}) + g_A(z)g_B(\bar{z}) \quad (2.61)$$

and

$$g(z, \bar{z}) = f_A(z)g_B(\bar{z}) + g_A(z)f_B(\bar{z}) \quad (2.62)$$

and apply (2.59) to find the error $\hat{\delta}_P$ in measuring P_τ . We again set $P_\tau = 0$ in the formula for simplicity.

A^-	B^+	$\hat{\delta}_P$	combined branching fraction, B_c	$\hat{\delta}_P/\sqrt{B_c}$
π^-	π^+	1.37	0.0121	12.5
π^-	ℓ^+	1.66	0.0779	5.97
ℓ^-	ℓ^+	3.23	0.125	9.13
$\pi^- + \pi^{0's}$	π^+	1.54	0.0664	5.99
$\pi^- + \pi^{0's}$	ℓ^+	2.29	0.214	4.95
$\pi^- + \pi^{0's}$	$\pi^+ + \pi^{0's}$	1.91	0.0912	6.34
$\pi^+ + 2\pi^-$	π^+	1.64	0.0156	13.1
$\pi^+ + 2\pi^-$	ℓ^+	2.96	0.0503	13.2
$\pi^+ + 2\pi^-$	$\pi^+ + \pi^{0's}$	2.21	0.043	10.7
$\pi^+ + 2\pi^-$	$\pi^- + 2\pi^+$	2.9	0.0050	41

Table 2.4: The errors associated with measuring the τ^- polarisation from a massive spin one boson X decaying as $X \rightarrow \tau^- \tau^+ \rightarrow A^- B^+ \nu$'s (or $X \rightarrow A^+ B^- \nu$'s). These errors should be compared with the 'best' value for A or B from Table 2.2, i.e. the lowest error of measurement using only one of the modes. We set $P_\tau = 0$ in (2.59). The product B_c of the branching fractions is simply B_A^2 if $B = A$ and is $2B_A B_B$ when $A \neq B$, since the last two columns refer to $A^- B^+ + A^+ B^-$.

In Table 2.4, we show the values of $\hat{\delta}_P$ for each of the ten possible combinations of ℓ , π , $\pi^\pm + \pi^{0's}$ and $a_1^\pm \rightarrow \pi^\mp 2\pi^\pm$ pairs. These values of $\hat{\delta}_P$ for correlated decays should be compared with the lower error of the two separate decays given in Table 2.2. We see that, as expected, there is an improvement in every case. By "adding up" all the entries in the end column of Table 2.4, and by accounting for those decays which have only a single useful mode, we find an ultimate 'theoretical' limit of the τ polarimeter, $\hat{\delta}_P = 2.37$. For comparison we note that when only the $\tau \rightarrow \pi \nu$ decay mode is used, the polarimeter power is $\hat{\delta}_P/\sqrt{2B_\pi - B_\pi^2} = 3.79$.

2.6.3 Measuring P_τ at hadron colliders

Finally we quantify the errors in the measurement of P_τ at hadron colliders. As mentioned in Section 2.4, only τ decays to high z particles can be detected in a hadronic environment; the fraction $f_A(\tau_\alpha, z_{\min})$ of $\tau \rightarrow A$ decay events with energy fraction $z > z_{\min}$ can be deduced from Table 2.1. Since the measurement of z at hadron colliders is expected to have poor resolution we treat the region $z_{\min} < z < 1$ as a single bin. (Thus the integration over z is of the form (2.58), with a single bin, $n_b = 1$, rather than (2.59)).

The P_τ dependence of that fraction of $\tau \rightarrow A$ decays that we can observe is given by

$$f_A(P_\tau, z_{\min}) = \frac{1}{2}(1 - P_\tau)f_A(\tau_L, z_{\min}) + \frac{1}{2}(1 + P_\tau)f_A(\tau_R, z_{\min}) \quad (2.63)$$

where the fractions $f_A(\tau_L, z_{\min})$ and $f_A(\tau_R, z_{\min})$ are defined in (2.46). The polarimeter power of the $\tau \rightarrow A$ mode is then obtained from the general formula (2.58). The error per one observed event (in the region $z_{\min} < z < 1$) is found to be

$$(\hat{\delta}_P)_A = \left(\sum_A f_A(P_\tau, z_{\min}) \right)^{1/2} \frac{2(f_A(P_\tau, z_{\min}))^{1/2}}{|f_A(\tau_L, z_{\min}) - f_A(\tau_R, z_{\min})|}. \quad (2.64)$$

The resulting values are listed in Table 5 for the choice $z_{\min} = 0.8$.

We first comment on the results shown in the upper part of Table 5. Even though the fraction of single π events is tiny if $P_\tau = -1$ (corresponding e.g. to $W^- \rightarrow \tau^- \rightarrow \pi^-$ decays) we see from Table 2.1 that it has a strong P_τ dependence and can provide a sensitive measure of P_τ if sufficiently large statistics can be achieved. Indeed $P_\tau = +1$ is expected for H^- or W_R^- decays (and certain Z' models), and so the sensitivity of the rate of single π decays to P_τ offers a powerful signature for new physics. Despite the larger observed fractions of ρ and a_1 events these decays have poorer sensitivity to P_τ , unless the subsequent decays to pions are studied (see Table 2.1). The large errors shown for the a_1 mode in Table 5 simply reflect the insensitivity of $\tau \rightarrow a_1$ decays to the value of P_τ , recall Fig. 2.3.

Just as for the previous studies, we find the subsequent ρ and a_1 decay distributions dramatically improve the accuracy in the measurement of P_τ . The middle section of Table 5 shows the improvement if just the distribution of the energy fraction of the π^- is studied and the accompanying π^0 's are not measured. We first give the accuracy arising from the ρ and a_1 modes separately and then the combined result in which the number of π^0 's is not detected. In this sample study we see that the contamination due to the a_1 mode can even lead to a small improvement in the measurement of P_τ from $\tau^- \rightarrow \rho^- \rightarrow \pi^-$ for values of $P_\tau \sim 0$ (arising from the increase in the number of events). This reflects the approximate similarity of the ρ and a_1 decay distributions shown in Fig. 2.12. Although there will be an additional small contamination arising from $\pi^- + 3\pi^0$ decays, which may decrease the accuracy in the determination of P_τ , it is encouraging that the major a_1 mode does not significantly reduce our ability to measure P_τ from $\tau \rightarrow \rho$ decays.

The three prong decay of the a_1 is a clean experimental signal. We therefore also give the accuracy corresponding to a one-dimensional analysis of these decays in Table 2.5, based on the x distributions of Fig. 2.12. The use of the two-dimensional decay distributions of Fig 5 does not significantly improve the sensitivity to P_τ .

decay mode	$\hat{\delta}_P$		
	$P_\tau = -1$	$P_\tau = 0$	$P_\tau = +1$
Zero dimensional results			
π	1.29	3.23	4.75
ℓ	5.48	4.77	3.06
ρ	3.48	4.79	6.07
a_1	25.0	28.9	32.6
One dimensional results (x)			
$\rho (\pi^- + \pi^0)$	1.15	2.67	2.88
$a_1 (\pi^- + 2\pi^0)$	3.90	6.42	7.44
$\pi^- + \pi^{0's}$	1.23	2.65	3.33
$a_1 (\pi^+ + 2\pi^-)$	4.01	6.60	7.65
Sum of errors over $\pi, \ell, \pi^- + \pi^{0's}, \pi^+ + 2\pi^-$			
sum	0.86	1.81	1.97

Table 2.5: The errors $\hat{\delta}_P$, as given by (2.64) per one observed event with $z > z_{\min}$, associated with measuring the τ^- polarisation at a hadron collider. We take $z_{\min} = 0.8$. We give results for $P_\tau = -1, 0$ and $+1$.

In the final row of Table 2.5 we give the expected theoretical error in the measurement of P_τ , per one observed event, obtained by combining all the decay modes: $\ell^-, \pi^-, \pi^-\pi^{0's}$ and $\pi^-\pi^-\pi^+$. In this ideal situation we expect a measurement of P_τ to 10% accuracy with 70 (400) observed events for values of $P_\tau \sim -1 (+1)$.

Again we must add similar words of caution to those given at the end of section 6.1. We have presented the idealized situation of complete detection of the specified τ decay products for $z > z_{\min}$, with a precisely known τ production rate and with neglect of possible background contaminations. For new heavy gauge bosons this assumes that the couplings respect the lepton universality. In practice there will be uncertainties in normalisation (both statistical, from the number of observed events, and systematic, from the detection efficiencies) and in the determination of the value of z (from the energy and angular resolution of the detector, the resolution in the missing p_T measurements, as well as from the width of the parent boson). A realistic measurement of P_τ will need to include these errors, which will depend on the specific details of the detector used in the analysis.

2.7 Conclusions

The tau polarisation measurement is a valuable probe of new physics. We examined in detail the specific cases of the τ decays of the charged and neutral Higgs bosons, and showed

how tau polarisation measurement can provide a signal of these particles. We showed that measurement of the tau polarisation can be greatly improved by using the decays of the intermediate vector mesons ρ and a_1 . We outlined the procedure for measuring the tau polarisation from these decays for highly energetic τ 's. We found that the use of these modes improves the power of the polarimeter, over using just the pion mode, by a factor of 60% for LEP, assuming perfect detection of final state charged particles.

We studied only the ρ and a_1 modes, since for these modes, we know the hadronic matrix elements with little ambiguity. It is relatively straightforward to include the rarer decay modes involving K , K^* and K_1 mesons. The matrix elements are not well known for the modes with more than three π 's or K 's. These modes are still non-negligible. Although further theoretical study on these modes may be necessary, it is also an important experimental question to measure the τ_L and τ_R decay functions phenomenologically at e^+e^- colliders.

The tables show the accuracy with which P_τ can be measured in an idealized situation of perfect detection, with precisely known τ production rates and with neglect of background contaminations. The results are indicative of what could be ultimately achieved using the decay products of the τ to measure its polarisation, but clearly the actual accuracy will depend on the particular experimental circumstances.

Chapter 3

Radiative corrections to top quark production and decay

The top quark is one of the two last missing pieces comprising the standard model (the other is the Higgs boson). It is vital for the theoretical consistency of the standard model that the top quark should exist. If it does not then anomalies occur which make the standard model unrenormalisable (see [27, 28] for details). However, the top quark has not, at the time of writing, been detected, because of its apparently huge mass. It is expected that it will either be discovered at the Fermilab experiments D0 or CDF, or if it is too massive to be produced at these experiments, at the upcoming LHC collider at CERN.

If the top quark does exist then its mass is almost certainly greater than the masses of any particles yet discovered. This makes it a particularly interesting probe for one of the most fundamental questions facing physicists today: how is mass generated? Because the top quark will interact strongly with a mass generating field, we may find in the behaviour of the top quark clues to the nature of mass generation.

Even if the top quark is discovered at Fermilab or the LHC collider, it is not anticipated that its properties will be accurately measured [29, 30]. Measurement of its mass to within ± 5 GeV, with no hope of accurately determining the relatively small top quark width, is considered the best that can be hoped for from the LHC collider. Therefore for using the top quark to detect new physics, e^+e^- collider experiments above the threshold for production of $t\bar{t}$ pairs, where the top's properties can be accurately measured, are more interesting. The projected e^+e^- accelerator to achieve these goals is known as the "Next Linear Collider". This collider will have a centre-of-mass energy greater than 500 GeV, sufficient to produce $t\bar{t}$ pairs.

In this chapter, as a background to studies of the effects of new physics on the production and decay of the top quark, we give complete analytic expressions for the one-loop elec-

trivial radiative corrections to top quark production and decay. Expressions for the one loop electroweak radiative corrections to production of $t\bar{t}$ pairs in e^+e^- collisions [31] and to the decay of the top quark [32, 33] have already been published. However, the radiative corrections presented in [31] to $t\bar{t}$ pair production were summed over the helicities of the t and \bar{t} quarks, and thus the decay of the top quark could not be incorporated. In our expressions for the radiative corrections to production of $t\bar{t}$ pairs in e^+e^- collisions, and the subsequent decay of the top quarks into b quarks and W bosons, we keep full polarisation information. We also introduce a new method for the evaluation of one loop radiative corrections to a vertex of two fermions and a gauge boson, which considerably simplifies the calculation.

At present, the lower limit on mass of the top quark, m_{top} , from experiments at Fermilab [29] is

$$m_{\text{top}} > 131 \text{ GeV}. \quad (3.1)$$

Restrictions on the mass of the top quark from consideration of standard model radiative corrections, using the accurate measurements of Z parameters at the LEP experiments and measurement of the W mass at hadron colliders [34] give

$$m_{\text{top}} \leq 200 \text{ GeV} \quad (3.2)$$

as an approximate upper limit. It has been shown [35] that if the mass of the top quark is greater than 100 GeV then a $t\bar{t}$ pair does not hadronise before it decays. The large mass and consequent large width of the top and antitop quarks act together as an infrared cutoff on soft gluon exchange between the quark pair, and so the top quark decays before any hadronisation can occur. This implies that the polarisation of the produced top quark is not dissipated in the hadronisation process, and provides another reason for keeping full polarisation information in our expressions for the radiative corrections.

The structure of the rest of the chapter is as follows. In the first section, we outline our approach to the problem. In the following two sections we establish our conventions for kinematics and spinors, and in the fourth we give the analytic expressions for the tree level amplitude. In the subsequent three sections, we give the radiative corrections to this amplitude. The radiative corrections are divided into three classes depending on the structure of their Feynman diagrams, which comprise these three sections. The first class, which we denote box diagrams, are diagrams in which two gauge bosons are exchanged between the e^+e^- and the $t\bar{t}$ pair. The second class, which we denote vertex diagrams, contains radiative corrections to diagrams where the loop has three external legs. The third class, which we denote self-energy diagrams, consists of radiative corrections which only affect the propagators of particles. In the following section, we discuss the removal of ultraviolet

divergences and the renormalisation of the amplitude in the modified minimal subtraction ($\overline{\text{MS}}$) scheme. In the final section, we give complete expressions for the total cross section.

3.1 Approach to the problem.

In our approach we consider production and decay processes together. This can be done in a simple way by calculating the radiative corrections as helicity amplitudes rather than using the traditional matrix element squared method. We also present a compact and convenient method for calculating the radiative corrections to the vertex of two fermions and a gauge boson, which can be readily extended to incorporate new physics effects.

Unitarity considerations on the structure of the Kobayashi-Maskawa (KM) matrix suggest that $V_{tb} \simeq 1$. Therefore in considering the decay of the top quark we may assume to a good approximation that only the processes

$$t \rightarrow bW^+, \quad \bar{t} \rightarrow \bar{b}W^-, \quad (3.3)$$

are significant.

We also make the approximation of factorising the radiative corrections into production and decay parts. This means that the top quark is treated as an on-shell particle. By making this approximation we avoid the technical difficulty of calculating loop level Feynman diagrams with more than four loop propagators, so-called pentagon and hexagon loop diagrams. We expect these diagrams to have an insignificant contribution to the amplitude, and by approximating that the top quark is on-shell we can avoid calculating them. However, since our corrections are expressed as helicity amplitudes rather than in matrix element squared form, we can combine the production and the decay amplitudes of the t and \bar{t} together. In our final expressions for the cross section, we insert a propagator factor for the top quark and integrate over the phase space volume, ignoring the virtuality of the top quark.

We choose to work entirely in the t'Hooft-Feynman gauge (corresponding to the R_ξ gauge of Appendix C with $\xi_{A,W,Z} = 1$), because in this gauge the gauge boson propagators have a very simple form proportional to the metric tensor $g^{\mu\nu}$.

We use the scheme of [36, 37] to carry out the loop integrals. Self-contained formulas for the loop integrals are presented here, and a discussion of the method is given in appendix D.

Our treatment of ultraviolet divergences is as follows. It can be seen from power counting arguments that the box diagrams do not contain divergences. The divergences of the vertex diagrams all cancel, due to the Ward-Takahashi identity, except for the diagrams containing a non-Abelian gauge boson coupling vertex. However, the divergence of the non-Abelian

graphs cancels against a term arising from gauge boson self-coupling in the propagator of the gauge boson. This term is known as the pinch term [38, 39]. Therefore the only divergence that needs to be renormalised in our expressions is the self energy of the gauge bosons, and thus we discuss renormalisation in the same section as the discussion of self energy graphs.

3.2 Kinematics

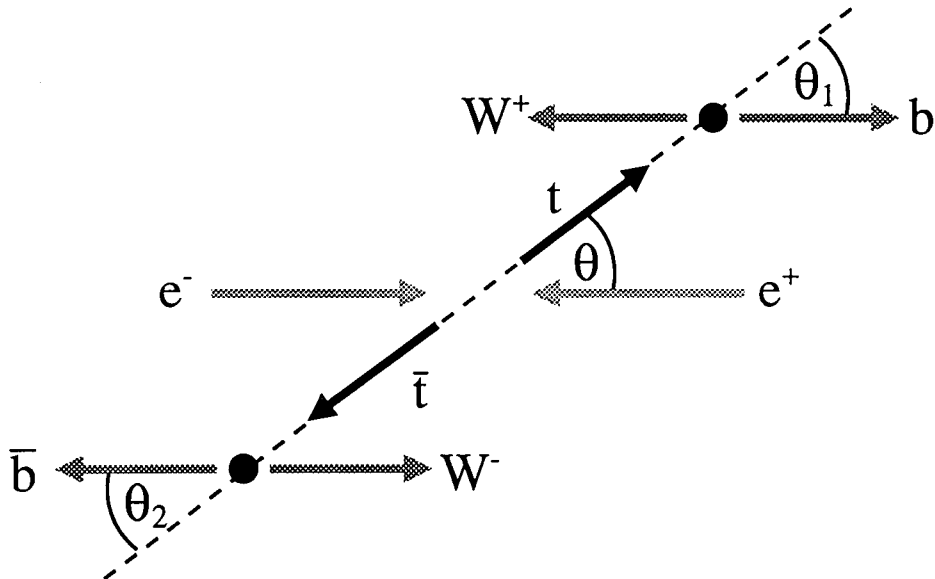


Figure 3.1: Momenta of e^- , e^+ , t and \bar{t} in the centre of mass frame of the e^+e^- pair, momenta of b , W^+ in the centre of mass frame of the decaying t quark and momenta of \bar{b} , W^- in the centre of mass frame of the decaying \bar{t} quark.

We approximate that the electron and b quark are massless. We denote the four momenta of e^+ and e^- by \bar{k}^μ and k^μ respectively, and the four momenta of t and \bar{t} by p^μ and \bar{p}^μ respectively. We define the momentum of the b and \bar{b} quarks produced in the t and \bar{t} decays to be r and \bar{r} respectively, and the momenta of the W^+ and W^- bosons to be w and \bar{w} respectively. Thus

$$k^2 = \bar{k}^2 = 0, \quad (3.4)$$

$$p^2 = \bar{p}^2 = m^2, \quad (3.5)$$

$$r^2 = \bar{r}^2 = 0, \quad (3.6)$$

$$w^2 = \bar{w}^2 = M_W^2, \quad (3.7)$$

where m denotes the mass of the top quark and M_W denotes the mass of the W boson.

We define Mandelstam variables [40]

$$s \equiv (k + \bar{k})^2 = (p + \bar{p})^2 = 2k\bar{k} = 2p\bar{p} + 2m^2, \quad (3.8)$$

$$t \equiv (k - p)^2 = (\bar{k} - \bar{p})^2, \quad (3.9)$$

$$u \equiv (k - \bar{p})^2 = (\bar{k} - p)^2, \quad (3.10)$$

for use in the $e^+e^- \rightarrow t\bar{t}$ amplitudes. The relation

$$s + t + u = 2m^2 \quad (3.11)$$

follows from conservation of four-momentum.

In the centre of mass frame of the e^+e^- pair, that is the laboratory frame of a prospective e^+e^- linear collider, we choose the four momenta of the electron and positron to be

$$k^\mu = (E, 0, 0, -E), \quad (3.12)$$

$$\bar{k}^\mu = (E, 0, 0, E). \quad (3.13)$$

where $E = \sqrt{s}/2$, and we choose the four momenta of the t and \bar{t} quark to be

$$p^\mu = (E, \mathbf{p}), \quad (3.14)$$

$$\bar{p}^\mu = (E, -\mathbf{p}), \quad (3.15)$$

where

$$\mathbf{p} = (\sqrt{E^2 - m^2})(\sin \theta \cos \phi, \sin \theta \sin \phi, \cos \theta), \quad (3.16)$$

and θ is shown in Fig. 3.1. ϕ is an arbitrary azimuthal angle included for completeness.

In the rest frame of the decaying t quark, we choose

$$r = ((m^2 - M_W^2)/2m, \mathbf{p}_1) \quad (3.17)$$

$$w = ((m^2 + M_W^2)/2m, -\mathbf{p}_1) \quad (3.18)$$

where

$$\mathbf{p}_1 = \frac{m^2 - M_W^2}{2m} (\sin \theta_1 \cos \phi_1, \sin \theta_1 \sin \phi_1, \cos \theta_1), \quad (3.19)$$

and θ_1 is shown in Fig. 3.1. ϕ_1 is the azimuthal angle between the $e^+e^-t\bar{t}$ plane and the tbW^+ plane, with $\phi_1 = 0$ for the situation shown in Fig. 3.1 and increasing clockwise when looked at from the point of impact of the e^+ and e^- . In other words, ϕ increases in a right handed sense relative to the laboratory direction of motion of the t quark.

Similarly in the rest frame of the decaying \bar{t} quark we choose

$$\bar{\mathbf{r}} = ((m^2 - M_W^2)/2m, \mathbf{p}_2) \quad (3.20)$$

$$\bar{\mathbf{w}} = ((m^2 + M_W^2)/2m, -\mathbf{p}_2) \quad (3.21)$$

with

$$\mathbf{p}_2 = \frac{m^2 - M_W^2}{2m} (\sin \theta_2 \cos \phi_2, \sin \theta_2 \sin \phi_2, \cos \theta_2), \quad (3.22)$$

where θ_2 is shown in Fig. 3.1. ϕ_2 is defined as a right handed rotation with respect to the motion of the \bar{t} quark in the same way as ϕ_1 is defined with respect to the motion of the t quark.

3.3 Spinors

In this section we give the necessary expressions for the products of Dirac spinors of the electron and positron, top and anti-top quarks and b and \bar{b} quarks. We use the momentum choices of the previous section and the spinor conventions of [41]. A summary of these conventions is given in Appendix A. A spinor representing a particle is denoted u , and a spinor representing an antiparticle is denoted v . Their conjugates are denoted \bar{u} and \bar{v} .

We first consider the various types of products of two spinors that we will use in the rest of the chapter. There are exactly sixteen linearly independent products that can be formed from a pair of Dirac spinors, known as bilinear covariants [42]. Any product of gamma matrices sandwiched between two spinors can be reduced to a linear combination of these bilinear covariants together with some combination of metric or Levi-Civita tensors by the method of Fierz projection [43]. The bilinear covariants of two Dirac spinors ψ and $\bar{\psi}$ are usually grouped as follows:

product	name
$\bar{\psi}\psi$	scalar,
$\bar{\psi}\gamma^\mu\psi$	current <i>or</i> vector,
$\bar{\psi}\sigma^{\mu\nu}\psi$	tensor,
$\bar{\psi}\gamma^\mu\gamma^5\psi$	axial current <i>or</i> axial vector,
$\bar{\psi}\gamma^5\psi$	pseudoscalar.

However, more naturally occurring objects are linear combinations of these bilinears which have definite chiralities. Defining the chirality projection operators

$$\mathcal{P}_\pm = \frac{1}{2}(1 \pm \gamma^5) \quad (3.23)$$

where γ^5 is the totally anticommuting gamma matrix, we denote the combinations of current and axial current $\bar{\psi}\gamma^\mu\mathcal{P}_-\psi$ and $\bar{\psi}\gamma^\mu\mathcal{P}_+\psi$ left- and right-handed currents, and the combinations of scalar and pseudoscalar $\bar{\psi}\mathcal{P}_-\psi$ and $\bar{\psi}\mathcal{P}_+\psi$ we denote left- and right-handed scalars.

Non-zero scalar, pseudoscalar and tensor products cannot be formed from spinors that represent massless particles. These types of product involve a flip of helicity between the two spinors, but helicity is exactly conserved for interactions of massless fermions. Since the electron is approximately massless, the only non-zero spinor product which the e^+ and e^- spinors can form is a left- or right-handed current. This current is

$$j_\alpha^\mu \equiv \bar{v}(e^+)\gamma^\mu\mathcal{P}_\alpha u(e^-) = 2E(0, -1, i\alpha, 0) \quad (3.24)$$

where $\alpha = \pm 1$ is the chirality, which for the massless electron is identical to its helicity.

Since the top and anti-top are massive, they can form non-zero scalar products. The non-zero scalar products of the t and \bar{t} spinors are

$$S_\alpha \equiv \bar{u}(t)\mathcal{P}_\alpha v(\bar{t}) = \begin{cases} \alpha & \sigma & \bar{\sigma} & | \\ \hline + & + & + & | (E - |\mathbf{p}|)e^{-i\phi} \\ + & - & - & | (E + |\mathbf{p}|)e^{i\phi} \\ - & + & + & | -(E + |\mathbf{p}|)e^{-i\phi} \\ - & - & - & | -(E - |\mathbf{p}|)e^{i\phi} \end{cases} \quad (3.25)$$

where σ and $\bar{\sigma}$ denote the helicity of t and \bar{t} respectively.

The currents formed from the t and \bar{t} spinors are

$$J_\alpha^\mu \equiv \bar{u}(t)\gamma^\mu\mathcal{P}_\alpha v(\bar{t}) = \begin{cases} \alpha & \sigma & \bar{\sigma} & | \\ \hline + & + & + & | me^{-i\phi}(1, \hat{\mathbf{p}}), \\ + & + & - & | (E + |\mathbf{p}|)(0, \hat{\mathbf{v}} + i\hat{\mathbf{w}}), \\ + & - & + & | (E - |\mathbf{p}|)(0, \hat{\mathbf{v}} - i\hat{\mathbf{w}}), \\ + & - & - & | me^{i\phi}(1, -\hat{\mathbf{p}}), \\ - & + & + & | -me^{-i\phi}(1, -\hat{\mathbf{p}}), \\ - & + & - & | (E - |\mathbf{p}|)(0, \hat{\mathbf{v}} + i\hat{\mathbf{w}}), \\ - & - & + & | (E + |\mathbf{p}|)(0, \hat{\mathbf{v}} - i\hat{\mathbf{w}}), \\ - & - & - & | -me^{i\phi}(1, \hat{\mathbf{p}}), \end{cases} \quad (3.26)$$

where σ and $\bar{\sigma}$ are as defined after (3.25), and we have defined vectors

$$\hat{\mathbf{p}} = (\sin\theta \cos\phi, \sin\theta \sin\phi, \cos\theta), \quad (3.27)$$

$$\hat{\mathbf{v}} = (\cos\theta \cos\phi, \cos\theta \sin\phi, -\sin\theta), \quad (3.28)$$

$$\hat{\mathbf{w}} = (\sin\phi, -\cos\phi, 0). \quad (3.29)$$

It is easy to see that

$$\hat{\mathbf{p}} \cdot \hat{\mathbf{p}} = \hat{\mathbf{v}} \cdot \hat{\mathbf{v}} = \hat{\mathbf{w}} \cdot \hat{\mathbf{w}} = 1, \quad (3.30)$$

$$\hat{\mathbf{p}} \cdot \hat{\mathbf{v}} = \hat{\mathbf{p}} \cdot \hat{\mathbf{w}} = \hat{\mathbf{v}} \cdot \hat{\mathbf{w}} = 0, \quad (3.31)$$

that is, $\hat{\mathbf{p}}$, $\hat{\mathbf{v}}$ and $\hat{\mathbf{w}}$ form an orthonormal triad of vectors.

In addition to the current and scalar product of the t and \bar{t} spinors, the tensor product

$$\Sigma^{\mu\nu} \equiv \bar{u}(t)\sigma^{\mu\nu}v(\bar{t}) \quad (3.32)$$

also occurs in our calculation. It is possible to rewrite this tensor product in terms of currents, scalars and momenta by using equations of motion, as is shown in [43], but we find that it is simpler not to. The explicit forms of the tensor products are relatively straightforward, as can be seen from (3.35), whereas their expansion into currents and scalars is in general lengthy. In our calculation, it turns out that $\sigma^{\mu\nu}$ always occurs in combination with the Levi-Civita tensor $\epsilon_{\alpha\beta\mu\nu}\sigma^{\mu\nu}$. Therefore it is easiest to use the relation

$$\epsilon_{\alpha\beta\mu\nu}\sigma^{\mu\nu} = \frac{i}{2}\sigma_{\alpha\beta}\gamma^5 \quad (3.33)$$

to eliminate the need for contracting the Levi-Civita tensor. We therefore define a new product

$$\Sigma_5^{\mu\nu} \equiv \bar{u}(t)\sigma^{\mu\nu}\gamma^5v(\bar{t}). \quad (3.34)$$

The six independent values of this tensor are

$$\Sigma_5^{\mu\nu} = \left\{ \begin{array}{cc|cc} \sigma & \bar{\sigma} & (01, 02, 03) & (23, 31, 12) \\ + & + & 2me^{-i\phi}\hat{\mathbf{p}} & 0 \\ + & - & 2E(\hat{\mathbf{v}} + i\hat{\mathbf{w}}) & 2|\mathbf{p}|(i\hat{\mathbf{v}} - \hat{\mathbf{w}}) \\ - & + & 2E(\hat{\mathbf{v}} - i\hat{\mathbf{w}}) & 2|\mathbf{p}|(i\hat{\mathbf{v}} + \hat{\mathbf{w}}) \\ - & - & -2me^{i\phi}\hat{\mathbf{p}} & 0 \end{array} \right. \quad (3.35)$$

where σ and $\bar{\sigma}$ are as defined after (3.25), and (01,02,03) and (23,31,12) represent triplets of values of $\mu\nu$. These six cover all the linearly independent components of the σ tensor.

It is interesting to note that the tensor products occur only in the expansion of the $e^+e^- \rightarrow t\bar{t}$ box diagram. A tensor product of two spinors transforms under Lorentz transformations as a spin 2 representation of the Lorentz group. The tensor product terms arise in the calculation of $e^+e^- \rightarrow t\bar{t}$ box diagrams because two spin one bosons pass between the $t\bar{t}$ pair and the e^+e^- pair. Such products cannot occur, for instance, when a single spin one boson is exchanged between e^+e^- and $t\bar{t}$.

The final set of currents and spinors that we require are those for the processes $t \rightarrow bW^+$ and $\bar{t} \rightarrow \bar{b}W^-$. For the decay $t \rightarrow bW^+$ we define

$$S_{1\alpha} \equiv \bar{u}(b)\mathcal{P}_\alpha u(t) = \sqrt{m^2 - M_W^2} \left\{ \begin{array}{ccc|c} \alpha & \sigma(b) & \sigma(t) & \\ + & - & + & c_1 \\ + & - & - & s_1 \\ - & + & + & s_1^* \\ - & + & - & -c_1 \end{array} \right. \quad (3.36)$$

$$\begin{aligned}
J_{1\alpha}^\mu &\equiv \bar{u}(b)\gamma^\mu\mathcal{P}_\alpha u(t) = \sqrt{m^2 - M_W^2} \\
&\times \left\{ \begin{array}{c|c} \alpha & \sigma(b) & \sigma(t) \\ \hline + & + & + \\ + & + & - \\ - & - & + \\ - & - & - \end{array} \right| \begin{array}{l} (s_1^*, c_1, -ic_1, -s_1^*), \\ (-c_1, -s_1^*, -is_1^*, -c_1), \\ (c_1, s_1, -is_1, -c_1), \\ (s_1, c_1, ic_1, -s_1), \end{array} \end{array} \quad (3.37)
\end{aligned}$$

where we have defined $c_1 \equiv \cos(\theta_1/2)$, $s_1 \equiv \sin(\theta_1/2)e^{i\phi_1}$ and $s_1^* \equiv \sin(\theta_1/2)e^{-i\phi_1}$, with those scalars and currents which are zero due to the approximate masslessness of the b quark omitted, and where $\sigma(t)$ and $\sigma(b)$ represent the helicity of the top quark and the b quark respectively.

For the equivalent \bar{t} decay,

$$S_{2\alpha} \equiv \bar{v}(\bar{t})\mathcal{P}_\alpha v(\bar{t}) = \sqrt{m^2 - M_W^2} \left\{ \begin{array}{c|c} \alpha & \sigma(b) & \sigma(t) \\ \hline + & + & - \\ + & - & - \\ - & + & + \\ - & - & + \end{array} \right| \begin{array}{l} c_2 \\ s_2 \\ s_2^* \\ -c_2 \end{array} \quad (3.38)$$

$$\begin{aligned}
J_{2\alpha}^\mu &\equiv \bar{v}(\bar{b})\gamma^\mu\mathcal{P}_\alpha v(\bar{t}) = \sqrt{m^2 - M_W^2} \\
&\times \left\{ \begin{array}{c|c} \alpha & \sigma(b) & \sigma(t) \\ \hline + & + & - \\ + & - & - \\ - & + & + \\ - & - & + \end{array} \right| \begin{array}{l} (-c_2, -s_2, is_2, -c_2) \\ (-s_2, -c_2, -ic_2, s_2) \\ (-s_2^*, -c_2, ic_2, s_2^*) \\ (c_2, s_2^*, -is_2^*, c_2) \end{array} \end{array} \quad (3.39)
\end{aligned}$$

where $c_2 \equiv \cos(\theta_2/2)$, $s_2 \equiv \sin(\theta_2/2)e^{i\phi_2}$ and $s_2^* \equiv \sin(\theta_2/2)e^{-i\phi_2}$, are the relevant scalar and current products of the \bar{t} and \bar{b} spinors.

3.4 Tree level amplitudes

Since we have made the approximation that the top quark is on shell, the tree level amplitude is simply the product of the helicity amplitudes for top quark production and decay. The amplitude for production of $t\bar{t}$ from e^+e^- collisions via Z boson exchange is

$$\begin{aligned}
\mathcal{M}_{\text{tree}}^Z &= g_Z^2 [(\frac{1}{2} - s_W^2)(\frac{2}{3}s_W^2 - \frac{1}{2})j_- \cdot J_- - s_W^2(\frac{2}{3}s_W^2 - \frac{1}{2})j_+ \cdot J_- \\
&+ \frac{2}{3}s_W^2(\frac{1}{2} - s_W^2)j_- \cdot J_+ - \frac{2}{3}s_W^4 j_+ \cdot J_+] / (s - M_Z^2 + i\epsilon) \end{array} \quad (3.40)$$

where $s_W \equiv \sin\theta_W$ is the sine of the Weinberg weak mixing angle, and the amplitude for production by photon exchange is

$$\mathcal{M}_{\text{tree}}^\gamma = e^2 [j_- \cdot J_- + j_+ \cdot J_- + j_- \cdot J_+ + j_+ \cdot J_+] / (s + i\epsilon) \quad (3.41)$$

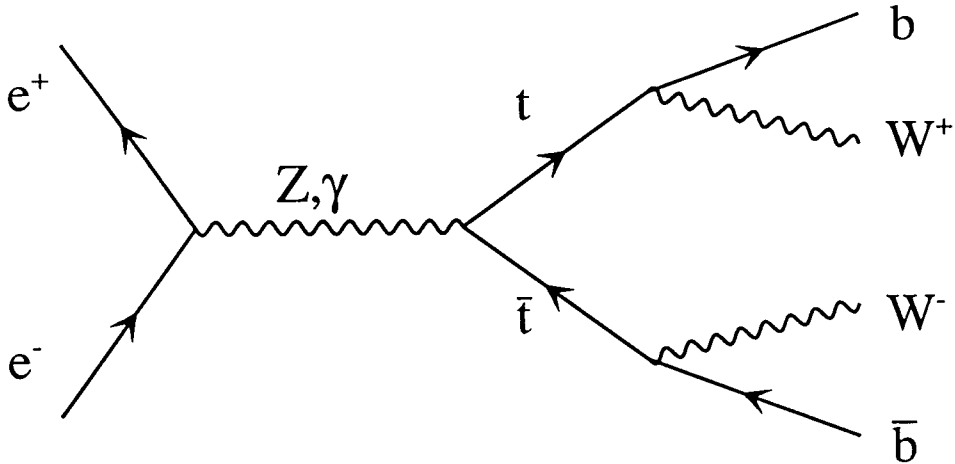


Figure 3.2: The Feynman diagram for $e^+e^- \rightarrow t\bar{t} \rightarrow bW^+ \bar{b}W^-$ at tree level

where e is the charge of the proton. We do not need to consider scalar exchange diagrams since scalars cannot couple to the massless electron pair.

The tree level amplitudes for top quark and anti-top quark decay are

$$\mathcal{M}_{\text{tree}}^{tbW} = J_1 \cdot \epsilon^*(W^+), \quad (3.42)$$

$$\mathcal{M}_{\text{tree}}^{\bar{t}bW} = J_2 \cdot \epsilon^*(W^-), \quad (3.43)$$

where $\epsilon(W^\pm)$ is the wavefunction of the emitted W^\pm boson. We neglect diagrams where the W is replaced by a scalar boson by approximating that the W is produced on its mass shell. We insert the t and \bar{t} propagator factors

$$D_t = \frac{1}{p^2 - m_t^2 + im_t\Gamma_t} \quad (3.44)$$

$$\bar{D}_t = \frac{1}{\bar{p}^2 - m_t^2 + im_t\Gamma_t} \quad (3.45)$$

The total tree level amplitude, summed over the helicities of unobserved particles, is then

$$\mathcal{M}_{\text{tree}} = \sum_{\sigma(t,\bar{t},b,\bar{b})=\pm} (\mathcal{M}_{\text{tree}}^Z + \mathcal{M}_{\text{tree}}^\gamma) D_t \mathcal{M}(t \rightarrow bW^+) \bar{D}_t \mathcal{M}(\bar{t} \rightarrow \bar{b}W^-). \quad (3.46)$$

We sum over the helicity of the b quark, because the polarisation of the b quark is virtually unobservable due to hadronisation effects, and because the decay amplitude is dominated by the left handed b quark.

3.5 Box diagrams

In this section we consider the evaluation of the three Feynman graphs shown in Fig. 3.3 which form part of the radiative corrections to $e^+e^- \rightarrow t\bar{t}$. In the first subsection we present the amplitudes, and carry out algebraic simplification and integration over the unfixed momentum of the loop expressing the results in terms of the one loop form factors of [36]. In the second subsection we give the reduction of these form factors to scalar one loop integrals.

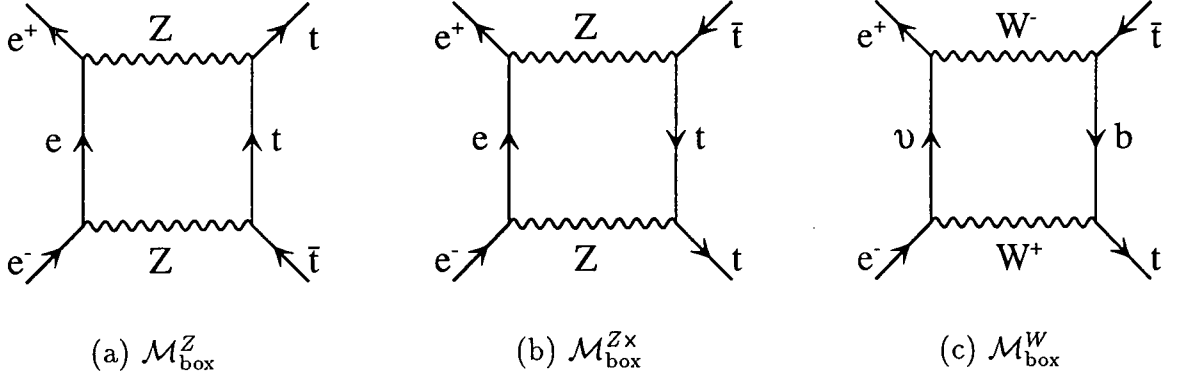


Figure 3.3: The three box diagrams.

3.5.1 Amplitudes

The three diagrams of Fig. 3.3 can be divided into two categories, depending on the direction of the arrow on the internal quark line relative to the direction of the arrow on the internal lepton line. We call these the uncrossed and crossed box diagrams. The conventions we use to describe these two categories are shown in Fig. 3.4.

We label the unfixed momentum in the loop by q as shown in Fig. 3.4.

The amplitudes for diagrams (a), (b) and (c) of Fig. 3.3 are

$$\begin{aligned} \mathcal{M}_{\text{box}}^Z &= g_Z^4 \int \frac{d^4 q}{(2\pi)^4 d} [\gamma_\mu \not{q} \gamma_\nu \left(\left(\frac{1}{2} - s_W^2\right)^2 \mathcal{P}_- + s_W^4 \mathcal{P}_+ \right)]_e \\ &\times \left[\left(\frac{2}{3} s_W^2 - \frac{1}{2}\right)^2 \gamma^\mu \not{Q} \gamma^\nu \mathcal{P}_- + \left(\frac{2}{3} s_W^2\right)^2 \gamma^\mu \not{Q} \gamma^\nu \mathcal{P}_+ + \left(\frac{2}{3} s_W^2\right) \left(\frac{2}{3} s_W^2 - \frac{1}{2}\right) m \gamma^\mu \gamma^\nu \right]_t, \end{aligned} \quad (3.47)$$

$$\begin{aligned} \mathcal{M}_{\text{box}}^{Zx} &= g_Z^4 \int \frac{d^4 q}{(2\pi)^4 d} [\gamma_\mu \not{q} \gamma_\nu \left(\left(\frac{1}{2} - s_W^2\right)^2 \mathcal{P}_- + s_W^4 \mathcal{P}_+ \right)]_e \\ &\times \left[\left(\frac{2}{3} s_W^2 - \frac{1}{2}\right)^2 \gamma^\nu \not{Q} \gamma^\mu \mathcal{P}_- + \left(\frac{2}{3} s_W^2\right)^2 \gamma^\nu \not{Q} \gamma^\mu \mathcal{P}_+ + \left(\frac{2}{3} s_W^2\right) \left(\frac{2}{3} s_W^2 - \frac{1}{2}\right) m \gamma^\nu \gamma^\mu \right]_t, \end{aligned} \quad (3.48)$$

$$\mathcal{M}_{\text{box}}^W = g^4 \int \frac{d^4 q}{(2\pi)^4 d} [\gamma_\mu \not{q} \gamma_\nu \mathcal{P}_-]_e [\gamma^\nu \not{Q} \gamma^\mu \mathcal{P}_-]_t, \quad (3.49)$$

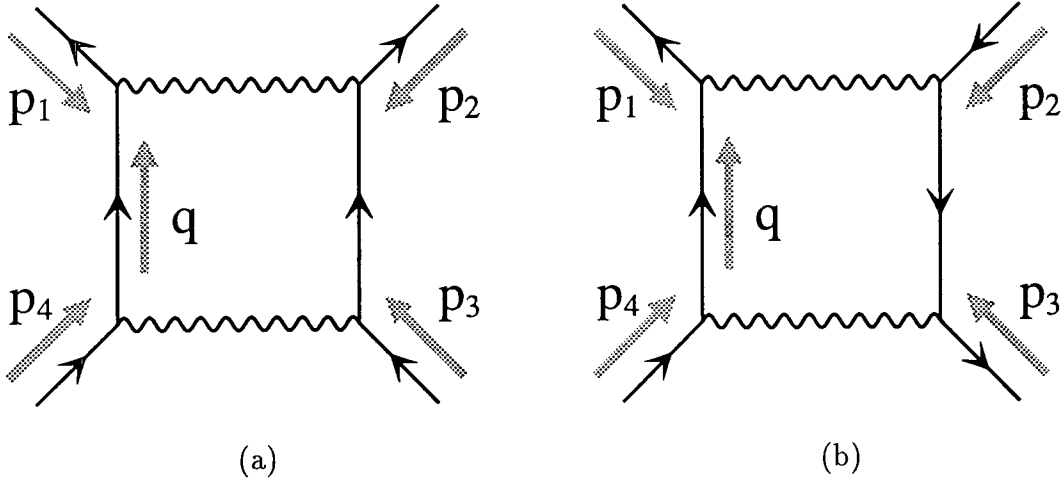


Figure 3.4: The uncrossed (a) and crossed (b) box diagrams with their assignments of momenta.

where

$$d = q^2((q + p_1)^2 - M^2)((q + p_1 + p_2)^2 - m'^2)((q - p_4)^2 - M^2), \quad (3.50)$$

with $m' = m$, $M = M_Z$, the mass of the Z boson, for $\mathcal{M}_{\text{box}}^Z$ and $\mathcal{M}_{\text{box}}^{Z\times}$ and $m' = 0$, $M = M_W$ for $\mathcal{M}_{\text{box}}^W$, and we abbreviate

$$\bar{u}(e^-) \dots v(e^+) \equiv [\dots]_e, \quad (3.51)$$

$$\bar{v}(t) \dots u(\bar{t}) \equiv [\dots]_t, \quad (3.52)$$

and define

$$Q \equiv q + p_1 + p_2 \quad (3.53)$$

for compactness.

We first consider how to carry out the gamma matrix algebra necessary to simplify the expressions for the amplitudes (3.47-3.49). We wish to simplify terms of the form

$$[\gamma_\mu \not{p}_\nu \mathcal{P}_\alpha]_e [\gamma^\mu \not{Q} \gamma^\nu \mathcal{P}_\beta]_t, \quad (3.54)$$

$$[\gamma_\mu \not{p}_\nu \mathcal{P}_\alpha]_e [\gamma^\mu \gamma^\nu]_t, \quad (3.55)$$

from the uncrossed box diagram, and

$$[\gamma_\mu \not{p}_\nu \mathcal{P}_\alpha]_e [\gamma^\nu \not{Q} \gamma^\mu \mathcal{P}_\beta]_t, \quad (3.56)$$

$$[\gamma_\mu \not{p}_\nu \mathcal{P}_\alpha]_e [\gamma^\nu \gamma^\mu]_t, \quad (3.57)$$

from the crossed box diagrams.

Using the identities [44]

$$\gamma^\mu \gamma^\rho \gamma^\nu = g^{\mu\rho} \gamma^\nu - g^{\mu\nu} \gamma^\rho + g^{\nu\rho} \gamma^\mu - i\epsilon^{\mu\rho\nu\lambda} \gamma_\lambda \gamma^5, \quad (3.58)$$

$$\epsilon^{\mu\rho\nu\lambda} \epsilon_{\alpha\beta\nu\lambda} = \delta_\alpha^\mu \delta_\beta^\rho - \delta_\beta^\mu \delta_\alpha^\rho, \quad (3.59)$$

(3.54) and (3.56) can be simplified to

$$[\gamma_\mu \not{q} \gamma_\nu \mathcal{P}_\alpha]_e [\gamma^\mu \not{Q} \gamma^\nu \mathcal{P}_\alpha]_t = 4q \cdot Q j_\alpha \cdot J_\alpha, \quad (3.60)$$

$$[\gamma_\mu \not{q} \gamma_\nu \mathcal{P}_\alpha]_e [\gamma^\mu \not{Q} \gamma^\nu \mathcal{P}_{-\alpha}]_t = 4j_\alpha \cdot Q J_{-\alpha} \cdot q, \quad (3.61)$$

$$[\gamma_\mu \not{q} \gamma_\nu \mathcal{P}_\alpha]_e [\gamma^\nu \not{Q} \gamma^\mu \mathcal{P}_\alpha]_t = 4j_\alpha \cdot Q J_\alpha \cdot q, \quad (3.62)$$

$$[\gamma_\mu \gamma_\rho \gamma_\nu \mathcal{P}_\alpha]_e [\gamma^\nu \gamma_\tau \gamma^\mu \mathcal{P}_{-\alpha}]_t = 4q \cdot Q j_\alpha \cdot J_{-\alpha}. \quad (3.63)$$

Relations of this type were first derived in [45].

In order to deal with (3.55) and (3.57) we need further relations. Using the gamma matrix identities [42]

$$\gamma_\mu \gamma_\nu = g_{\mu\nu} - i\sigma_{\mu\nu}, \quad (3.64)$$

$$\epsilon^{\mu\nu\rho\sigma} \sigma_{\sigma\rho} = 2i\sigma^{\mu\nu} \gamma^5, \quad (3.65)$$

$$\gamma^5 \mathcal{P}_\alpha = \alpha \mathcal{P}_\alpha, \quad (3.66)$$

and (3.58), it is straightforward to derive

$$[\gamma_\mu \not{q} \gamma_\nu \mathcal{P}_\alpha]_e [\gamma^\mu \gamma^\nu]_t = -2j_\alpha \cdot q (S_+ + S_-) + 2i\alpha j_{\alpha\lambda} \Sigma_5^{\rho\lambda} q_\rho, \quad (3.67)$$

$$[\gamma_\mu \not{q} \gamma_\nu \mathcal{P}_\alpha]_e [\gamma^\nu \gamma^\mu]_t = -2j_\alpha \cdot q (S_+ + S_-) - 2i\alpha j_{\alpha\lambda} \Sigma_5^{\rho\lambda} q_\rho. \quad (3.68)$$

We now consider the integration over the unfixed momentum q . The concepts of this method are explained in Appendix D and here we merely give the formulas without derivation or detailed explanation. We first consider the case of a general box diagram with the momentum assignments of Fig. 3.4. We introduce the notation

$$D_{(0,\mu,\mu\nu)} = \int \frac{d^4 q (1, q_\mu, q_\mu q_\nu)}{i\pi^2 d}. \quad (3.69)$$

D^μ and $D^{\mu\nu}$ are expanded into Lorentz invariant functions D_{1i} , $i = 1, 2, 3$,

$$D^\mu = p_1^\mu D_{11} + p_2^\mu D_{12} + p_3^\mu D_{13} \quad (3.70)$$

and D_{2i} , $i = 1, \dots, 7$,

$$\begin{aligned} D^{\mu\nu} &= p_1^\mu p_1^\nu D_{21} + p_2^\mu p_2^\nu D_{22} + p_3^\mu p_3^\nu D_{23} \\ &+ p_1^{\{\mu} p_2^{\nu\}} D_{24} + p_1^{\{\mu} p_3^{\nu\}} D_{25} + p_2^{\{\mu} p_3^{\nu\}} D_{26} + g^{\mu\nu} D_{27} \end{aligned} \quad (3.71)$$

where $a^{\{\mu b^\nu\}} \equiv a^\mu b^\nu + a^\nu b^\mu$, respectively.

The various factors of the formulas (3.60-3.63) and (3.67-3.68) become

$$\int \frac{d^4 q}{d} q \cdot Q j_\alpha \cdot J_\beta = \frac{1}{2}(C_0^{(234)} + C_0^{(124)} + (f_1 + f_2)D_0)j_\alpha \cdot J_\beta, \quad (3.72)$$

$$\begin{aligned} \int \frac{d^4 q}{d} j_\alpha \cdot Q J_\beta \cdot q &= j_\alpha \cdot p_2 J_\beta \cdot (p_1(D_{12} + D_{24}) + p_2 D_{22} + p_3 D_{26}) \\ &+ j_\alpha \cdot p_3 J_\beta \cdot (p_1 D_{25} + p_2(D_{13} + D_{22} + D_{26}) + p_3 D_{23}) \\ &+ j_\alpha \cdot J_\beta D_{27}, \end{aligned} \quad (3.73)$$

$$\int \frac{d^4 q}{d} j_\alpha \cdot q S_\beta = j_\alpha \cdot (p_2 D_{12} + p_3 D_{13}) S_\beta, \quad (3.74)$$

$$\int \frac{d^4 q}{d} j_{\alpha\lambda} \Sigma_\beta^{\mu\lambda} q_\mu = j_{\alpha\lambda} \Sigma_\beta^{\mu\lambda} (p_{1\mu} D_{11} + p_{2\mu} D_{12} + p_{3\mu} D_{13}), \quad (3.75)$$

where f_1 and f_2 are defined in (3.102) and (3.103) respectively, and $C_0^{(ijk)}$ is defined in (3.91).

Inserting these expressions into the amplitudes $\mathcal{M}_{\text{box}}^{Z, Z^\times, W}$ gives

$$\begin{aligned} \mathcal{M}_{\text{box}}^Z &= \frac{8}{9} j_+ \cdot J_+ s_W^8 ((f_1 + f_2)D_0 + C_0^{(234)} + C_0^{(124)}) \\ &+ 4j_+ \cdot J_- s_W^4 [\frac{2}{3}s_W^2 - \frac{1}{2}]^2 D_{27} \\ &+ 4j_+ \cdot pJ_- \cdot \bar{k} s_W^4 [\frac{2}{3}s_W^2 - \frac{1}{2}]^2 (-D_{12} - D_{24} + D_{25}) \\ &+ 4mj_+ \cdot pS_+ s_W^4 [\frac{2}{3}s_W^2 - \frac{1}{2}] (\frac{1}{3}s_W^2 (D_{12} - D_{13}) + [\frac{2}{3}s_W^2 - \frac{1}{2}] (D_{23} - D_{26})) \\ &+ 4mj_+ \cdot pS_- s_W^4 [\frac{2}{3}s_W^2 - \frac{1}{2}] (\frac{1}{3}s_W^2 (D_{12} - D_{13}) - [\frac{2}{3}s_W^2 - \frac{1}{2}] (D_{13} + D_{26})) \\ &+ \frac{16}{9} j_- \cdot J_+ [\frac{1}{2} - s_W^2]^2 s_W^4 D_{27} \\ &+ 2j_- \cdot J_- [\frac{1}{2} - s_W^2]^2 [\frac{2}{3}s_W^2 - \frac{1}{2}]^2 ((f_1 + f_2)D_0 + C_0^{(234)} + C_0^{(124)}) \\ &+ \frac{16}{9} j_- \cdot pJ_+ \cdot \bar{k} [\frac{1}{2} - s_W^2]^2 s_W^4 (-D_{12} - D_{24} + D_{25}) \\ &+ \frac{4}{3} mj_- \cdot pS_+ [\frac{1}{2} - s_W^2]^2 s_W^2 (-\frac{4}{3}s_W^2 (D_{13} + D_{26}) + [\frac{2}{3}s_W^2 - \frac{1}{2}] (D_{12} - D_{13})) \\ &+ \frac{4}{3} mj_- \cdot pS_- [\frac{1}{2} - s_W^2]^2 s_W^2 (\frac{4}{3}s_W^2 (D_{23} - D_{26}) + [\frac{2}{3}s_W^2 - \frac{1}{2}] (D_{12} - D_{13})) \\ &+ \frac{8i}{3} \Sigma_{5\mu\lambda} j_+^\lambda m s_W^6 [\frac{2}{3}s_W^2 - \frac{1}{2}] [\bar{k}^\mu D_{11} - \bar{p}^\mu D_{12} - p^\mu D_{13}] \\ &- \frac{8i}{3} \Sigma_{5\mu\lambda} j_-^\lambda m [\frac{1}{2} - s_W^2]^2 s_W^2 [\frac{2}{3}s_W^2 - \frac{1}{2}] [\bar{k}^\mu D_{11} - \bar{p}^\mu D_{12} - p^\mu D_{13}] \end{aligned} \quad (3.76)$$

for the uncrossed box with Z boson exchange,

$$\begin{aligned} \mathcal{M}_{\text{box}}^{Z^\times} &= \frac{16}{9} s_W^8 j_+ \cdot J_+ D_{27} \\ &+ 2j_+ \cdot J_- s_W^4 [\frac{2}{3}s_W^2 - \frac{1}{2}]^2 ((f_1 + f_2)D_0 + C_0^{(234)} + C_0^{(124)}) \\ &+ \frac{16}{9} j_+ \cdot \bar{p} J_+ \cdot \bar{k} s_W^8 (-D_{12} - D_{24} + D_{25}) \\ &+ \frac{4}{3} j_+ \cdot \bar{p} S_+ m s_W^6 (\frac{4}{3}s_W^2 (-D_{23} + D_{26}) + [\frac{2}{3}s_W^2 - \frac{1}{2}] (D_{12} - D_{13})) \end{aligned}$$

$$\begin{aligned}
& + \frac{4}{3}j_+ \cdot \bar{p}S_- m s_W^6 \left(\frac{4}{3}s_W^2(D_{13} + D_{26}) + \left[\frac{2}{3}s_W^2 - \frac{1}{2} \right] (D_{12} - D_{13}) \right) \\
& + \frac{8}{9}j_- \cdot J_+ \left[\frac{1}{2} - s_W^2 \right]^2 s_W^4 \left((f_1 + f_2)D_0 + C_0^{(234)} + C_0^{(124)} \right) \\
& + 4j_- \cdot J_- \left[\frac{1}{2} - s_W^2 \right]^2 \left[\frac{2}{3}s_W^2 - \frac{1}{2} \right]^2 D_{27} \\
& + 4j_- \cdot \bar{p}J_- \cdot \bar{k} \left[\frac{1}{2} - s_W^2 \right]^2 \left[\frac{2}{3}s_W^2 - \frac{1}{2} \right]^2 (-D_{12} - D_{24} + D_{25}) \\
& + 4j_- \cdot \bar{p}S_+ m \left[\frac{1}{2} - s_W^2 \right]^2 \left[\frac{2}{3}s_W^2 - \frac{1}{2} \right] \left(\frac{1}{3}s_W^2(D_{12} - D_{13}) + \left[\frac{2}{3}s_W^2 - \frac{1}{2} \right] (D_{13} + D_{26}) \right) \\
& + 4j_- \cdot \bar{p}S_- m \left[\frac{1}{2} - s_W^2 \right]^2 \left[\frac{2}{3}s_W^2 - \frac{1}{2} \right] \left(\frac{1}{3}s_W^2(D_{12} - D_{13}) + \left[\frac{2}{3}s_W^2 - \frac{1}{2} \right] (D_{26} - D_{23}) \right) \\
& - \frac{8i}{3}\Sigma_{5\mu\lambda}j_+^\lambda m s_W^6 \left[\frac{2}{3}s_W^2 - \frac{1}{2} \right] (\bar{k}^\mu D_{11} - p^\mu D_{12} - \bar{p}^\mu D_{13}) \\
& + \frac{8i}{3}\Sigma_{5\mu\lambda}j_-^\lambda m \left[\frac{1}{2} - s_W^2 \right]^2 s_W^2 \left[\frac{2}{3}s_W^2 - \frac{1}{2} \right] (\bar{k}^\mu D_{11} - p^\mu D_{12} - \bar{p}^\mu D_{13})
\end{aligned} \tag{3.77}$$

for the crossed box with Z boson exchange, and

$$\begin{aligned}
\mathcal{M}_{\text{box}}^W &= \frac{g^4}{4\pi^4} \left(j_- \cdot J_- D_{27} + j_- \cdot \bar{p} \left[J_- \cdot \bar{k} (D_{25} - D_{12} - D_{24}) \right. \right. \\
&\quad \left. \left. + m(S_+(D_{13} + D_{26}) + S_-(D_{26} - D_{23})) \right] \right)
\end{aligned} \tag{3.78}$$

for the crossed box with W boson exchange. The relation

$$j_\pm \cdot p_3 = -j_\pm \cdot p_2 \tag{3.79}$$

was used to reduce the number of terms in these expressions.

3.5.2 Reduction of the D_{1n} and D_{2n} form factors

In this subsection we present a complete reduction of the form factor D_{2i} , $i = 1, \dots, 7$ of (3.71), and the factors D_{1i} , $i = 1, \dots, 3$ of (3.70) into the three types of scalar integrals D_0 , C_0 , and B_0 defined below. For explanation of the concepts of this reduction please refer to Appendix D.

In this section we present the reduction for the case of the uncrossed box diagram, so that we have identified

$$p_1 = \bar{k}, \tag{3.80}$$

$$p_2 = -p, \tag{3.81}$$

$$p_3 = -\bar{p}, \tag{3.82}$$

$$p_4 = k. \tag{3.83}$$

The corresponding expressions for the crossed box are identical to those presented here except for the interchange of u with t . This is because for the crossed box,

$$p_2 = -\bar{p}, \tag{3.84}$$

$$p_3 = -p, \tag{3.85}$$

and so the association of p_2 and p_3 with the four momentum of top and anti-top quarks is exchanged.

Defining the propagator factors

$$P_1 \equiv q^2, \quad (3.86)$$

$$P_2 \equiv (q + p_1)^2 - M^2, \quad (3.87)$$

$$P_3 \equiv (q + p_1 + p_2)^2 - m'^2, \quad (3.88)$$

$$P_4 \equiv (q - p_4)^2 - M^2, \quad (3.89)$$

where m' and M are defined immediately after (3.50), we define the scalar integral functions

$$B_0^{(ij)} = \int \frac{d^D q}{P_i P_j}, \quad (3.90)$$

$$C_0^{(ijk)} = \int \frac{d^4 q}{P_i P_j P_k}, \quad (3.91)$$

$$D_0 = \int \frac{d^4 q}{P_1 P_2 P_3 P_4}. \quad (3.92)$$

The analytic solutions to these integrals have been published in [37, 46] and are also available as numerical computer programs [47] thus we do not present their lengthy analytic forms here. The B_0 integral is carried out using dimensional regularisation, over $D = 4 - 2\epsilon$ dimensions, because it is ultraviolet divergent. The ultraviolet divergence appears as a pole in $1/\epsilon$ as the limit of $D = 4$ dimensions is taken. However, the B_0 functions always appear in pairs such that the poles cancel each other out, because the D_{2i} and D_{1i} functions are ultraviolet finite, as can be seen from counting the number of factors of q in numerator and denominator.

The factors D_{2i} and D_{1i} are reduced to B_0 , C_0 and D_0 by

$$\begin{pmatrix} D_{21} \\ D_{24} \\ D_{25} \end{pmatrix} = \frac{1}{2} X^{-1} \begin{pmatrix} C_{11}^{(134)} + C_0^{(234)} + f_1 D_{11} + D_{27} \\ C_{11}^{(124)} - C_{11}^{(134)} + f_2 D_{11} \\ C_{11}^{(123)} - C_{11}^{(124)} + f_3 D_{11} \end{pmatrix} \quad (3.93)$$

$$\begin{pmatrix} D_{24} \\ D_{22} \\ D_{26} \end{pmatrix} = \frac{1}{2} X^{-1} \begin{pmatrix} C_{11}^{(134)} - C_{11}^{(234)} + f_1 D_{12} \\ C_{12}^{(124)} - C_{11}^{(134)} + f_2 D_{12} + D_{27} \\ C_{12}^{(123)} - C_{12}^{(124)} + f_3 D_{12} \end{pmatrix} \quad (3.94)$$

$$\begin{pmatrix} D_{25} \\ D_{26} \\ D_{23} \end{pmatrix} = \frac{1}{2} X^{-1} \begin{pmatrix} C_{12}^{(134)} - C_{12}^{(234)} + f_1 D_{13} \\ C_{12}^{(124)} - C_{12}^{(134)} + f_2 D_{13} \\ -C_{12}^{(124)} + f_3 D_{13} + D_{27} \end{pmatrix} \quad (3.95)$$

$$D_{27} = m_1^2 D_0 + \frac{1}{2} C_0^{(234)} - \frac{1}{2} (f_1 D_{11} + f_2 D_{12} + f_3 D_{13}) \quad (3.96)$$

$$\begin{pmatrix} D_{11} \\ D_{12} \\ D_{13} \end{pmatrix} = \frac{1}{2} X^{-1} \begin{pmatrix} C_0^{(134)} - C_0^{(234)} + f_1 D_0 \\ C_0^{(124)} - C_0^{(134)} + f_2 D_0 \\ C_0^{(123)} - C_0^{(124)} + f_3 D_0 \end{pmatrix}, \quad (3.97)$$

$$\begin{pmatrix} C_{11}^{(123)} \\ C_{12}^{(123)} \end{pmatrix} = \frac{1}{(u-m^2)^2} \begin{pmatrix} 2m^2 & u-m^2 \\ u-m^2 & 0 \end{pmatrix} \begin{pmatrix} B_0^{(13)} - B_0^{(23)} + f_1 C_0^{(123)} \\ B_0^{(12)} - B_0^{(13)} + f_2 C_0^{(123)} \end{pmatrix} \quad (3.98)$$

$$\begin{pmatrix} C_{11}^{(124)} \\ C_{12}^{(124)} \end{pmatrix} = \frac{1}{(s+2m^2)^2} \begin{pmatrix} 2s & s+2m^2 \\ s+2m^2 & 0 \end{pmatrix} \times \begin{pmatrix} B_0^{(14)} - B_0^{(24)} + f_1 C_0^{(124)} \\ B_0^{(12)} - B_0^{(14)} + (f_2 + f_3) C_0^{(124)} \end{pmatrix} \quad (3.99)$$

$$\begin{pmatrix} C_{11}^{(134)} \\ C_{12}^{(134)} \end{pmatrix} = \frac{1}{4um^2 - (t-m^2)^2} \begin{pmatrix} 2m^2 & t-m^2 \\ t-m^2 & 2u \end{pmatrix} \times \begin{pmatrix} B_0^{(14)} - B_0^{(34)} + (f_1 + f_2) C_0^{(134)} \\ B_0^{(13)} - B_0^{(14)} + f_3 C_0^{(134)} \end{pmatrix} \quad (3.100)$$

$$\begin{pmatrix} C_{11}^{(234)} \\ C_{12}^{(234)} \end{pmatrix} = \frac{1}{s(s+4m^2)} \begin{pmatrix} -2m^2 & s+2m^2 \\ s+2m^2 & -2m^2 \end{pmatrix} \times \begin{pmatrix} B_0^{(23)} - B_0^{(34)} + f_2 C_0^{(234)} \\ B_0^{(24)} - B_0^{(23)} + f_3 C_0^{(234)} \end{pmatrix} \quad (3.101)$$

where

$$f_1 = m_2^2 - m_1^2, \quad (3.102)$$

$$f_2 = m_3^2 - m_2^2 - u, \quad (3.103)$$

$$f_3 = m_4^2 - m_3^2 + u. \quad (3.104)$$

and

$$X^{-1} = \frac{1}{s(tu-m^4)} \begin{pmatrix} -s^2 + 4sm^2 & s(t+m^2) & s(u+m^2) \\ s(t+m^2) & -(t-m^2)^2 & (u-m^2)(t-m^2) \\ s(u+m^2) & (u-m^2)(t-m^2) & -(u-m^2)^2 \end{pmatrix}. \quad (3.105)$$

As was claimed, the B_0 integrals appear in pairs such that their ultraviolet poles cancel.

3.6 Vertex diagrams

In this section we consider the one loop Feynman diagrams with three external legs attached to the loop that arise in the process $e^+e^- \rightarrow t\bar{t} \rightarrow bW^+ \bar{b}W^-$. We denote this type of diagram a vertex diagram because it is a radiative correction to a tree level vertex. Each vertex where these radiative corrections arise in top quark production and decay is shown in Fig. 3.5 as a

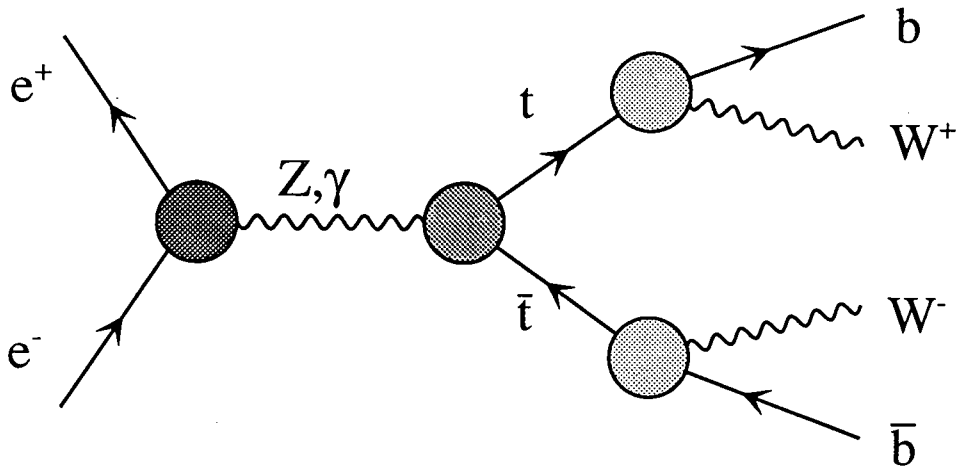


Figure 3.5: The locations of the vertex radiative corrections to $e^+e^- \rightarrow t\bar{t} \rightarrow bW^+ \bar{b}W^-$ shown by shaded circles on the Feynman diagram

shaded circle. The first subsection of this section deals with the general framework in which these radiative corrections have been calculated, and the following three subsections deal with each of the vertices shown in Fig. 3.5 by shaded circles. The radiative corrections to $t \rightarrow bW^+$ and $\bar{t} \rightarrow \bar{b}W^-$ vertices are dealt with as one case since they are CP conjugates, and so the expression for one is directly related to the other at the one loop level of the standard model where no CP violating amplitudes appear in the process.

3.6.1 Vertices with external on-shell fermions

For any given scattering process, in each order of perturbation theory, only a finite number of Feynman diagrams can connect the initial and final particles. In this section, we show that for one loop radiative corrections to vertices involving a pair of external fermions and a spin one boson there are only six types of Feynman graph that need to be considered in standard model calculations. This is because in the standard model, within any particular choice of gauge, the essential structure of Feynman rules for interactions are independent of all properties of the particles except their spin, up to multiplicative coupling factors. That is, almost all Feynman rules, even when they involve completely different particles with only their intrinsic angular momentum in common, have almost identical structures.

For example, the term of the Standard model Lagrangian density representing interaction of a Higgs boson with two W bosons

$$gM_W W^{+\mu} W_{\mu}^- H$$

and the term representing interaction of a positively charged Goldstone boson χ^+ with a W^- and a Z boson

$$\frac{s_W^2 g g_Z}{2} Z^\mu W_\mu^- \chi^+$$

(see appendix C for notation) have identical relationships between the different fields of the same spin, up to a multiplicative factor, and thus lead to almost identical Feynman rules.

We take advantage of this similarity between Feynman diagrams involving different particles with the same spin, to give complete solutions for one loop diagrams involving two external fermions and one external boson. Six spin structures can occur with the particles of the standard model. These six cases are shown in Fig. 3.6. We call these diagrams generic Feynman diagrams, and the resulting expressions corresponding to each diagram, we call generic expressions. These generic expressions we denote by $\Delta_{a,b,c,d,e,f}^\mu$, where μ is the four vector index that is contracted with the propagator of the vector boson, and a, b, c, d, e and f correspond to Fig. 3.6(a),(b),...,(f).

In order to evaluate these generic expressions, we choose the following conventions. We calculate in the t'Hooft-Feynman gauge, in which the propagator of the gauge boson is proportional to the metric tensor. In this gauge Feynman graphs that do not occur in the unitary gauge, involving scalar Goldstone bosons, must be included in some calculations. However, the simple structure of the gauge boson propagator facilitates loop level calculations. At each vertex of two fermions and a boson we expand the Feynman rule into left and right handed chirality couplings. In order to use our formalism, in the standard model a vector boson coupling to fermions should be expressed in the form

$$\gamma^\mu (h_{V+} \mathcal{P}_+ + h_{V-} \mathcal{P}_-), \quad (3.106)$$

and a scalar boson coupling to fermions should be expressed in the form

$$h_{S+} \mathcal{P}_+ + h_{S-} \mathcal{P}_-, \quad (3.107)$$

where $h_{S,V\pm}$ are coupling constants. For particles such as the photon or the Higgs boson, whose interactions do not distinguish between left and right chirality states, clearly $h_+ = h_-$.

Our generic expressions for the vertex radiative corrections also include the two external spinors, in the form of current or scalar spinor products, plus a free Lorentz index μ which is contracted with the appropriate free index of the propagator of the external vector boson.

The most general expression which can be constructed from Lorentz invariance for a two fermion and one gauge boson vertex contains six independent Lorentz invariant form factors. This can be seen from counting the number of possible helicity states of the three external

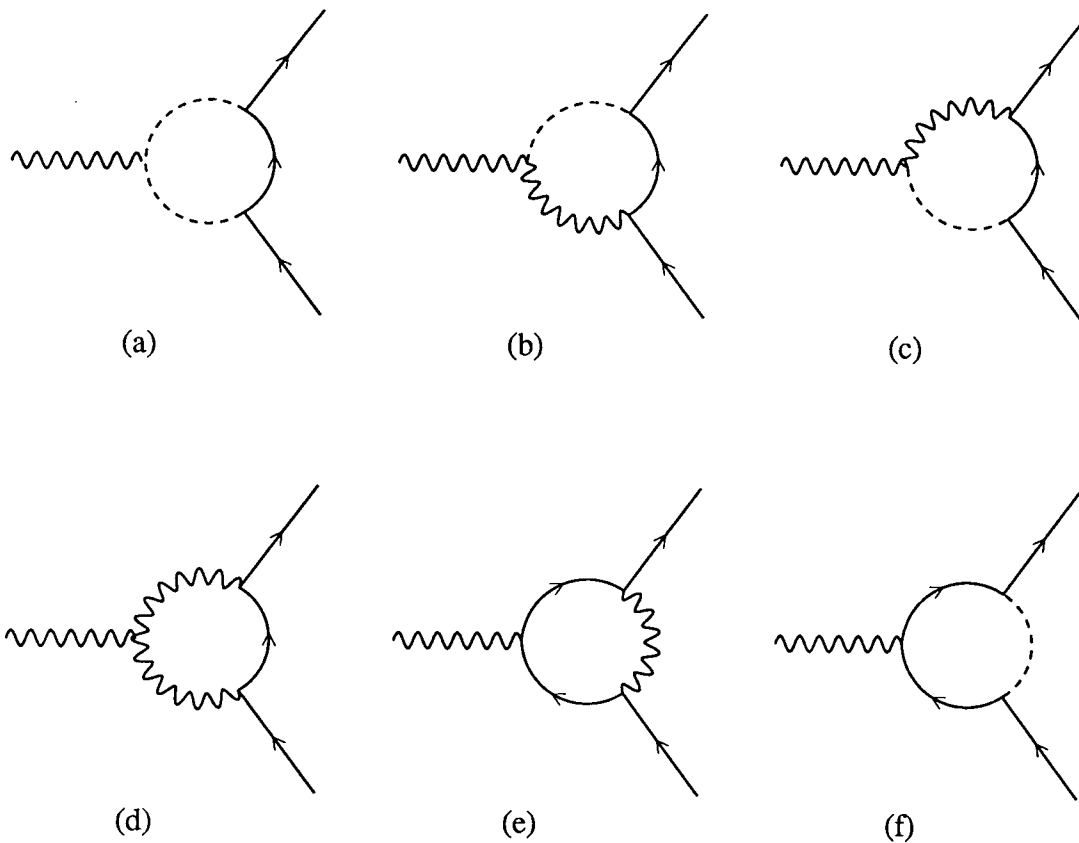


Figure 3.6: The six possible structures of one loop vertex occurring in the standard model

particles. There are three allowed helicity states for a massive vector boson, and these are multiplied by a factor of two from the two possible fermion pair helicity states. Two of the four states of fermion pair helicity cannot occur, since interaction of a fermion pair with a spin one boson (or a conserved current) can never involve a helicity flip. We choose to expand in chiral spinor currents and scalar product states, that is

$$J_\alpha^\mu \equiv \bar{\psi} \gamma^\mu \mathcal{P}_\alpha \psi \quad \text{and} \quad S_\alpha \equiv \bar{\psi} \mathcal{P}_\alpha \psi, \quad (3.108)$$

where ψ is the spinor with the arrow pointing into the vertex, and $\bar{\psi}$ is the spinor with the arrow pointing away from the vertex. (Note that these are different definitions for J_α and S_α from those used in the rest of the chapter where they denote t and \bar{t} spinor products.) The most general expansion of the vertex in terms of these chiral currents and scalars is

$$\Delta_{\text{general}}^\mu = f_1 J_+^\mu + f_2 J_-^\mu + f_3 p^\mu S_+ + f_4 p^\mu S_- + f_5 \bar{p}^\mu S_+ + f_6 \bar{p}^\mu S_-, \quad (3.109)$$

where we denote the momenta of ψ and $\bar{\psi}$ by p and \bar{p} respectively. (Again these definitions of p and \bar{p} are different from those of the rest of the chapter where they denote t and \bar{t} momenta.) which as stated contains six multiplicative factors. We denote their particle numbers $\eta = \pm 1$ and $\bar{\eta} = \pm 1$, depending on whether the spinors ψ and $\bar{\psi}$ respectively represent particle or antiparticle, the helicities of ψ and $\bar{\psi}$ by σ and $\bar{\sigma}$ respectively, and masses by m and \bar{m} respectively. Our choice of conventions is shown in Fig. 3.7. Using the Dirac equation,

$$p \cdot J_\alpha = m\eta S_{-\alpha}, \quad (3.110)$$

$$\bar{p} \cdot J_\alpha = \bar{m}\bar{\eta} S_\alpha. \quad (3.111)$$

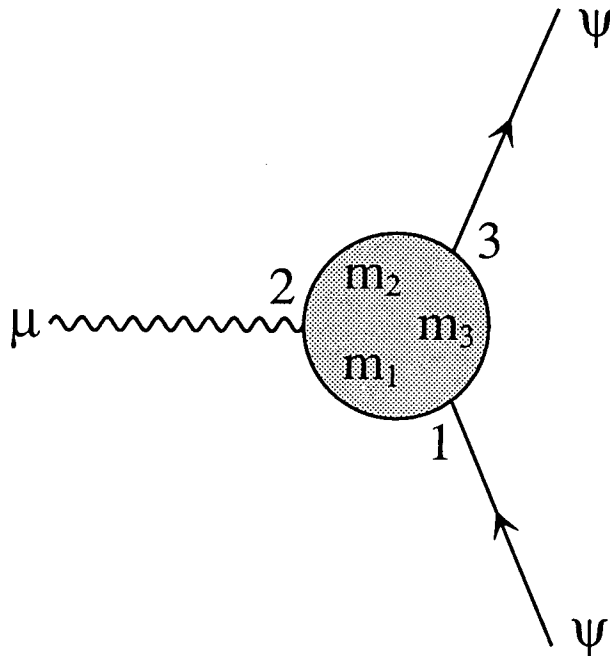


Figure 3.7: Conventions for the vertex one loop diagrams

We now consider integration over the unfixed momentum of the loop. We define integrals

$$C_{(0,\mu,\mu\nu)} = \int \frac{d^n k}{i\pi^2} \frac{\{1, k_\mu, k_\mu k_\nu\}}{P_1 P_2 P_3} \quad (3.112)$$

where the propagator factors

$$P_1 = (k + p)^2 - m_1^2 + i\epsilon, \quad (3.113)$$

$$P_2 = (k + \bar{p})^2 - m_2^2 + i\epsilon, \quad (3.114)$$

$$P_3 = k^2 - m_3^2 + i\epsilon. \quad (3.115)$$

The integrals C^μ and $C^{\mu\nu}$ are expanded using the formalism of [36] into Lorentz invariant form factors as follows

$$C^\mu = p^\mu C_{11} + \bar{p}^\mu C_{12} \quad (3.116)$$

$$C^{\mu\nu} = p^\mu p^\nu C_{21} + \bar{p}^\mu \bar{p}^\nu C_{22} + (p^\mu \bar{p}^\nu + p^\nu \bar{p}^\mu) C_{23} + g^{\mu\nu} C_{24} \quad (3.117)$$

We will consider the reduction of the terms C_{2n} , $n = 1, \dots, 4$, C_{1n} , $n = 1, 2$ after the final expressions for the Δ functions have been given.

Writing down the Feynman rules for the six structures of Fig. 3.6 gives

$$\begin{aligned} \Delta_a^\mu &= \frac{-h_2}{(2\pi)^4} \int \frac{d^D k}{P_1 P_2 P_3} \bar{\psi}(h_{3-} \mathcal{P}_- + h_{3+} \mathcal{P}_+) (-\not{k} + m_3) (h_{1-} \mathcal{P}_- + h_{1+} \mathcal{P}_+) \psi \\ &\times (-2k^\mu - p^\mu - \bar{p}^\mu) \end{aligned} \quad (3.118)$$

$$\Delta_b^\mu = \frac{h_2}{(2\pi)^4} \int \frac{d^D k}{P_1 P_2 P_3} \bar{\psi}(h_{3-} \mathcal{P}_- + h_{3+} \mathcal{P}_+) (-\not{k} + m_3) \gamma^\mu (h_{1-} \mathcal{P}_- + h_{1+} \mathcal{P}_+) \psi \quad (3.119)$$

$$\Delta_c^\mu = \frac{h_2}{(2\pi)^4} \int \frac{d^D k}{P_1 P_2 P_3} \bar{\psi} \gamma^\mu (h_{3-} \mathcal{P}_- + h_{3+} \mathcal{P}_+) (-\not{k} + m_3) (h_{1-} \mathcal{P}_- + h_{1+} \mathcal{P}_+) \psi \quad (3.120)$$

$$\begin{aligned} \Delta_d^\mu &= \frac{-h_2}{(2\pi)^4} \int \frac{d^D k}{P_1 P_2 P_3} \bar{\psi} \gamma_\rho (h_{3-} \mathcal{P}_- + h_{3+} \mathcal{P}_+) (-\not{k} + m_3) \gamma_\sigma (h_{1-} \mathcal{P}_- + h_{1+} \mathcal{P}_+) \psi \\ &\times (g^{\sigma\rho} (-2k^\mu - p^\mu - \bar{p}^\mu) + g^{\mu\rho} (k^\sigma - p^\sigma + 2\bar{p}^\sigma) + g^{\mu\sigma} (k^\rho + 2p^\rho - \bar{p}^\rho)) \end{aligned} \quad (3.121)$$

$$\begin{aligned} \Delta_e^\mu &= \frac{1}{(2\pi)^4} \int \frac{d^D k}{P_1 P_2 P_3} \bar{\psi} \gamma^\alpha (h_{3-} \mathcal{P}_- + h_{3+} \mathcal{P}_+) (\not{k} + \not{p} + m_2) \gamma^\mu (h_{2-} \mathcal{P}_- + h_{2+} \mathcal{P}_+) \\ &\times (\not{k} + \not{p} + m_1) \gamma_\alpha (h_{1-} \mathcal{P}_- + h_{1+} \mathcal{P}_+) \psi \end{aligned} \quad (3.122)$$

$$\begin{aligned} \Delta_f^\mu &= \frac{-1}{(2\pi)^4} \int \frac{d^D k}{P_1 P_2 P_3} \bar{\psi} (h_{3-} \mathcal{P}_- + h_{3+} \mathcal{P}_+) (\not{k} + \not{p} + m_2) \gamma^\mu (h_{2-} \mathcal{P}_- + h_{2+} \mathcal{P}_+) \\ &\times (\not{k} + \not{p} + m_1) (h_{1-} \mathcal{P}_- + h_{1+} \mathcal{P}_+) \psi \end{aligned} \quad (3.123)$$

where Δ_a corresponds to the Feynman diagram of Fig. 3.6(a) and so on, and the couplings $h_{1,2,3}$ refer to vertices 1, 2 and 3 respectively in Fig. 3.7. The couplings $h_{1,2,3\pm}$ should be read directly from the Lagrangian (all other numerical factors have been taken into account). The arguments to $\Delta_{a,b,c,d}$ are

$$(\eta, \bar{\eta}, p, \bar{p}, m, \bar{m}, h_{1+}, h_{1-}, h_2, h_{3+}, h_{3-}, m_1, m_2, m_3). \quad (3.124)$$

In the case of $\Delta_{e,f}$ the only difference is that there are left- and right-chirality h_2 couplings h_{2-} and h_{2+} instead of simply h_2 in these arguments, because for diagrams Fig. 3.6(e) and (f) there is a fermion-boson coupling at vertex 2 instead of a boson-boson-boson coupling.

We first insert the integral expansions (3.116) and (3.117). We then contract all the dummy indices, applying gamma matrix relations in D dimensions [48] and the Dirac equation

of motion for the on-shell spinors $\psi, \bar{\psi}$. The generic expressions are

$$\begin{aligned}\Delta_a^\mu &= \frac{-h_2}{16\pi^2} \sum_{\alpha=\pm} \left(2h_{-\alpha\alpha} C_{24} J_\alpha^\mu + \{h_{-\alpha\alpha} \bar{\eta} \bar{m} (C_{12} + 2C_{22}) - h_{\alpha\alpha} m_3 (C_0 + 2C_{12})\} S_\alpha \bar{p}^\mu \right. \\ &+ \left. \{h_{-\alpha\alpha} \bar{\eta} \bar{m} (C_{12} + 2C_{23}) - h_{\alpha\alpha} m_3 (C_0 + 2C_{11})\} S_\alpha p^\mu \right. \\ &+ \left. h_{-\alpha\alpha} \eta m \{(C_{11} + 2C_{23}) \bar{p}^\mu + (C_{11} + 2C_{21}) p^\mu\} S_{-\alpha} \right) \quad (3.125)\end{aligned}$$

$$\begin{aligned}\Delta_b^\mu &= \frac{h_2}{16\pi^2} \sum_{\alpha=\pm} \left(\{h_{-\alpha\alpha} m_3 C_0 - h_{\alpha\alpha} \bar{\eta} \bar{m} C_{12}\} J_\alpha^\mu \right. \\ &+ \left. h_{\alpha\alpha} \eta m C_{11} J_{-\alpha}^\mu - 2h_{\alpha\alpha} C_{11} S_\alpha p^\mu \right) \quad (3.126)\end{aligned}$$

$$\begin{aligned}\Delta_c^\mu &= \frac{h_2}{16\pi^2} \sum_{\alpha=\pm} \left(\{h_{-\alpha\alpha} \bar{\eta} \bar{m} C_{12} + h_{\alpha\alpha} m_3 C_0\} J_\alpha^\mu \right. \\ &- \left. h_{-\alpha\alpha} \eta m C_{11} J_{-\alpha}^\mu - 2h_{-\alpha\alpha} C_{12} S_\alpha \bar{p}^\mu \right) \quad (3.127)\end{aligned}$$

$$\begin{aligned}\Delta_d^\mu &= \frac{-h_2}{16\pi^2} \sum_{\alpha=\pm} \left(-3h_{-\alpha\alpha} C_0 m_3 \{\bar{\eta} \bar{m} J_\alpha^\mu + \eta m J_{-\alpha}^\mu\} - 3\eta \bar{\eta} m \bar{m} h_{\alpha\alpha} (C_{11} + C_{12}) J_{-\alpha}^\mu \right. \\ &- h_{\alpha\alpha} \{m^2 (C_{11} + 2C_{21}) + \bar{m}^2 (C_{12} + 2C_{22}) + 4p \cdot \bar{p} (C_{11} + C_{12} + C_{23}) + 12C_{24} + 2\} J_\alpha^\mu \\ &+ 2h_{\alpha\alpha} \bar{\eta} \bar{m} \{(C_{11} + C_{12} - 2C_{23}) p^\mu - (C_{12} + 2C_{22}) \bar{p}^\mu\} S_\alpha \\ &+ 2h_{\alpha\alpha} \eta m \{(C_{11} + C_{12} - 2C_{23}) \bar{p}^\mu - (C_{11} + 2C_{21}) p^\mu\} S_{-\alpha} \\ &- \left. 6h_{-\alpha\alpha} m_3 \{C_{11} p^\mu + C_{12} \bar{p}^\mu\} S_\alpha \right) \quad (3.128)\end{aligned}$$

$$\begin{aligned}\Delta_e^\mu &= \frac{-1}{16\pi^2} \sum_{\alpha=\pm} \left(4h_{\alpha\alpha\alpha} (C_0 + C_{11} + C_{12} + C_{23}) (p \cdot \bar{p} J_\alpha^\mu - \bar{\eta} \bar{m} S_\alpha p^\mu - \eta m S_{-\alpha} \bar{p}^\mu) \right. \\ &+ 2h_{\alpha\alpha\alpha} \left[m^2 (C_{11} + C_{21}) + \bar{m}^2 (C_{12} + C_{22}) + 2C_{24} + 1 \right] J_\alpha^\mu - 2h_{\alpha-\alpha\alpha} m_1 m_2 C_0 J_\alpha^\mu \\ &+ 2h_{\alpha\alpha\alpha} \eta \bar{\eta} m \bar{m} (C_0 + C_{11} + C_{12}) J_{-\alpha}^\mu - 4h_{\alpha\alpha\alpha} \eta m (C_{11} + C_{21}) S_{-\alpha} p^\mu \\ &+ 4 \{h_{-\alpha-\alpha\alpha} m_1 (C_0 + C_{12}) + h_{-\alpha\alpha\alpha} m_2 C_{12} - h_{\alpha\alpha\alpha} \bar{\eta} \bar{m} (C_{12} + C_{22})\} S_\alpha \bar{p}^\mu \\ &+ \left. 4 \{h_{-\alpha-\alpha\alpha} m_1 C_{11} + h_{-\alpha\alpha\alpha} m_2 (C_0 + C_{11})\} S_\alpha p^\mu \right) \quad (3.129)\end{aligned}$$

$$\begin{aligned}\Delta_f^\mu &= \frac{1}{16\pi^2} \sum_{\alpha=\pm} \left(\{h_{-\alpha\alpha\alpha} m_1 m_2 C_0 + \bar{\eta} \bar{m} [h_{\alpha\alpha\alpha} m_1 (C_0 + C_{12}) - h_{\alpha-\alpha\alpha} m_2 C_{12}]\} J_\alpha^\mu \right. \\ &- h_{-\alpha-\alpha\alpha} \left\{ m^2 (C_{11} + C_{21}) + \bar{m}^2 (C_{12} + C_{22}) + 2p \cdot \bar{p} C_{23} + 2C_{24} + \frac{1}{2} \right\} J_\alpha^\mu \\ &+ \eta m \{h_{\alpha-\alpha\alpha} m_2 (C_0 + C_{11}) - h_{\alpha\alpha\alpha} m_1 C_{11} + h_{-\alpha-\alpha\alpha} \bar{\eta} \bar{m} (C_0 + C_{11} + C_{12})\} J_{-\alpha}^\mu \\ &+ 2h_{-\alpha-\alpha\alpha} \{\bar{\eta} \bar{m} [(C_{12} + C_{22}) \bar{p}^\mu + C_{23} p^\mu] S_\alpha + \eta m [C_{23} \bar{p}^\mu + (C_{11} + C_{21}) p^\mu] S_{-\alpha}\} \\ &+ \left. 2 \{h_{\alpha\alpha\alpha} m_1 C_{11} p^\mu + h_{\alpha-\alpha\alpha} m_2 C_{12} \bar{p}^\mu\} S_\alpha \right) \quad (3.130)\end{aligned}$$

where we abbreviate

$$h_{\alpha\beta} \equiv h_{1\alpha}h_{3\beta}, \quad (3.131)$$

$$h_{\alpha\beta\gamma} \equiv h_{1\alpha}h_{2\beta}h_{3\gamma}, \quad (3.132)$$

with the chiralities $\alpha, \beta, \gamma = \pm 1$.

Notice that the function C_{24} , which is the only ultraviolet divergent C_{2n} function, as can be seen from counting powers of momentum in (3.117), only occurs in conjunction with J_{\pm}^{μ} , the term proportional to the tree level vertex.

We now turn to the reduction of the C_{2n} and C_{1n} functions into simpler integrals. We first define

$$B_{(0,\mu)}(i, j) = \int \frac{d^n k \{1, k_{\mu}\}}{i\pi^2 P_i P_j}. \quad (3.133)$$

where the P_i , $i = 1, 2, 3$, are defined in (3.113-3.115) Then

$$B^{\mu}(1, 2) = -p^{\mu} B_0(1, 2) + (\bar{p}^{\mu} - p^{\mu}) B_1(1, 2), \quad (3.134)$$

$$B^{\mu}(1, 3) = -p^{\mu} (B_0(1, 3) + B_1(1, 3)), \quad (3.135)$$

$$B^{\mu}(2, 3) = \bar{p}^{\mu} B_1(2, 3). \quad (3.136)$$

We can reduce all C_{1n} and C_{2n} functions to C_0 , B_0 and B_1 functions by using

$$\begin{aligned} \begin{pmatrix} C_{11} \\ C_{12} \end{pmatrix} &= \frac{1}{2} X^{-1} \begin{pmatrix} B_0(2, 3) - B_0(1, 2) + f_1 C_0 \\ B_0(1, 3) - B_0(1, 2) + f_2 C_0 \end{pmatrix}, \\ \begin{pmatrix} C_{21} \\ C_{23} \end{pmatrix} &= \frac{1}{2} X^{-1} \begin{pmatrix} B_0(1, 2) + B_1(1, 2) + f_1 C_{11} - 2C_{24} \\ B_1(1, 3) + B_0(1, 3) + B_1(1, 2) + f_2 C_{11} \end{pmatrix}, \\ \begin{pmatrix} C_{23} \\ C_{22} \end{pmatrix} &= \frac{1}{2} X^{-1} \begin{pmatrix} B_1(2, 3) - B_1(1, 2) + f_1 C_{12} \\ -B_1(1, 2) + f_2 C_{12} - 2C_{24} \end{pmatrix}, \\ C_{24} &= \frac{1}{4} + m_3^2 C_0 + \frac{1}{4} [B_0(1, 2) - f_1 C_{11} - f_2 C_{12}] \end{aligned} \quad (3.137)$$

where

$$X \equiv \begin{pmatrix} m^2 & p \cdot \bar{p} \\ p \cdot \bar{p} & \bar{m}^2 \end{pmatrix}, \quad f_1 \equiv m_1^2 - m_3^2 - m^2, \quad f_2 \equiv m_2^2 - m_3^2 - \bar{m}^2. \quad (3.138)$$

The complete analytic solution for the C_0 scalar integral has been published in [37] and a complete set of $B_{0,1}$ integrals can be found in [49].

With these generic expressions for the vertex diagrams, any standard model one loop vertex can be compactly expressed. We take advantage of this compactness to express all the vertex radiative corrections to $e^+ e^- \rightarrow t \bar{t}$ and $t \rightarrow bW$ in a very simple way.

3.6.2 e^+e^- vertex corrections

In this subsection we give the expressions for the radiative corrections to the vertex of the e^+e^- and the Z boson or photon, in the form of the Δ functions of the previous subsection.

Omitting the arguments involving the e^+e^- spinors in the Δ functions, $(1, -1, k, \bar{k}, 0, 0)$, which are the same for all cases, the amplitude from the e^+e^- vertex corrections is

$$\mathcal{M}_\Delta^{e^+e^-} \frac{2}{3} e (J_{-\mu} + J_{+\mu}) \frac{\Delta_\gamma^\mu}{q^2 + i\epsilon} + g_Z \left(\left(\frac{2}{3} s_W^2 - \frac{1}{2} \right) J_{-\mu} + \frac{2}{3} s_W^2 J_{+\mu} \right) \frac{\Delta_Z^\mu}{q^2 - M_Z^2 + i\epsilon} \quad (3.139)$$

where α is the chirality of the $t\bar{t}$ current.

	γ Z boson
	$\Delta_d^\mu(e\nu W; e; e\nu W; m_W, m_W, 0)$ $\Delta_d^\mu(e\nu W; g_Z; e\nu W; m_W, m_W, 0)$
	0 $\Delta_e^\mu(e\nu W; \nu\nu Z; e\nu W; 0, 0, m_W)$
	$\Delta_e^\mu(ee Z; ee\gamma; ee Z; 0, 0, m_Z)$ $\Delta_e^\mu(ee Z; ee Z; ee Z; 0, 0, m_Z)$

Table 3.1: Radiative corrections to e^+e^- vertex

The symbols which appear in the tables are

$$\begin{aligned} eeZ &= g_Z \left(\frac{1}{2} - s_W^2, -s_W^2 \right) \\ ee\gamma &= (e, e) \\ \nu\nu Z &= \left(-\frac{1}{2} g_Z, 0 \right) \\ e\nu W &= \left(-\frac{g}{\sqrt{2}}, 0 \right) \end{aligned}$$

where the first member of each pair refers to the left- and the second to the right-chirality couplings of the fermions.

$$s_W \equiv \sin \theta_W \quad (3.140)$$

is the Weinberg weak mixing angle, and further details of the notation for coupling constants are given in Appendix C.

3.6.3 $t\bar{t}$ vertex corrections

In this subsection we give complete expressions for the non-infrared divergent radiative corrections to the $t\bar{t}$ vertex, again in the Δ function formalism.

In Table 3.2 we show the Δ functions arising from each Feynman diagram shown. Similarly to Table 3.1 we omit the arguments involving the e^+e^- spinors in the Δ functions $(-1, 1, p, \bar{p}, m, m)$, which are the same for all cases. The symbols presented as arguments to the Δ functions in Table 3.2, Table 3.3 and Table 3.4 have the following meanings

$$tbW^+ = \left(-\frac{g}{\sqrt{2}}, 0\right) \quad (3.141)$$

$$ttZ = \left(\frac{2}{3}s_W^2 - \frac{1}{2}, \frac{2}{3}s_W^2\right) \quad (3.142)$$

$$bbZ = \left(\frac{1}{2} - \frac{1}{3}s_W^2, -\frac{1}{3}s_W^2\right) \quad (3.143)$$

$$tt\chi^3 = \left(\frac{im}{v}, -\frac{im}{v}\right) \quad (3.144)$$

$$tb\chi^+ = \left(\frac{i\sqrt{2}m}{v}, 0\right) \quad (3.145)$$

$$bt\chi^- = \left(0, -\frac{i\sqrt{2}m}{v}\right) \quad (3.146)$$

$$bb\gamma = \left(-\frac{1}{3}e, -\frac{1}{3}e\right) \quad (3.147)$$

$$tt\gamma = \left(\frac{2}{3}e, \frac{2}{3}e\right) \quad (3.148)$$

where the first and second members of each pair represent left- and right-chirality couplings of boson to fermion. The sums of the upper and lower sets of corrections are denoted Δ_γ^μ and Δ_Z^μ respectively. The total radiative correction is then

$$\mathcal{M}_\Delta^{t\bar{t}} = -e(j_{-\mu} + j_{+\mu})\frac{\Delta_\gamma^\mu}{q^2 + i\epsilon} + \left(\left(\frac{1}{2} - s_W^2\right)j_{-\mu} - s_W^2 j_{+\mu}\right)\frac{\Delta_Z^\mu}{q^2 - M_Z^2 + i\epsilon}. \quad (3.149)$$

3.6.4 tbW vertex corrections

In this subsection we give complete expressions for the electroweak radiative corrections to the tbW vertex. In this section we include the full soft photon radiative corrections. The soft photon corrections to the tbW vertex do not form a gauge invariant subset of the total set of diagrams, because there is no neutral external current. Thus the soft photon diagrams must be included to maintain gauge invariance, unlike the e^+e^- and $t\bar{t}$ vertices.

In Table 3.3 we show the full set of radiative corrections to the vertex $t \rightarrow bW^+$. Similarly to Table 3.1 we omit the arguments involving the e^+e^- spinors in the Δ functions $(1, 1, p, r, m, 0)$, which are the same for all the Δ functions of the table. The sum of these corrections we denote Δ_{tot}^μ .

In addition to these expressions, we also need to calculate the infrared divergent diagrams involving virtual photons. These are shown in Table 3.4. The dependence of the expressions for the radiative corrections of Table 3.3 on λ , the fictitious photon mass, and m_b , in the limit $\lambda \rightarrow 0$ and $m_b \rightarrow 0$, cancels against the dependence on λ in (3.150), such that the S-matrix does not contain infrared divergences, by the Kinoshita-Lee-Nauenberg theorem. Dependence on the mass of the b quark, denoted m_b , has been retained since there is an infrared collinear divergence associated with the massless limit $m_b = 0$. After summing the infrared divergent diagrams together in the S-matrix element, the massless limits $m_b \rightarrow 0$ and $\lambda \rightarrow 0$ can be taken.

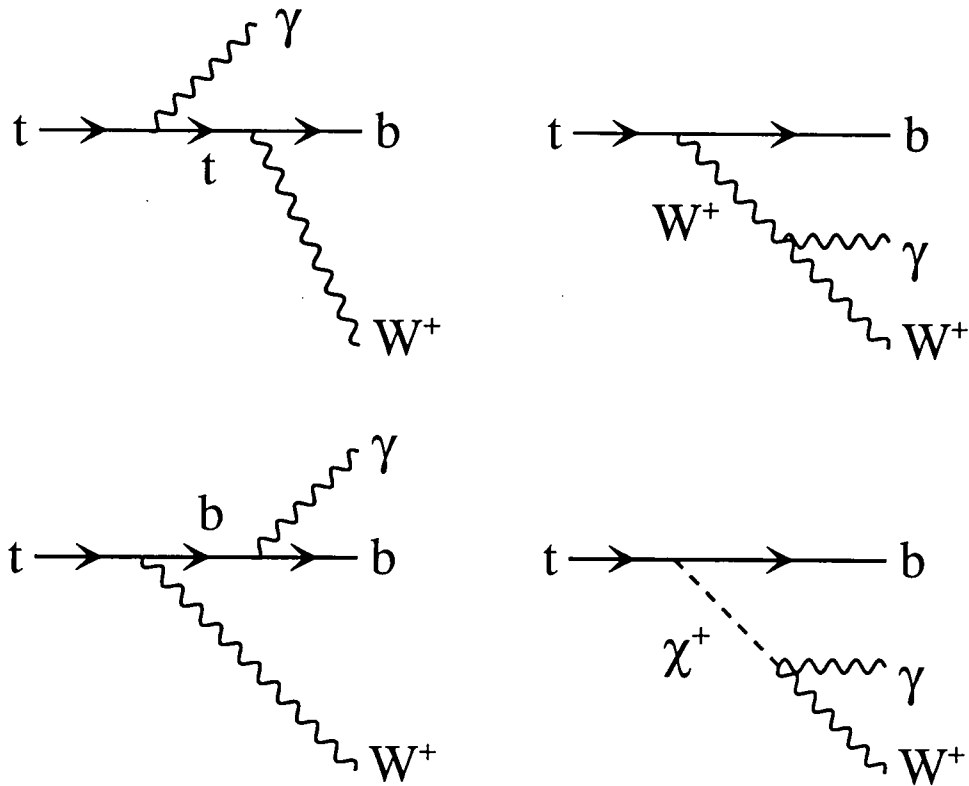


Figure 3.8: Soft photon radiative corrections to $t \rightarrow bW^+$.

The expressions for the photonic corrections of Fig. 3.8 are treated in the eikonal approximation, in which the soft photon momenta appearing in the numerators are neglected. Introducing the upper limit ω on the soft photon energy in the rest frame of the top quark, which may be regarded as the energy resolution of the experimental apparatus, the contri-

bution of the soft photon radiation can be computed by the strategy outlined in [37]. The amplitude is [32]

$$\begin{aligned}
\mathcal{M}_{\text{soft}}^{tbW} = & \frac{e^2 g}{(4\pi)^2 \sqrt{2}} J_{1-} \cdot \epsilon^*(W^+) \left[-2\left(\frac{2}{3}\right)^2 \left(\log \frac{2\omega}{\lambda} - 1 \right) \right. \\
& - 2\left(-\frac{1}{3}\right)^2 \left(\log \frac{2\omega}{\lambda} + \log \frac{mm_b}{m^2 - M_W^2} \right) \\
& - 2 \left(\log \frac{2\omega}{\lambda} + \frac{m^2 + M_W^2}{m^2 - M_W^2} \log \frac{M_W}{m} \right) \\
& + 2\left(\frac{2}{3}\right)\left(-\frac{1}{3}\right) \left(\log \frac{m^2 - M_W^2}{mm_b} \log \frac{2\omega}{\lambda} - \log^2 \frac{mm_b}{m^2 - M_W^2} - \frac{\pi^2}{4} + \frac{1}{2} \log^2 2 \right) \\
& - 2\left(-\frac{1}{3}\right) \left(2 \log \frac{m^2 - M_W^2}{M_W m_b} \log \frac{2\omega}{\lambda} - \log^2 \frac{mm_b}{m^2 - M_W^2} + \log^2 \frac{M_W}{m} \right. \\
& \left. + \text{Li}_2 \left(-\frac{m^2 - M_W^2}{M_W^2} \right) - \frac{\pi^2}{6} \right) \\
& \left. + \frac{4}{3} \frac{m_t^2 + M_W^2}{m^2 - M_W^2} \left(2 \log \frac{m}{M_W} \log \frac{2\omega}{\lambda} - \log^2 \frac{M_W}{m} - \text{Li}_2 \left(\frac{m^2 - M_W^2}{m^2} \right) \right) \right] \quad (3.150)
\end{aligned}$$

where $\epsilon^*(W^+)$ is the wavefunction of the outgoing W^+ boson and where Li_2 is the dilogarithm function

$$\text{Li}_2(x) = - \int_0^x dt \frac{\log(1-t)}{t}. \quad (3.151)$$

This real photon correction, and the corresponding cancellation between real and virtual photon amplitudes, actually appears at amplitude squared level. The expression (3.150) is in reality a factor that multiplies the tree level amplitude squared for the decay of the top quark without a soft photon, $\mathcal{M}_{\text{tree}}^{tbW}$, which has already been integrated over the phase space volume of the soft photon. It is here presented it as if it were a one loop correction to a tree level amplitude. This is because, as we will see in the final section, this term $\mathcal{M}_{\text{soft}}^{tbW}$ is multiplied only by the tree level amplitude anyway when we form the final cross section, and thus its actual contribution to the cross section is not affected by presenting it in this form. The advantage of this is that in the form (3.150), it is simple to show the cancellation between the real and virtual photon infrared divergences.

The overall helicity amplitude from the radiative correction diagrams is then

$$\mathcal{M}_{\Delta}^{tbW} = \Delta_{\text{tot}}^{\mu} \epsilon_{\mu}^*(W^+) + \frac{1}{2} \mathcal{M}_{\text{soft}}^{tbW} \quad (3.152)$$

where $\epsilon^*(W^+)$ is the wavefunction of the outgoing W^+ boson. This expression is free of infrared divergences in the limit $\lambda \rightarrow 0$ and $m_b \rightarrow 0$. The factor of $1/2$ before $\mathcal{M}_{\text{soft}}^{tbW}$ arises because both the total amplitude and its complex conjugate are added to the cross section as

interference terms with the tree level amplitude. Since $\mathcal{M}_{\text{soft}}^{tbW}$ is not really a loop amplitude (see the discussion above), we should not apply this double counting to it.

The $\bar{t}bW$ decay amplitudes are the CP conjugates of the tbW amplitudes. We can obtain them from the above results by a straightforward inversion of each Feynman diagram of Table 3.3, and by replacing the spinor products of (3.36) and (3.37) by those of (3.38) and (3.39) in the relevant Δ functions.

Thus we have complete radiative corrections to all vertex processes.

3.7 Self energy diagrams

By self energy diagrams we refer to radiative corrections to particle propagators. We first define the B functions in terms of which we express our results, and then give expressions for the gauge boson and fermion self energies to one loop order in the electroweak standard model.

Following Passarino and Veltman, [36], we define

$$A(m) = \int \frac{d^D k}{i\pi^2} \frac{1}{k^2 - m^2 + i\epsilon}, \quad (3.153)$$

$$\{B_0, B_\mu, B_{\mu\nu}\}(q; m_1, m_2) = \int \frac{d^D k}{i\pi^2} \frac{\{1, k_\mu, k_\mu k_\nu\}}{(k^2 - m_1^2 + i\epsilon)[(k+q)^2 - m_2^2 + i\epsilon]}, \quad (3.154)$$

$$B_\mu = q_\mu B_1, \quad (3.155)$$

$$B_{\mu\nu} = q_\mu q_\nu B_{21} + g_{\mu\nu} B_{22}. \quad (3.156)$$

Explanation of the concepts underlying this form factor expansion appears in Appendix D. We use the Bjorken and Drell metric [50] and so our definitions of the B functions differ from those of [36] by signs. The functions B_0 , B_1 and B_{21} are logarithmically divergent, and the functions A and B_{22} are quadratically divergent. In fact these two quadratically divergent functions always cancel in the way of the B_5 function defined in (3.160).

In order to make our expressions for self-energy corrections compact, we introduce the following four scalar B functions in addition to B_0 and B_1 above;

$$B_2(q^2; m_1, m_2) = B_{21}(q^2; m_1, m_2), \quad (3.157)$$

$$B_3(q^2; m_1, m_2) = -B_1(q^2; m_1, m_2) - B_2(q^2; m_1, m_2), \quad (3.158)$$

$$B_4(q^2; m_1, m_2) = -m_1^2 B_1(q^2; m_2, m_1) - m_2^2 B_1(q^2; m_1, m_2), \quad (3.159)$$

$$B_5(q^2; m_1, m_2) = A(m_1) + A(m_2) - 4B_{22}(q^2; m_2, m_1). \quad (3.160)$$

All the two-point functions of the standard model and its extensions can be expressed using the above six B_n functions (where $n = 0, \dots, 5$), which are no more than logarithmically

divergent. Comprehensive analytic expressions for these functions, and their derivatives with respect to q^2 can be found in [49].

We now turn to the self energy corrections to the gauge boson propagators. We only need to consider the transverse components of the gauge boson propagators, that is, the corrections to the propagator which are proportional to the metric tensor part of the boson propagator (that is, the part proportional to $g^{\mu\nu}$). This is because in all processes that we consider at least one end of the gauge boson propagators joins a light fermion line. A light fermion line cannot couple with the part of the gauge boson propagator proportional to the momentum of the gauge boson because of that would create a helicity flip interaction. Therefore only the transverse part of the propagator can contribute to the amplitude.

We add the so-called pinch term [38, 39] of the gauge boson self energy to the gauge boson propagators. The gauge boson propagator of the electroweak bosons does not in itself take the gauge invariant form

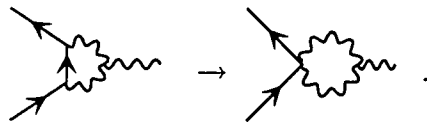
$$(g^{\mu\nu} - q^\mu q^\nu / q^2) f(q^2) \quad (3.161)$$

where f is some Lorentz invariant function of q^2 , the boson's four momentum, and other Lorentz invariant factors. The term which violates gauge invariance arises from the non-Abelian part of the gauge boson self energy



$$(3.162)$$

The non-gauge invariant part of the gauge boson propagator cancels against a term arising from the non-Abelian vertex



$$(3.163)$$

In fact, as is shown in (3.163), the term which cancels against the gauge non-invariant part is exactly the term arising from the cancellation of the fermion propagator factor $1/(q^2 - m_f^2)$ from the denominator of the integral over the loop momentum

$$\frac{1}{(q^2 - m_f^2)((q + p_1)^2 - m_B^2)((q + p_1 + p_2)^2 - m_B^2)} \quad (3.164)$$

where m_B represents the mass of the gauge bosons, in the non-Abelian vertex diagram against factors of q which appear in the numerator. There can be no dependence of terms in (3.162)

on the nature of the internal fermion line of the left hand side of (3.163), and if there were no non-Abelian terms in the propagator, then there would also be no non-Abelian vertex. Because this diagrammatically implies a pinching together of the two fermion-fermion-gauge boson vertices, this term is referred to as the “pinch” term.

There are four vector boson two-point functions that contribute to processes with external light quarks and leptons at one-loop order. We parameterise them, following [51], as

$$\Pi_T^{\gamma\gamma}(q^2) = \hat{e}^2 \Pi_T^{QQ}(q^2), \quad (3.165)$$

$$\Pi_T^{Z\gamma}(q^2) = \hat{e}\hat{g}_Z \left\{ \Pi_T^{3Q}(q^2) - \hat{s}^2 \Pi_T^{QQ}(q^2) \right\}, \quad (3.166)$$

$$\Pi_T^{ZZ}(q^2) = \hat{g}_Z^2 \left\{ \Pi_T^{33}(q^2) - 2\hat{s}^2 \Pi_T^{3Q}(q^2) + \hat{s}^4 \Pi_T^{QQ}(q^2) \right\}, \quad (3.167)$$

$$\Pi_T^{WW}(q^2) = \hat{g}^2 \Pi_T^{11}(q^2), \quad (3.168)$$

with the coupling factors

$$\hat{g}_Z = \frac{\hat{g}}{\hat{c}} = \frac{\hat{e}}{\hat{s}\hat{c}} \quad (3.169)$$

where we denote

$$\hat{s}^2 = 1 - \hat{c}^2 = \sin^2 \hat{\theta}_W, \quad (3.170)$$

where θ_W is the Weinberg weak mixing angle, throughout this section. We renormalise these two-point functions and the coupling factors in the modified minimal subtraction ($\overline{\text{MS}}$) scheme, and hence they depend on the 'tHooft unit of mass μ which appears explicitly in the B functions defined in (3.154-3.160). The coupling factors of (3.169) and (3.170) also depend on the unit of mass μ implicitly.

The bosonic contributions to the transverse part of the propagator, and their corresponding pinch terms, which are the B_0 functions, are

$$\overline{\Pi}_T^{QQ}(q^2) = \Pi_T^{QQ}(q^2) - \frac{1}{4\pi^2} q^2 B_0(q^2; W, W) \quad (3.171)$$

$$\overline{\Pi}_T^{3Q}(q^2) = \Pi_T^{3Q}(q^2) - \frac{1}{4\pi^2} \left(q^2 - \frac{1}{2}m_W^2 \right) B_0(q^2; W, W) \quad (3.172)$$

$$\overline{\Pi}_T^{33}(q^2) = \Pi_T^{33}(q^2) - \frac{1}{4\pi^2} (q^2 - m_W^2) B_0(q^2; W, W) \quad (3.173)$$

$$\overline{\Pi}_T^{11}(q^2) = \Pi_T^{11}(q^2) - \frac{1}{4\pi^2} (q^2 - m_W^2) \left[\hat{c}^2 B_0(q^2; W, Z) + \hat{s}^2 B_0(q^2; W, \gamma) \right] \quad (3.174)$$

where we abbreviate

$$B_n(q^2; A, B) = B_n(q^2, m_A^2, m_B^2). \quad (3.175)$$

and where the overline denotes a self energy correction with the pinch term added. The $\Pi_T(q^2)$ functions were calculated in the 'tHooft-Feynman gauge. The self energies, without

the pinch terms, are

$$\bar{\Pi}_T^{QQ}(q^2) = -\frac{q^2}{16\pi^2} \left\{ \left[5B_0 + 12B_3 \right] (q^2; W, W) + \frac{2}{3} \right\} \quad (3.176)$$

$$\bar{\Pi}_T^{3Q}(q^2) = -\frac{q^2}{16\pi^2} \left\{ \left[\frac{11}{2}B_0 + 10B_3 \right] (q^2; W, W) + \frac{2}{3} \right\} \quad (3.177)$$

$$\begin{aligned} \bar{\Pi}_T^{33}(q^2) &= \frac{1}{16\pi^2} \left[m_Z^2 B_0 - \frac{1}{4} B_5 \right] (q^2, Z, H) \\ &\quad - \frac{1}{16\pi^2} \left[\left(\frac{23}{4} q^2 - 2m_W^2 \right) B_0 + 9q^2 B_3 \right] (q^2, W, W) - \frac{q^2}{24\pi^2} \end{aligned} \quad (3.178)$$

$$\begin{aligned} \bar{\Pi}_T^{11}(q^2) &= \frac{1}{16\pi^2} \left[m_W^2 B_0 - \frac{1}{4} B_5 \right] (q, W, H) \\ &\quad - \frac{1}{16\pi^2} \left[\left(8\hat{c}^2 q^2 - (1 - 4\hat{s}^2) m_W^2 - m_Z^2 \right) B_0 - \left(\frac{9}{4} - 2\hat{s}^2 \right) B_5 \right] (q^2; W, Z) \\ &\quad - \frac{\hat{s}^2}{8\pi^2} \left[(4q^2 - 2m_W^2) B_0 - B_5 \right] (q^2; W, \gamma) - \frac{q^2}{24\pi^2} \end{aligned} \quad (3.179)$$

The two first terms of (3.178) and (3.179) are the only two terms in the transverse part of the vector boson propagators that depend on the Higgs boson mass m_H at the level of one-loop corrections to the minimal standard model.

The contributions to the transverse part of the gauge boson propagators from fermion loops are

$$\Pi_T^{QQ}(q^2) = \frac{q^2}{2\pi^2} \left[\sum_{f=\ell_i} Q_\ell^2 B_3(q^2; \ell_i, \ell_i) + 3 \sum_{f=u_i, d_i} Q_f^2 B_3(q^2; f, f) \right] \quad (3.180)$$

$$\Pi_T^{3Q}(q^2) = \frac{q^2}{4\pi^2} \left[\sum_{f=\ell_i} Q_\ell I_{3\ell} B_3(q^2; \ell_i, \ell_i) + 3 \sum_{f=u_i, d_i} Q_f I_{3f} B_3(q^2; f, f) \right] \quad (3.181)$$

$$\begin{aligned} \Pi_T^{33}(q^2) &= \frac{1}{16\pi^2} \left[\sum_{f=\ell_i, \nu_i} (I_{3f})^2 \left[4q^2 B_3 - 2m_f^2 B_0 \right] (q^2; f, f) \right. \\ &\quad \left. + 3 \sum_{f=u_i, d_i} (I_{3f})^2 \left[4q^2 B_3 - 2m_f^2 B_0 \right] (q^2; f, f) \right], \end{aligned} \quad (3.182)$$

$$\begin{aligned} \Pi_T^{11}(q^2) &= \frac{1}{16\pi^2} \left[\sum_{f=\ell_i, \nu_i} \left[2q^2 B_3 - B_4 \right] (q^2; \nu_i, \ell_i) \right. \\ &\quad \left. + 3 \sum_{f=u_i, d_i} |U_{u_i d_j}|^2 \left[2q^2 B_3 - B_4 \right] (q^2; u_i, d_j) \right]. \end{aligned} \quad (3.183)$$

The factors of 3 arise from colour summation. Here the three generations

$$\begin{array}{rcl}
 i & = & 1 \quad 2 \quad 3 \\
 \nu_i & = & \nu_e \quad \nu_\mu \quad \nu_\tau, \\
 \ell_i & = & e \quad \mu \quad \tau, \\
 u_i & = & u \quad c \quad t, \\
 d_i & = & d \quad s \quad b,
 \end{array} \tag{3.184}$$

Q_f is the electric charge of f in units of the proton charge, I_{3f} is the weak isospin

$$I_{3f} = \begin{cases} +\frac{1}{2} & \text{for } f = \nu_i \text{ or } u_{iL}, \\ -\frac{1}{2} & \text{for } f = \ell_{iL} \text{ or } d_{iL}, \\ 0 & \text{for } f = \ell_{iR}, u_{iR} \text{ or } d_{iR}, \end{cases} \tag{3.185}$$

and U_{u,d_j} denotes the Kobayashi-Maskawa quark mixing matrix elements.

We finally turn to self-energy corrections to fermion propagators. There are only two classes of this type of diagram, corrections involving emission and reabsorption of a virtual gauge boson and corrections involving a virtual scalar boson. The scalar boson corrections apply only to the top quark line since it is the only fermion that is not massless in our approximation.

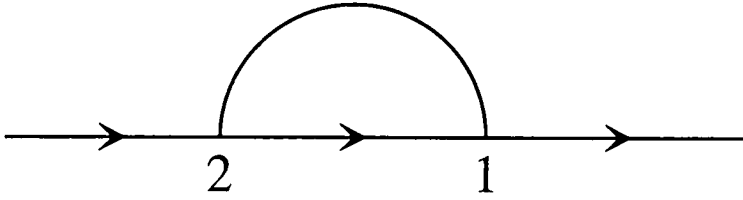


Figure 3.9: Fermionic self energy Feynman diagram. The lines with arrows represent fermion propagators, the curved line represents either a spin one or a spin zero boson propagator. The numbers label the two vertices.

The generic self energy for a spin one boson correction to a fermion propagator is

$$\Sigma^1 = - \int \frac{d^D k}{(2\pi)^D} \frac{\gamma^\mu (h_{1+} \mathcal{P}_+ + h_{1-} \mathcal{P}_-) \not{k} + m \gamma_\mu (h_{2+} \mathcal{P}_+ + h_{2-} \mathcal{P}_-)}{(k^2 - m^2)((p - k)^2 - M^2)} \tag{3.186}$$

$$\begin{aligned}
 &= \frac{-1}{16\pi^2} [(h_{1+} h_{2+} \not{p} \mathcal{P}_+ + h_{1-} h_{2-} \not{p} \mathcal{P}_-) (2B_1(p^2, m, M) + 1) \\
 &+ m(h_{1+} h_{2-} \mathcal{P}_- + h_{1-} h_{2+} \mathcal{P}_+) (4B_0(p^2, m, M) - 2)] \tag{3.187}
 \end{aligned}$$

and the generic self energy for a spin zero boson correction to a fermion propagator is

$$\Sigma^0 = \int \frac{d^D k}{(2\pi)^D} \frac{(h_{1+} \mathcal{P}_+ + h_{1-} \mathcal{P}_-) \not{k} + m(h_{2+} \mathcal{P}_+ + h_{2-} \mathcal{P}_-)}{(k^2 - m^2)((p - k)^2 - M^2)} \tag{3.188}$$

$$\begin{aligned}
&= \frac{1}{16\pi^2} [(h_{1+}h_{2-}\not{p}\mathcal{P}_- + h_{1-}h_{2+}\not{p}\mathcal{P}_+)B_1(p^2, m, M) \\
&+ m(h_{1+}h_{2+}\mathcal{P}_+ + h_{1-}h_{2-}\mathcal{P}_-)B_0(p^2, m, M)]
\end{aligned} \tag{3.189}$$

where the factors $h_{1,2\pm}$ represent the couplings of the boson to the fermions, with 1 and 2 the labels of Fig. 3.9, and the arguments to $G^{0,1}$ are

$$(h_{1-}, h_{1+}, h_{2-}, h_{2+}, m, M) \tag{3.190}$$

with m the mass of the internal fermion, and M the mass of the internal boson. The four-momentum squared of the external particle does not need to be explicitly specified. Thus the electroweak one loop corrections to the electron propagator are

$$\begin{aligned}
\Sigma^e &= \Sigma^1(g, 0, g, 0, 0, M_W) + \Sigma^1((g_Z(\frac{1}{2} - s^2), -g_Z s^2, g_Z(\frac{1}{2} - s^2), -g_Z s^2, 0, M_Z) \\
&+ \Sigma^1(e, e, e, e, 0, \lambda),
\end{aligned} \tag{3.191}$$

where a finite photon mass λ has been retained to regulate infrared divergences; the electroweak one loop corrections to the b quark propagator are

$$\begin{aligned}
\Sigma^b &= \Sigma^1(g, 0, g, 0, 0, M_W) + \Sigma^1(g_Z(\frac{1}{2} - \frac{1}{3}s^2), -g_Z \frac{1}{3}s^2, g_Z(\frac{1}{2} - \frac{1}{3}s^2), -g_Z \frac{1}{3}s^2, 0, M_Z) \\
&+ \Sigma^1(\frac{1}{3}e, \frac{1}{3}e, \frac{1}{3}e, \frac{1}{3}e, 0, \lambda),
\end{aligned} \tag{3.192}$$

and the electroweak one loop corrections to the t quark propagator are

$$\begin{aligned}
\Sigma^t &= \Sigma^1(g, 0, g, 0, 0, M_W) + \Sigma^1(g_Z(\frac{2}{3}s^2 - \frac{1}{2}), g_Z \frac{2}{3}s^2, g_Z(\frac{2}{3}s^2 - \frac{1}{2}), g_Z \frac{2}{3}s^2, m, M_Z) \\
&+ \Sigma^1(-\frac{2}{3}e, -\frac{2}{3}e, -\frac{2}{3}e, -\frac{2}{3}e, m, \lambda) + \Sigma^0(0, -i\sqrt{2}m/v, i\sqrt{2}m/v, 0, m, M_W) \\
&+ \Sigma^0(im/v, -im/v, im/v, -im/v, m, M_Z) \\
&+ \Sigma^0(-m/v, -m/v, -m/v, -m/v, m, M_H).
\end{aligned} \tag{3.193}$$

In Σ^b and Σ^e , because the internal masses are set to zero, all the Σ^1 functions are proportional to \not{p} and so there is no mass renormalisation. The ultraviolet divergence in the \not{p} term is absorbed into the renormalisation of the wavefunction. In Σ^t , in the $\overline{\text{MS}}$ scheme, the divergence in the mass term is reabsorbed into the mass renormalisation of the top quark mass. The \not{p} divergence is again absorbed into the wavefunction renormalisation.

3.8 Renormalisation

The renormalisation of the amplitudes is the process of absorbing the ultraviolet divergences that appear in the loop integrals of the one loop diagrams into experimentally measured

parameters. In the standard electroweak model, there are four parameters that require renormalisation. These are g and g' , the couplings of the SU(2) and U(1) component fields respectively, v , the vacuum expectation value of the Higgs field, and λ , the self-coupling of the Higgs field (see appendix C for details). The self-coupling of the Higgs field does not contribute to processes with light external fermions. The self coupling of the Higgs field only influences the Higgs field's self interactions, and since there are no Higgs boson propagators at tree level because the external fermions are light and thus do not have significant interactions with the Higgs field, and thus there are no one loop corrections to a Higgs boson propagator, which are the only place that Higgs self couplings could occur.

Thus we only need to consider the renormalisation of three of the four electroweak parameters. Divergences occurring in the Green's functions of the process $e^+e^- \rightarrow t\bar{t} \rightarrow bW^+ \bar{b}W^-$ must be reabsorbed into these three electroweak parameters. The remaining divergences must be reabsorbed either into mass or wavefunction renormalisations, where the ultraviolet divergence is reabsorbed into the measured mass or normalisation of the wavefunction to one particle per unit volume. Once this process has been carried out, the sum of the diagrams in the S-matrix must be ultraviolet finite.

For the case of the box diagrams, in the t'Hooft-Feynman gauge, only two powers of the loop momentum, arising from the propagators of the two virtual fermions, appear in the numerator of the amplitudes. Eight powers of the loop momentum appear in the denominator which originate from the four virtual particle propagators occurring in the loop. Therefore by power counting the loop integrals are finite and consequently all the box diagram amplitudes must be finite.

Because we approximate the mass of the electron and the b quark to be zero, there is no renormalisation of these masses, as can be seen explicitly by inserting the value $m = 0$ into (3.189) and (3.187), and the only fermion which requires mass renormalisation is the top quark. The masses of the Z and W bosons also require renormalisation.

After resumming the one-loop irreducible self energy diagrams, a particle's propagator takes the form

$$G(q^2) = \frac{1}{q^2 - m^2 + \Sigma(q^2)} \quad (3.194)$$

where q^2 is the particle's four-momentum squared, \hat{m} is the bare mass of the particle, and Σ is the self energy. We then find the (complex) pole mass

$$m_p^2 = m^2 - im\Gamma \quad (3.195)$$

where Γ is the on-shell width of the particle, and m is its renormalised mass, by the condition

$$m_P^2 - \hat{m}^2 + \Pi(m_P^2) = 0. \quad (3.196)$$

We then have

$$G(q^2) = \frac{1}{q^2 - m_P^2 + \Pi(q^2) - \Pi(m_P^2)} \quad (3.197)$$

which can be perturbatively expanded as

$$G(q^2) = \frac{1}{q^2 - m_P^2} \left(1 - \frac{\Pi(q^2) - \Pi(m_P^2)}{q^2 - m_P^2} \right), \quad (3.198)$$

$$= \frac{1}{q^2 - m_P^2} \left(1 - \Pi'(q^2) \right), \quad (3.199)$$

where we have defined

$$\Pi'(q^2) \equiv \frac{\Pi(q^2) - \Pi(m_P^2)}{q^2 - m_P^2}. \quad (3.200)$$

The first term of the right side of (3.199) is just the tree level propagator after mass renormalisation. The second part is still ultraviolet divergent. This ultraviolet divergence is absorbed into the wavefunction normalisation of the particle. The extension of this method to a fermion propagator with its extra spin factor in the numerator follows on almost identical lines.

Once these ultraviolet divergences have been absorbed, the remaining divergences from the vertex diagrams are absorbed by coupling constant renormalisation. The two couplings, the SU(2) coupling g and the U(1) coupling g' , are redefined in the $\overline{\text{MS}}$ renormalisation scheme by replacing the bare coupling and a factor of the pole term, (which is $\frac{1}{\epsilon} + \frac{1}{2}(\gamma_E - \log 4\pi)$ in the $\overline{\text{MS}}$ scheme), with the experimentally measured coupling. We can check the correctness of the calculation (since the theory is renormalisable) by seeing whether by making only one redefinition of each coupling all divergences can be reabsorbed.

This $\overline{\text{MS}}$ renormalisation leaves us with a logarithm of the unit of mass $\log \mu$ in place of the pole term. This term can be adjusted at will. We leave consideration of the physics of this renormalisation scale dependence to future works.

3.9 The total cross section

In this section we consider the total cross section for the electroweak radiatively corrected production and decay of top quarks to order g^4 in the weak coupling constant.

The sum of the one-loop radiative correction amplitudes to the $e^+e^- \rightarrow t\bar{t}$ process is

$$\mathcal{M}_{\text{O}}^{e^+e^-t\bar{t}} = \mathcal{M}_{\text{box}}^Z + \mathcal{M}_{\text{box}}^{Z\chi} + \mathcal{M}_{\text{box}}^W + \mathcal{M}_{\Delta}^{e^+e^-} + \mathcal{M}_{\Delta}^{t\bar{t}}$$

$$\begin{aligned}
& + \mathcal{M}_{\text{tree}}^\gamma \Pi_T^{\gamma\gamma} + \mathcal{M}_{\text{tree}}^Z \Pi_T^{ZZ} + \mathcal{M}^{\gamma Z} + \mathcal{M}^{Z\gamma} \\
& + (\Sigma'^e + \Sigma'^t)(\mathcal{M}_{\text{tree}}^\gamma + \mathcal{M}_{\text{tree}}^Z). \tag{3.201}
\end{aligned}$$

The sum of one loop radiatively corrected amplitudes to the $t \rightarrow bW^+$ and $\bar{t} \rightarrow \bar{b}W^-$ processes is

$$\mathcal{M}_\Delta^{tbW} = \mathcal{M}_\Delta^{tbW} + \frac{1}{2}(\Sigma'^t + \Sigma'^b + \Pi_T'^{WW})\mathcal{M}_{\text{tree}}^{tbW} \tag{3.202}$$

$$\mathcal{M}_\Delta^{\bar{t}\bar{b}W} = \mathcal{M}_\Delta^{\bar{t}\bar{b}W} + \frac{1}{2}(\Sigma'^t + \Sigma'^b + \Pi_T'^{WW})\mathcal{M}_{\text{tree}}^{\bar{t}\bar{b}W} \tag{3.203}$$

In the case of the on-shell particles, e^\pm , t and b and their antiparticle partners, and W^\pm , Σ' and Π' denote the derivative with respect to the four momentum squared for the on-shell particle. The order g^3 one-loop amplitude

$$\begin{aligned}
\mathcal{M}_\Delta & = \left(\mathcal{M}_\Delta^{e^+e^-t\bar{t}} \mathcal{M}_{\text{tree}}^{tbW} \mathcal{M}_{\text{tree}}^{\bar{t}\bar{b}W} + (\mathcal{M}_{\text{tree}}^\gamma + \mathcal{M}_{\text{tree}}^Z) \right. \\
& \times \left. \left[\mathcal{M}_\Delta^{tbW} \mathcal{M}_{\text{tree}}^{\bar{t}\bar{b}W} + \mathcal{M}_{\text{tree}}^{tbW} \mathcal{M}_\Delta^{\bar{t}\bar{b}W} \right] \right) D_t \bar{D}_t. \tag{3.204}
\end{aligned}$$

The differential cross section is

$$d\sigma = \frac{1}{2s} \left(\mathcal{M}_{\text{tree}} \mathcal{M}_{\text{tree}}^* + \mathcal{M}_\Delta \mathcal{M}_{\text{tree}}^* + \mathcal{M}_{\text{tree}} \mathcal{M}_\Delta^* \right) d\Phi_4, \tag{3.205}$$

the phase space volume

$$\begin{aligned}
d\Phi_4 & = (2\pi)^4 \delta^4(k + \bar{k} - r - \bar{r} - w - \bar{w}) \\
& \times \frac{dr}{(2\pi)^3 2r^0} \frac{d\bar{r}}{(2\pi)^3 2\bar{r}^0} \frac{dw}{(2\pi)^3 2w^0} \frac{d\bar{w}}{(2\pi)^3 2\bar{w}^0}, \tag{3.206}
\end{aligned}$$

$$= d\Phi_2(\theta, \phi) \frac{dp^2}{2\pi} d\Phi_2(\theta_1, \phi_1) \frac{d\bar{p}^2}{2\pi} d\Phi_2(\theta_2, \phi_2), \tag{3.207}$$

where

$$d\Phi_2(\theta, \phi) \equiv \frac{d \cos \theta}{2} \frac{d\phi}{2\pi} \tag{3.208}$$

and $\mathbf{r}, \dots, \bar{\mathbf{w}}$ indicate the three-vector part of the equivalent four-vector. See [52] for details of this phase space integral decomposition.

We leave the presentation of the numerical results for the cross section to later works.

3.10 Conclusions

The production and decay of the top quark may hold valuable clues to the nature of the symmetry breaking sector of the standard model. In this chapter, we gave complete analytic

expressions for helicity amplitudes for radiative corrections to the production and decay of the top quark at an e^+e^- linear collider. We also gave a general formalism for these radiative corrections which can be extended to new physics.

We approximated that the electron and b quarks were massless, and did not include the soft photon radiation to the $e^+e^- \rightarrow t\bar{t}$ production.

Even though the radiative corrections to top quark production and decay have already been calculated separately, our work makes it possible to combine the sequence of events by keeping full information on the correlations among final state particles.


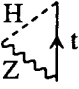
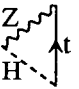
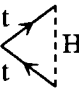
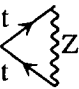

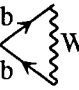
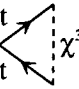
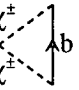
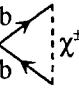
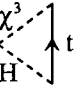
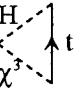
	γ Z boson
	0 $\Delta_b^\mu(ttZ; ivg_Z^2/4; ttH; M_Z, M_H, m)$
	0 $\Delta_c^\mu(ttH; ivg_Z^2/4; ttZ; M_H, M_Z, m)$
	$\Delta_f^\mu(ttH; tt\gamma; ttH; m, m, M_H)$ $\Delta_f^\mu(ttHZ; ttZ; ttH; m, m, M_H)$
	$\Delta_e^\mu(ttZ; tt\gamma; ttZ; m, m, M_Z)$ $\Delta_e^\mu(ttZ; ttZ; ttZ; m, m, M_Z)$
	$\Delta_d^\mu(tbW; WW\gamma; tbW; M_W, m, M_H)$ $\Delta_d^\mu(tbW; WWZ; tbW; M_W, m, M_H)$
	$\Delta_e^\mu(tbW; bb\gamma; tbW; 0, 0, M_W)$ $\Delta_e^\mu(tbW; bbZ; tbW; 0, 0, M_W)$
	$\Delta_f^\mu(tt\chi^3; tt\gamma; tt\chi^3; m, m, M_Z)$ $\Delta_f^\mu(tt\chi^3; ttZ; tt\chi^3; m, m, M_Z)$
	$\Delta_a^\mu(tb\chi^+; bb\gamma; bt\chi^-; M_W, M_W, 0)$ $\Delta_a^\mu(tb\chi^+; bbZ; bt\chi^-; M_W, M_W, 0)$
	$\Delta_f^\mu(tb\chi^+; bb\gamma; bt\chi^-; 0, 0, M_W)$ $\Delta_f^\mu(tb\chi^+; bbZ; bt\chi^-; 0, 0, M_W)$
	0 $\Delta_a^\mu(ttH; ig_Z/2; tt\chi^3; M_H, M_Z, m)$
	0 $\Delta_a^\mu(tt\chi^3; ig_Z/2; ttH; M_Z, M_H, m)$

Table 3.2: Radiative corrections to $t\bar{t}$ vertex

	$\Delta_c^\mu(ttH, gM_W, tbW^+; M_H, M_W, m)$
	$\Delta_d^\mu(ttZ, -g_Z, tbW^+; M_Z, M_W, m)$
	$\Delta_a^\mu(tt\chi^3, -ig/2, tb\chi^+; M_Z, M_W, m)$
	$\Delta_d^\mu(tbW^+, -g_Z, bbZ; M_W, M_Z, 0)$
	$\Delta_a^\mu(ttH, -ig/2, tb\chi^+; M_H, M_W, m)$
	$\Delta_c^\mu(ttZ, -iM_Wg_Zs^2, tb\chi^+; M_Z, M_W, m)$
	$\Delta_e^\mu(ttZ, tbW^+, bbZ; m, 0, M_Z)$
	$\Delta_c^\mu(tb\chi^+, -iM_Wg_Zs^2, bbZ; M_W, M_Z, 0)$

Table 3.3: The radiative corrections to tbW vertex which do not involve virtual photon corrections

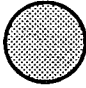

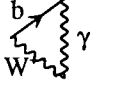
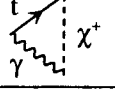
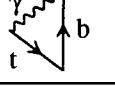
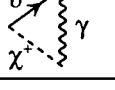
	
	$\Delta_d^\mu(tt\gamma, e, tbW^+; \lambda, M_W, m)$
	$\Delta_d^\mu(tbW^+, e, bb\gamma; M_W, \lambda, m_b)$
	$\Delta_c^\mu(tt\gamma, -ieM_W, tb\chi^+; \lambda, M_W, m)$
	$\Delta_e^\mu(tt\gamma, tbW^+, bb\gamma; m, m_b, \lambda)$
	$\Delta_c^\mu(tb\chi^+, -ieM_W, bb\gamma; M_W, \lambda, m_b)$

Table 3.4: The radiative corrections to the tbW vertex that involve virtual photons. The fictitious mass of the photon is denoted λ .

Appendices

Appendix A. Gamma matrices

In this section we give the conventions and notations used for the Dirac gamma matrices in this thesis. Most of the results about gamma matrices are proved in [42].

The specific choice of representation of gamma matrix used to construct spinors is that of [41].

The gamma matrices themselves are denoted γ^μ .

The sigma tensor

$$\sigma^{\mu\nu} \equiv \frac{i}{2}[\gamma^\mu, \gamma^\nu] \quad (\text{A.1})$$

The Levi-Civita tensor or totally anticommuting tensor in four dimensions is denoted by $\epsilon^{\mu\nu\sigma\rho}$ with $\epsilon_{0123} = 1 \Rightarrow \epsilon^{0123} = -1$.

The γ^5 matrix is defined by

$$\gamma^5 \equiv i\gamma^0\gamma^1\gamma^2\gamma^3 = (i/4!)\epsilon_{\mu\nu\sigma\rho}\gamma^\mu\gamma^\nu\gamma^\sigma\gamma^\rho. \quad (\text{A.2})$$

The chirality projection operator

$$\mathcal{P}_\alpha \equiv (\mathbf{1} + \alpha\gamma^5)/2 \quad (\text{A.3})$$

where $\alpha = \pm 1$, frequently shortened to $\alpha = \pm$. Also define $\mathcal{P}_L \equiv \mathcal{P}_-$, $\mathcal{P}_R \equiv \mathcal{P}_+$.

In the chiral representation the linearly independent components of $\sigma^{\mu\nu}$ take the form

$$\{\sigma^{01}, \sigma^{02}, \sigma^{03}, \sigma^{12}, \sigma^{31}, \sigma^{23}\} \equiv \left\{ \begin{pmatrix} -i\sigma^1 & 0 \\ 0 & i\sigma^1 \end{pmatrix}, \begin{pmatrix} -i\sigma^2 & 0 \\ 0 & i\sigma^2 \end{pmatrix}, \begin{pmatrix} -i\sigma^3 & 0 \\ 0 & i\sigma^3 \end{pmatrix}, \right. \\ \left. \begin{pmatrix} \sigma^3 & 0 \\ 0 & \sigma^3 \end{pmatrix}, \begin{pmatrix} \sigma^2 & 0 \\ 0 & \sigma^2 \end{pmatrix}, \begin{pmatrix} \sigma^1 & 0 \\ 0 & \sigma^1 \end{pmatrix} \right\} \quad (\text{A.4})$$

where σ^i are 2×2 Pauli matrices. The $\sigma^{\mu\nu}$ tensor generates proper Lorentz transformations, and the diagonal form of these matrices in the chiral representation demonstrates the well known result that proper Lorentz transformations do not mix chirality eigenstates.

Appendix B. Rougé's formula

Rougé's formula states that when one particle decays to three, the angle ψ that the normal of the plane made by the three decay products, in its rest frame, makes with the laboratory direction of motion of the decaying particle, has cosine

$$\cos \psi = \frac{8M^2 \mathbf{p}_1 \cdot (\mathbf{p}_2 \times \mathbf{p}_3)}{|\mathbf{p}_1 + \mathbf{p}_2 + \mathbf{p}_3| \sqrt{-\lambda(\lambda(M^2, m_{12}^2, m^2), \lambda(M^2, m_{13}^2, m^2), \lambda(M^2, m_{23}^2, m^2))}} \quad (\text{B.1})$$

where M is the mass of the decaying particle, m is the mass of the product particle, m_{ij} is the sum of the four-momenta of particle i and j squared,

$$m_{ij}^2 = (p_i + p_j)^2, \quad (\text{B.2})$$

\mathbf{p}_i is the momentum of particle i as labelled in Fig. B.1, and λ is the triangle function

$$\lambda(a, b, c) = a^2 + b^2 + c^2 - 2(ab + ac + bc). \quad (\text{B.3})$$

See [52] for details about this function. The meaning of ψ is shown in Fig. B.1.

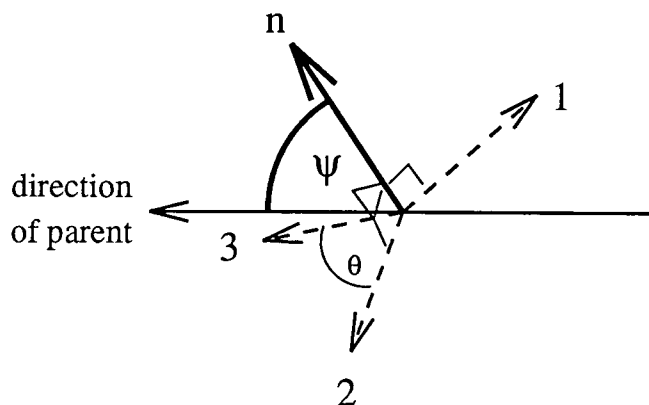


Figure B.1: The angle ψ between the normal, n , to the plane that the three decaying bodies make in their parent's rest frame and the direction of motion of the parent particle in the lab frame.

Proof

We label quantities in the rest frame of the decaying particle with an asterisk, $*$, and the same quantities in the laboratory frame without an asterisk. Thus, for instance the laboratory momentum of particle 1 is denoted \mathbf{p}_1 and its momentum in the rest frame of the decaying particle is denoted \mathbf{p}_1^* . We denote the three momentum of the decaying particle as \mathbf{P} and its rest mass as M .

Using the relations $|\mathbf{p}_1 + \mathbf{p}_2 + \mathbf{p}_3| = |\mathbf{P}|$ and $|\mathbf{P}| = \gamma\beta M$, where $\beta = |\mathbf{P}|/E$ and $\gamma = \sqrt{1 - \beta^2}$. Thus

$$|\mathbf{p}_1 + \mathbf{p}_2 + \mathbf{p}_3| = \gamma\beta M. \quad (\text{B.4})$$

Without loss of generality, we can take the direction of the decaying particle's motion in the laboratory frame to be in the z direction. The factor from the numerator of (B.1),

$$\mathbf{p}_1 \cdot (\mathbf{p}_2 \times \mathbf{p}_3) = \begin{vmatrix} p_{1x} & p_{1y} & p_{1z} \\ p_{2x} & p_{2y} & p_{2z} \\ p_{3x} & p_{3y} & p_{3z} \end{vmatrix} = \begin{vmatrix} p_{1x}^* & p_{1y}^* & \gamma(p_{1z}^* + \beta E_1^*) \\ p_{2x}^* & p_{2y}^* & \gamma(p_{2z}^* + \beta E_2^*) \\ p_{3x}^* & p_{3y}^* & \gamma(p_{3z}^* + \beta E_3^*) \end{vmatrix}, \quad (\text{B.5})$$

where $|A|$ denotes the determinant of a matrix A . Since the \mathbf{p}_i^* 's are coplanar,

$$\begin{vmatrix} p_{1x}^* & p_{1y}^* & p_{1z}^* \\ p_{2x}^* & p_{2y}^* & p_{2z}^* \\ p_{3x}^* & p_{3y}^* & p_{3z}^* \end{vmatrix} = 0. \quad (\text{B.6})$$

After eliminating \mathbf{p}_1 and E_1 from (B.5) using four momentum conservation, we obtain

$$\mathbf{p}_1 \cdot (\mathbf{p}_2 \times \mathbf{p}_3) = \gamma\beta M \hat{z} \cdot (\mathbf{p}_2^* \times \mathbf{p}_3^*) \quad (\text{B.7})$$

where \hat{z} is the unit vector in the z direction, the laboratory direction of motion of the decaying particle.

Let θ be the angle between \mathbf{p}_2^* and \mathbf{p}_3^* , as shown in Fig. B.1. By momentum conservation, the momentum vectors of the decay products in the decaying particle's rest frame form a triangle. Using the cosine rule

$$2|\mathbf{p}_2^*||\mathbf{p}_3^*| \cos(2\pi - \theta) = |\mathbf{p}_1^*|^2 - |\mathbf{p}_2^*|^2 - |\mathbf{p}_3^*|^2. \quad (\text{B.8})$$

In the decay of one particle to two bodies, in the rest frame of the decaying particle, the absolute value of the equal and opposite momenta of the two bodies, \mathbf{p} and $-\mathbf{p}$, is given by

$$|\mathbf{p}|^2 = \frac{1}{2M} \sqrt{\lambda(M^2, m_1^2, m_2^2)} \quad (\text{B.9})$$

where M denotes the mass of the decaying particle, and m_1 and m_2 denote the masses of the two product particles. Thus, treating particles 2 and 3 of the three body decay as a one body system with invariant mass m_{ij} as defined in (B.2), the absolute value of \mathbf{p}_1^* is given by

$$|\mathbf{p}_1^*|^2 = \frac{1}{2M} \sqrt{\lambda(M^2, m_{23}^2, m_1^2)} \quad (\text{B.10})$$

and similarly for $|\mathbf{p}_2^*|$ and $|\mathbf{p}_3^*|$. Now

$$|\mathbf{p}_2 \times \mathbf{p}_3| = |\mathbf{p}_2||\mathbf{p}_3| \sin \theta \quad (\text{B.11})$$

$$= \sqrt{|\mathbf{p}_2|^2|\mathbf{p}_3|^2 - (|\mathbf{p}_1^*|^2 - |\mathbf{p}_2^*|^2 - |\mathbf{p}_3^*|^2)^2/4} \quad (\text{B.12})$$

$$= \frac{1}{2}\sqrt{-\lambda(|\mathbf{p}_1^*|^2, |\mathbf{p}_2^*|^2, |\mathbf{p}_3^*|^2)} \quad (\text{B.13})$$

and so, using (B.10),

$$\sqrt{-\lambda(\lambda(M^2, m_{12}^2, m^2), \lambda(M^2, m_{13}^2, m^2), \lambda(M^2, m_{23}^2, m^2))} = 8M^2|\mathbf{p}_2^* \times \mathbf{p}_3^*| \quad (\text{B.14})$$

Combining (B.14), (B.7) and (B.4),

$$\begin{aligned} & \frac{8M^2\mathbf{p}_1 \cdot (\mathbf{p}_2 \times \mathbf{p}_3)}{|\mathbf{p}_1 + \mathbf{p}_2 + \mathbf{p}_3| \sqrt{-\lambda(\lambda(M^2, m_{12}^2, m^2), \lambda(M^2, m_{13}^2, m^2), \lambda(M^2, m_{23}^2, m^2))}} \\ &= \frac{8M^2 \times \gamma\beta M \hat{z} \cdot (\mathbf{p}_2^* \times \mathbf{p}_3^*)}{\gamma\beta M \times 8M^2|\mathbf{p}_2^* \times \mathbf{p}_3^*|} = \cos \psi, \end{aligned} \quad (\text{B.15})$$

which proves B.1.

Appendix C. The Standard Model Lagrangian

In this appendix, we give the complete Lagrangian of the standard electroweak model. We do not give explanation of its derivation. From this Lagrangian, the Feynman rules can be extracted by crossing out the fields. This Lagrangian was used to create the results of chapter 3.

We choose the linear representation of the Higgs field,

$$\Phi = \begin{pmatrix} i\chi^+ \\ (v + H - i\chi^3)/\sqrt{2} \end{pmatrix}. \quad (\text{C.1})$$

The coefficients

$$\lambda = \frac{m_H^2}{2v^2} \quad (\text{C.2})$$

$$M_W = \frac{1}{2}gv \quad (\text{C.3})$$

where m_H is the mass of the Higgs boson, v is the vacuum expectation of the Higgs field, and λ is the self coupling of the Higgs field. The symbol g denotes the coupling of the SU(2) part of the electroweak theory, and g' represents the coupling of the U(1) part. At tree level, these couplings are related by

$$\tan \theta_W = \frac{g}{g'} \quad (\text{C.4})$$

where θ_W is the Weinberg weak mixing angle. We also use the symbols

$$s = \sin \theta_W \quad (\text{C.5})$$

$$c = \cos \theta_W \quad (\text{C.6})$$

$$g_Z = g/c \quad (\text{C.7})$$

$$e = sg = cg' \quad (\text{C.8})$$

to represent various coupling factors. The component fields Z and A which result from the diagonalisation of the mass matrix of the weak bosons are defined in terms of the SU(2) field W_3 and the U(1) field B by

$$\begin{pmatrix} W_3^\mu \\ B^\mu \end{pmatrix} = \begin{pmatrix} c & s \\ -s & c \end{pmatrix} \begin{pmatrix} Z^\mu \\ A^\mu \end{pmatrix} \quad (\text{C.9})$$

The symbols m_Z, m_W denote the masses of the Z and W bosons respectively. We use three independent gauge-fixing terms for the photon, W boson and Z boson propagators. These introduce gauge parameters ξ_A, ξ_W and ξ_Z , and the Z and W boson gauge-fixing terms eliminate mixing terms between the Goldstone boson fields χ^3 and χ^\pm and the gauge boson fields of the Z and W boson which are here denoted by Z and W^\pm respectively.

For the annihilation operator, whose wavefunction contains a position dependence $e^{-ip \cdot x}$, where p^μ is the four momentum of the particle, and x^μ is its position, the derivative factors are replaced by a factor $-ip^\mu$. If the particle is created rather than annihilated, then we replace the derivative by ip^μ .

Once the Feynman rule has been read from the Lagrangian, it must be multiplied by a factor of i which arises from the perturbative expansion, and a symmetry factor $1/n!$ if it involves n identical particles.

Boson propagators

$$\begin{aligned} & W_\alpha^+ \left[(\partial^2 + m_W^2) g^{\alpha\beta} + \left(\frac{1}{\xi_W} - 1 \right) \partial^\alpha \partial^\beta \right] W_\beta^- + \frac{1}{2} Z_\alpha \left[(\partial^2 + m_Z^2) g^{\alpha\beta} + \left(\frac{1}{\xi_Z} - 1 \right) \partial^\alpha \partial^\beta \right] Z_\beta \\ & + \frac{1}{2} A_\alpha \left[\partial^2 g^{\alpha\beta} + \left(\frac{1}{\xi_A} - 1 \right) \partial^\alpha \partial^\beta \right] A_\beta - \chi^+ (\partial^2 + \xi_W m_W^2) \chi^- - \frac{1}{2} \chi^3 (\partial^2 + \xi_Z m_Z^2) \chi^3 \\ & - \frac{1}{2} H (\partial^2 + m_H^2) H \end{aligned} \quad (\text{C.10})$$

scalar-scalar interactions

$$+\frac{\lambda}{4} v^4 - (\lambda v^2 + \mu^2) \left[\chi^+ \chi^- + \frac{(\chi^3)^2}{2} + \frac{(v + H)^2}{2} \right]$$

$$\begin{aligned}
& -6\lambda \left[v \frac{H^3}{3!} + \frac{H^4}{4!} + \frac{(\chi^3)^4}{4!} \right] - 2\lambda v H \left[\chi^+ \chi^- + \frac{(\chi^3)^2}{2} \right] \\
& - 2\lambda \left[\left(\frac{H^2}{2} + \frac{(\chi^3)^2}{2} \right) \chi^+ \chi^- + \frac{H^2 (\chi^3)^2}{2} \right] - 4\lambda \frac{(\chi^+ \chi^-)^2}{4}
\end{aligned} \tag{C.11}$$

Scalar-gauge Boson interactions

$$\begin{aligned}
& + \frac{g}{2} W^{-\mu} \left[H \vec{\partial}_\mu \chi^+ + i \chi_3 \vec{\partial}_\mu \chi^+ \right] + \frac{g}{2} W^{+\mu} \left[H \vec{\partial}_\mu \chi^- - i \chi_3 \vec{\partial}_\mu \chi^- \right] \\
& + \frac{g_Z}{2} Z^\mu H \vec{\partial}_\mu \chi_3 + i \left[\left(\frac{1}{2} - s^2 \right) g_Z Z^\mu + e A^\mu \right] \chi^+ \vec{\partial}_\mu \chi^- \\
& + \left[\frac{s^2 g g_Z}{2} Z^\mu - \frac{e g}{2} A^\mu \right] \left[(W_\mu^+ \chi^- + W_\mu^- \chi^+) \chi_3 + i (W_\mu^+ \chi^- - W_\mu^- \chi^+) (v + H) \right] \\
& + \left[\frac{g^2}{2} W_\mu^+ W^{-\mu} + \left(\frac{1}{2} - s^2 \right)^2 g_Z^2 Z_\mu Z^\mu + (1 - 2s^2) g_Z e Z_\mu A^\mu + e^2 A_\mu A^\mu \right] \chi^+ \chi^- \\
& + \left[\frac{g^2}{2} W_\mu^+ W^{-\mu} + \frac{g_Z^2}{2} Z_\mu Z^\mu \right] \left[v H + \frac{H^2}{2} + \frac{(\chi_3)^2}{2} \right]
\end{aligned} \tag{C.12}$$

Gauge Boson-gauge Boson interactions

$$\begin{aligned}
& -ig \left[g^{\alpha\beta} \left(W_\alpha^+ \vec{\partial}^\gamma W_\beta^- \right) W_\gamma^3 + g^{\beta\gamma} \left(W_\beta^- \vec{\partial}^\alpha W_\gamma^3 \right) W_\alpha^+ + g^{\gamma\alpha} \left(W_\gamma^3 \vec{\partial}^\beta W_\alpha^+ \right) W_\beta^- \right] \\
& + g^2 \left(g^{\alpha\beta} g^{\gamma\delta} + g^{\alpha\delta} g^{\beta\gamma} - 2g^{\alpha\gamma} g^{\beta\delta} \right) \left[\frac{1}{2} W_\alpha^+ W_\beta^3 W_\gamma^- W_\delta^3 - \frac{1}{4} W_\alpha^+ W_\beta^- W_\gamma^+ W_\delta^- \right].
\end{aligned} \tag{C.13}$$

Faddeev-Popov ghost interactions

$$\begin{aligned}
& -\bar{c}^-(\partial^2 + \xi_W m_W^2) c^+ - \bar{c}^+(\partial^2 + \xi_W m_W^2) c^- - \bar{c}_Z(\partial^2 + \xi_Z m_Z^2) c_Z - \bar{c}_A \partial^2 c_A \\
& + ig(\partial^\mu \bar{c}^-)[W_\mu^3 c^+ - W_\mu^+ c_3] + ig(\partial^\mu \bar{c}^+)[W_\mu^- c_3 - W_\mu^3 c^-] + ig(\partial^\mu \bar{c}_3)[W_\mu^+ c^- - W_\mu^- c^+] \\
& - \frac{g}{2} \xi_W m_W [\bar{c}^-(H - i\chi_3) c^+ + \bar{c}^+(H + i\chi_3) c^-] + i \left(\frac{1}{2} - s^2 \right) g_Z \xi_W m_W [\bar{c}^+ \chi^- c_Z - \bar{c}^- \chi^+ c_Z] \\
& + ie \xi_W m_W [\bar{c}^+ \chi^- c_A - \bar{c}^- \chi^+ c_A] - \frac{g_Z}{2} \xi_Z m_Z \bar{c}_Z H c_Z + i \frac{g}{2} \xi_Z m_Z [\bar{c}_Z \chi^+ c^- - \bar{c}_Z \chi^- c^+],
\end{aligned} \tag{C.14}$$

where

$$c_3 = \cos \theta_W c_Z + \sin \theta_W c_A, \quad \bar{c}_3 = \cos \theta_W \bar{c}_Z + \sin \theta_W \bar{c}_A. \tag{C.15}$$

Lepton-Boson interactions

$$\sum_{\ell=e,\mu,\tau} \left\{ \bar{\nu}_\ell i \not{\partial} \mathcal{P}_L \nu_\ell + \bar{\ell} (i \not{\partial} - m_\ell) \ell - \frac{g}{\sqrt{2}} \left(\bar{\nu}_\ell \not{W}^+ \mathcal{P}_L \ell + \bar{\ell} \not{W}^- \mathcal{P}_L \nu_\ell \right) \right\}$$

$$\begin{aligned}
& +g_Z \left[\bar{\ell} \not{Z} \left(\left(\frac{1}{2} - s^2 \right) \mathcal{P}_L - s^2 \mathcal{P}_R \right) \ell - \frac{1}{2} \bar{\nu}_\ell \not{Z} \mathcal{P}_L \nu_\ell \right] + e \bar{\ell} A \ell \\
& + \frac{i m_\ell \sqrt{2}}{v} \left(\chi^- \bar{\ell} \mathcal{P}_L \nu_\ell - \chi^+ \bar{\nu}_\ell \mathcal{P}_R \ell \right) - \frac{m_\ell}{v} H \bar{\ell} \ell + i \frac{m_\ell}{v} \chi^3 \bar{\ell} (\mathcal{P}_R - \mathcal{P}_L) \ell \Big\}, \quad (\text{C.16})
\end{aligned}$$

where ℓ and ν_ℓ represent the field of the lepton and its neutrino, and m_ℓ represents the mass of the lepton (the neutrinos are assumed massless). $\mathcal{P}_{L,R}$ are the chirality projection operators

$$\mathcal{P}_L = \frac{1}{2}(1 - \gamma^5) \quad (\text{C.17})$$

$$\mathcal{P}_R = \frac{1}{2}(1 + \gamma^5) \quad (\text{C.18})$$

where γ^5 is the totally anticommuting gamma matrix (see Appendix A).

Quark-Boson interactions

$$\begin{aligned}
& \bar{T}(i\not{\phi} - m_T)T + \bar{B}(i\not{\phi} - m_B)B - \frac{2}{3}e\bar{T}AT + \frac{1}{3}e\bar{B}AB \\
& - \frac{g}{\sqrt{2}}U\bar{T}\not{W}^+\mathcal{P}_LB - \frac{g}{\sqrt{2}}U^*\bar{B}\not{W}^-\mathcal{P}_LT \\
& + g_Z\bar{T}\not{Z} \left[\left(\frac{2s^2}{3} - \frac{1}{2} \right) \mathcal{P}_L + \frac{2s^2}{3}\mathcal{P}_R \right] T + g_Z\bar{B}\not{Z} \left[\left(\frac{1}{2} - \frac{s^2}{3} \right) \mathcal{P}_L - \frac{s^2}{3}\mathcal{P}_R \right] B \\
& - \frac{H}{v} (m_B\bar{B}B + m_T\bar{T}T) + \frac{i\chi^3}{v} [m_T\bar{T}(\mathcal{P}_L - \mathcal{P}_R)T - m_B\bar{B}(\mathcal{P}_L - \mathcal{P}_R)B] \\
& + \frac{i\sqrt{2}}{v} [U\chi^+\bar{T}(m_T\mathcal{P}_L - m_B\mathcal{P}_R)B + U^*\chi^-\bar{B}(m_B\mathcal{P}_L - m_T\mathcal{P}_R)T] \quad (\text{C.19})
\end{aligned}$$

where

$$T = \begin{bmatrix} u \\ c \\ t \end{bmatrix}, \quad B = \begin{bmatrix} d \\ s \\ b \end{bmatrix}, \quad (\text{C.20})$$

The symbols u , c and t represent the fields of the charge $+2/3$ up, charm and top quarks, d , s and b represent the fields of the charge $-1/3$ down, strange and bottom quarks, and U represents the Kobayashi-Maskawa quark mixing matrix. The symbols m_T and m_B denote the mass matrices

$$m_T = \begin{pmatrix} m_u & 0 & 0 \\ 0 & m_c & 0 \\ 0 & 0 & m_t \end{pmatrix}, \quad (\text{C.21})$$

$$m_B = \begin{pmatrix} m_d & 0 & 0 \\ 0 & m_s & 0 \\ 0 & 0 & m_b \end{pmatrix}, \quad (\text{C.22})$$

of the quarks.

Appendix D. One loop integrals

In this section we outline the techniques used in the evaluation of the integrals arising from ‘one loop’ Feynman diagrams. In particular, we consider the Passarino-Veltman reduction scheme for the evaluation of loop integrals, and explain the concepts used in this scheme.

A Feynman diagram containing a loop has a path along the lines representing propagators of virtual particles which self-intersects. We cannot know what momentum is flowing through this path, since the particles whose propagators form the loop are in virtual, unobserved, states. Therefore every value of internal momentum is possible. In effect, we must integrate over every possible internal momentum that could be flowing around the loop.

In perturbation theory, the behaviour of a virtual particle, that is, a particle which is neither an initial or final state, is described by its propagator. In the momentum space representation every particle’s propagator contains a factor

$$\frac{1}{q^2 - m^2 + i\epsilon} \quad (\text{D.1})$$

where q^μ is the four momentum of the virtual particle and m is its mass. Further to this universal factor, the propagator may also contain a factor dependent on the particle’s momentum arising from the sum over the possible spin states of the virtual particle. For instance, fermion propagators have the form

$$i \frac{\gamma_\mu q^\mu + m}{q^2 - m^2 + i\epsilon}, \quad (\text{D.2})$$

where γ_μ are the Dirac gamma matrices. This contains a power of q in its numerator, arising from the sum over the possible spin states of the fermion. A gauge boson propagator in the unitary gauge has the form

$$-i \frac{g^{\mu\nu} - q^\mu q^\nu / m^2}{q^2 - m^2 + i\epsilon}, \quad (\text{D.3})$$

which has two powers of q in its numerator.

The usual way to write the amplitude from a Feynman graph containing a loop is to give the unfixed momentum a name and some arbitrarily chosen direction. The amplitude of the Feynman graph is then calculated by integrating the unfixed internal momentum over all possible values from zero to infinity in all directions.

There are two important points to notice about these integrals in the general case. First, the denominator of the integral contains only multiple propagator factors of the form of (D.1) depending only on the internal unfixed momentum q , the external momentum p and the mass of the electron. Secondly, we can ignore all factors occurring in the numerator except for

those which contain the unfixed loop momentum, since only these factors are affected by the integration. This is a drastic simplification, because in every one loop integral, q only appears in the form q^μ , and never in functions of its value such as $\sin(q^2)$.

In the case of one-loop integrals, that is, integrals with only one unfixed momentum, denoted q , the problem of one-loop integration is reduced to solving expressions of the form

$$\frac{q^\mu \dots q^\nu}{((q + p_a)^2 - m_a^2)((q + p_b)^2 - m_b^2) \dots ((q + p_z)^2 - m_z^2)} \quad (\text{D.4})$$

where p_a, \dots, p_z are some combinations of the external momenta and $m_a \dots m_z$ are masses.

The method we used to solve these types of integrals is that of [36, 37]. The first step in this scheme is to classify one loop integrals by the number of virtual particle propagators that feature in the loop integration. A one loop integral involving one propagator, or equivalently one external leg, is given the classifying letter 'A'. A one loop integral involving two propagators, or equivalently two external legs, is given the classifying letter 'B', and so on for 'C' and 'D' as is shown in Fig. D.1.

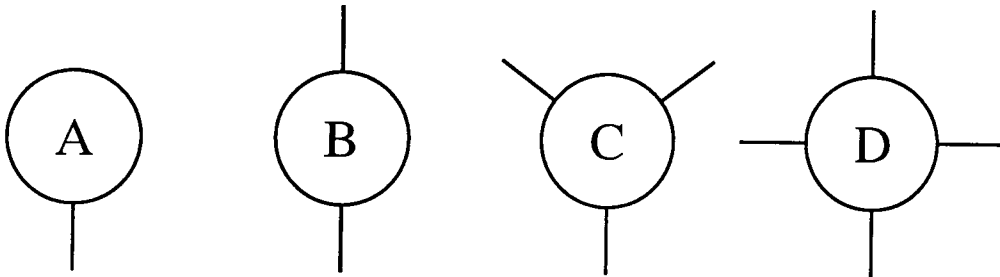


Figure D.1: The A, B, C, D classification scheme for one loop integrals.

Let the momentum unfixed inside the loop be q . The A , B , C and D integrals are further subdivided depending on the number of powers of q appearing in the numerator. For the case that there are no powers of q in the numerator, we label the integrals with a 0 subscript, that is A_0 , B_0 , C_0 and D_0 . For the case that there is one power of q in the numerator, we label the integral with the index of q , so that if q^μ appears in the numerator, we denote the integrals as B^μ , C^μ or D^μ . There is no need for an A^μ , because

$$\therefore A^\mu = \int_{-\infty}^{\infty} \frac{q^\mu d^4 q}{q^2 - m^2} = 0, \quad (\text{D.5})$$

since the integrand is odd under spatial reflection. We can further define $B^{\mu\nu}$, $C^{\mu\nu}$ and $D^{\mu\nu}$, which have $q^\mu q^\nu$ in their numerator, and $C^{\mu\nu\rho}$ and $D^{\mu\nu\rho}$, etc.



Having defined these integrals, the next step is to perform the integration over q . The first thing to note about these integrals is that several of them have so-called ultraviolet divergences. When we integrate the integrand over all values of momenta, we find that the total is divergent. These integrals must be regularised, that is we must find some way to make them finite. The method we choose in this thesis is the method of dimensional regularisation. In this method we change the number of dimensions of the integral from 4 to D , where $D = 4 - 2\epsilon$, and take the limit $\epsilon \rightarrow 0$. The divergences of the integrals show up as poles in $1/\epsilon$. The process of renormalisation consists of absorbing these poles into experimentally measured quantities. We do not discuss this topic any further here, since it is thoroughly covered in many textbooks (see for instance [48, 53, 54, 55]).

The integrals which contain powers of q in their numerators, which we denote as tensor integrals, have certain fixed Lorentz transformation properties. For instance, the integral

$$B^\mu = \int \frac{q^\mu d^D q}{(q^2 - m_1^2)((q+p)^2 - m_2^2)} \quad (\text{D.6})$$

is a four-vector under Lorentz transformations. Therefore the solution to the integral should also be a four-vector under Lorentz transformations. As we saw in (D.5), if the integral was totally symmetric in all space-time directions, then it would be equal to zero. The only part of the integral which is not symmetric is p . Therefore the solution to this integral must be proportional to p^μ , since it is the only possible object with the correct transformation properties. We define a scalar function B_1 such that

$$B^\mu = B_1 p^\mu. \quad (\text{D.7})$$

B_1 is a function of p^2 , m_1 and m_2 . Now for each type of tensor integral, we can apply the same argument, that it must be proportional to available four vectors. For

$$C^\mu = \int \frac{q^\mu d^D q}{(q^2 - m_1^2)((q+p_1)^2 - m_2^2)((q+p_1+p_2)^2 - m_3^2)} \quad (\text{D.8})$$

there are two available four vectors, p_1 and p_2 , and so we can express the integral as

$$C^\mu = p_1^\mu C_{11} + p_2^\mu C_{12} \quad (\text{D.9})$$

where again C_{11} and C_{12} are multiplicative scalar functions.

This process continues to the integrals with two or more indices, with the addition also of factors involving the metric tensor $g^{\mu\nu}$. Examples of this type of decomposition can be seen in (3.70), (3.71), (3.116) and (3.117).

Out of interest we note that a decomposition which never involves the $g^{\mu\nu}$ tensor has been invented by [46]. This scheme instead uses the linearly independent four vectors that appear in the denominator of the integral plus a four vector which is orthogonal to them as a basis for the decomposition. We will not consider this decomposition further here.

Having formed an expression in terms of the functions B_1 and so on, we now need a way to evaluate these functions. In order to do this, we use the method of decomposition to scalar integrals. In this method, each function is expressed in terms of the functions A_0 , B_0 , C_0 and D_0 . The complete solutions to these scalar integrals is known from [37].

The simplest example on which we can convincingly demonstrate this method is the C^μ integral of (D.8). For convenience we first define

$$P_1 = q^2 - m_1^2 \quad (\text{D.10})$$

$$P_2 = (q + p_1)^2 - m_2^2 \quad (\text{D.11})$$

$$P_3 = (q + p_1 + p_2)^2 - m_3^2 \quad (\text{D.12})$$

We contract the free index of C^μ with both $p_{1\mu}$ and $p_{2\mu}$,

$$p_{1\mu}C^\mu = p_1^2C_{11} + p_1p_2C_{12} = \int \frac{p_1q d^Dq}{P_1P_2P_3}, \quad (\text{D.13})$$

$$p_{2\mu}C^\mu = p_1p_2C_{11} + p_2^2C_{12} = \int \frac{p_2q d^Dq}{P_1P_2P_3}, \quad (\text{D.14})$$

then use the identities

$$p_1q = \frac{1}{2} [P_2 - P_1 - p_1^2 - m_1^2 + m_2^2], \quad (\text{D.15})$$

$$p_2q = \frac{1}{2} [P_3 - P_2 - (p_1 + p_2)^2 + p_1^2 - m_2^2 + m_3^2], \quad (\text{D.16})$$

to obtain

$$p_{1\mu}C^\mu = \frac{1}{2}(m_2^2 - m_1^2 - p_1^2) \int \frac{d^Dq}{P_1P_2P_3} + \frac{1}{2} \int \frac{d^Dq}{P_1P_3} - \frac{1}{2} \int \frac{d^Dq}{P_2P_3}, \quad (\text{D.17})$$

$$= \frac{1}{2}(m_2^2 - m_1^2 - p_1^2)C_0 + \frac{1}{2}B_0((p_1 + p_2)^2, m_1, m_3) - \frac{1}{2}B_0(p_2^2, m_2, m_3), \quad (\text{D.18})$$

$$p_{2\mu}C^\mu = \frac{1}{2}(-p_2^2 - 2p_1p_2 - m_2^2 + m_3^2) \int \frac{d^Dq}{P_1P_2P_3} + \frac{1}{2} \int \frac{d^Dq}{P_1P_2} - \frac{1}{2} \int \frac{d^Dq}{P_1P_3}, \quad (\text{D.19})$$

$$= \frac{1}{2}(-p_2^2 - 2p_1p_2 - m_2^2 + m_3^2)C_0 + \frac{1}{2}B_0(p_1^2, m_1, m_2) - \frac{1}{2}B_0((p_1 + p_2)^2, m_1, m_3), \quad (\text{D.20})$$

where

$$B_0(p^2, m_1, m_2) = \int \frac{d^Dq}{((q + p)^2 - m_1^2)(q^2 - m_2^2)}. \quad (\text{D.21})$$

Thus we have complete expressions for the reduction of the C_{11} and C_{12} functions.

Further examples of this type of reduction are given in subsection 3.5.2 and (3.137).

Bibliography

- [1] See, for instance, S. Jadach and Z. Was, in *Z Physics at LEP1*, CERN 89-08, edited by G. Altarelli, R. Kleiss and G. Verzegnassi, Vol. 1, p.235 (1990).
- [2] Y.-S. Tsai, *Phys. Rev. D* **4** (1971) 2821.
- [3] S.Y. Pi and A.I. Sanda, *Ann. Phys. (N.Y.)* **106** (1977) 16.
- [4] H. Kühn and F. Wagner, *Nucl. Phys. B* **236** (1984) 16.
- [5] K. Hagiwara, A.D. Martin and D. Zeppenfeld, *Phys. Lett. B* **235** (1989) 198.
- [6] A. Rougé, *Z. Phys. C* **48** (1990) 75.
- [7] B.K. Bullock, K. Hagiwara and A.D. Martin, *Phys. Rev. Lett.* **67** (1991) 3055.
- [8] R.M. Barnett, I. Hinchliffe, J.F. Gunion, B. Hubbard, H.E. Haber and H.-J. Trost, Davis preprint UCD-90-32, *Proc. of DPF Summer Study on High Energy Physics* (1990); R. Cruz, B. Grzadkowski and J.F. Gunion, Davis preprint UCD-92-15 (1992).
- [9] D.P. Roy, *Phys. Lett. B* **277** (1992) 183; *ibid*, *B* **283** (1992) 403; R.M. Godbole and D.P. Roy, *Phys. Rev. D* **43** (1992) 3640.
- [10] B.K. Bullock, K. Hagiwara and A.D. Martin, *Phys. Lett. B* **273** (1991) 501.
- [11] J.F. Gunion, H.E. Haber, G. Kane and S. Dawson, *Higgs Hunter's Guide* (Addison-Wesley 1990).
- [12] *Proceedings of the ECFA Large Hadron Collider Workshop*, edited by G. Jarlskog and C. Rein [CERN Yellow report No. 90-10 (1990)], Vols. I, II, and III.
- [13] V. Barger and R.J.N. Phillips, *Phys. Rev. D* **41** (1990) 884; A. C. Bawa, C. S. Kim and A. D. Martin, *Z. Phys. C* **47** (1990) 75;

- R. M. Godbole and D. P. Roy, Phys. Rev. D **43** (1991) 3640;
M. Drees and D.P. Roy, Phys. Lett. B **269** (1991) 155.
- [14] J.F. Gunion and H.E. Haber, *Proceedings of the 1984 Summer Study on the Design and Utilization of the Superconducting Super Collider*, Snowmass, Colorado, Eds. R. Donaldson and J.G. Morfin (1984) p.150;
H.E. Haber, *ibid*, p.157.
- [15] J.D. Anderson, M.H. Austern and R.N. Cahn, LBL reports, LBL-31858, LBL-32034 (1992).
- [16] See, for example, A.D. Martin and T.D. Spearman, *Elementary Particle Theory* (North-Holland, Amsterdam 1970) p.321.
- [17] J.H. Kühn and A. Santamaria, Z. Phys. C **48** (1990) 445.
- [18] N. Isgur, C. Morningstar and C. Reader, Phys. Rev. D **39** (1989) 1357.
- [19] S. M. Berman and M. Jacob, Phys. Rev. **139**, (1965) B1023.
- [20] J.E. Brau and G.J. Tarnpolsky, Phys. Rev. D **24** (1981) 2521;
P. Aurenche and R. Kinnunen, Z. Phys. C **28** (1985) 261;
E.W.N. Glover and A.D. Martin, Z. Phys. C **29** (1985) 399.
- [21] V. Barger, N.G. Deshpande, J.L. Rosner and K. Whisnant, Phys. Rev. D **35**, (1987) 2893;
F. del Aguila, M. Quirós and F. Zwirner, Nucl. Phys. B **287** (1987) 419.
- [22] UA1 Collaboration, Phys. Lett. B **185** (1987) 233;
CDF Collaboration, Fermilab preprint 91-356.
- [23] H. Murayama, I. Watanabe and K. Hagiwara, 'HELAS: helicity amplitude subroutines for Feynman diagram evaluations', KEK report 91-11 (1992).
- [24] Review of Particle Properties, Particle Data Group, Phys. Lett. B **239**, 1 (1990).
- [25] J.D. Anderson, M.H. Austern, R.N. Cahn, Phys. Rev. Lett. **69** (1992) 290.
- [26] C.A. Nelson, Phys. Rev. D **40** (1989) 123, Phys. Rev. D **43** (1991) 1465;
J. Bernabeu, A. Pich and N. Rius, Phys. Lett. B **257** (1991) 219;
R. Alemany, N. Rius, J. Bernabeu, J.J. Gómez-Cadenas and A. Pich, CERN-TH 6191/91 (1991).

- [27] T-P. Cheng and L-F. Li, *Gauge theory of elementary particle physics*, (Oxford University Press, 1989).
- [28] K. Huang, *Quarks, Leptons and Gauge fields*, (World Scientific, Singapore, 1992)
- [29] W.T. Giele, private communication.
- [30] *Large Hadron Collider Workshop, Proceedings Volume II, CERN 90-10, ECFA 90-133, Aachen, Eds. G. Jarlskog and D. Rein (1990) p.295;*
- [31] R.J. Guth and J.H. Kühn, Nucl. Phys. B **368**, (1992) 38.
- [32] T. Kuruma, Z. Phys. C 57, (1993) 551.
- [33] A. Denner and T. Sack, Nucl. Phys. B **358**, (1991) 46.
- [34] D. Levinthal, F. Bird, R.G. Stuart, B.W. Lynn, Z. Phys. C **53** 617 (1992).
- [35] V. Fadin and V. Khoze, Sov. J. Nucl. Phys. 48, (1988) 300.
- [36] G. Passarino and M. Veltman, Nucl. Phys. **B160**, (1979) 151.
- [37] G. 't Hooft and M. Veltman, Nucl. Phys. **B153**, (1979) 365.
- [38] J.M. Cornwall and J. Papavassiliou, Phys. Rev. D **40** (1989) 3474;
J. Papavassiliou, Phys. Rev. D **41** (1990) 3179.
- [39] G. Degrassi and A. Sirlin, Nucl. Phys. B **383** (1992) 73; Phys. Rev. D **46** (1992) 3104;
G. Degrassi, B.A. Kniehl and A. Sirlin, Phys. Rev. D **48** (1993) 3963.
- [40] A.D. Martin and F. Halzen, *Quarks and Leptons*, (Wiley, 1986).
- [41] K. Hagiwara, D. Zeppenfeld, Nucl. Phys. B **274**, (1986) 1.
See also [23] for a brief summary of their conventions for spinors.
- [42] D. Bailin, *Weak interactions*, (Sussex University Press 1977).
- [43] J. A. M. Vermaseren, *Spiders, a diagram building kit* (Unpublished).
- [44] L.B. Okun, *Leptons and Quarks*, (North Holland, 1982)
- [45] A. Sirlin, Nucl. Phys. B **192**, (1981) 93.

- [46] G. Van Oldenborgh and J.A.M. Vermaseren, *Z. Phys. C* **46** (1990) 425.
- [47] G. Van Oldenborgh.
- [48] F. Mandl and G. Shaw, *Quantum Field Theory*, (Wiley 1984).
- [49] S. Matsumoto, PhD thesis, Kanazawa University 1994.
- [50] J.D Bjorken and S.D. Drell *Relativistic Quantum Mechanics; Relativistic Quantum Field Theory* (McGraw-Hill, 1965).
- [51] D.C. Kennedy and B.W. Lynn, *Nucl. Phys. B* **322** (1989) 1.
- [52] Byckling and Kajantie, *Particle Kinematics*, (1979).
- [53] J.C. Collins, *Renormalization* (Cambridge University Press, 1984).
- [54] L.H. Ryder, *Quantum Field Theory*, (Cambridge University Press 1985).
- [55] B. De Wit and J. Smith *Field Theory in Particle Physics* (North Holland, 1986).

